

1. Report No. SPR-PL-1 (038) P535	2. Government Accession No.	3. Recipient's Catalog No.	
4. Title and Subtitle SPLICED I-GIRDER CONCRETE BRIDGE SYSTEM		5. Report Date December 2003	
		6. Performing Organization Code	
7. Author(s) Maher K. Tadros ,Amgad Girgis, Robert Pearce.		8. Performing Organization Report No.	
9. Performing Organization Name and Address Department of Civil Engineering University of Nebraska-Lincoln Omaha, Nebraska 68182		10. Work Unit No.	
		11. Contract or Grant No. SPR-PL-1 (038) P535	
12. Sponsoring Agency Name and Address Nebraska Department of Roads Bridge Division P. O. Box 94759 Lincoln, NE 68509-4759		13. Type of Report and Period Covered Final Report	
		14. Sponsoring Agency Code	
15. Supplementary Notes			
16. Abstract A number of prestressed concrete I-girder bridges built in the past several decades have demonstrated the ability of precast, prestressed spliced girder bridges to compete with structural steel plate girder bridges in the 120 ft - 300 ft span range. Some states limit the maximum transportable length of a member to 120 ft and the weight to 70 tons. Others, including Nebraska, have permitted lengths up to 175 ft and weights up to 100 tons. When span lengths exceed the maximum shippable length or weight, however, girder segments must be spliced at intermediate locations in the girder away from the piers. There are several other ways to extend the span capacity limits of standard products. These include using high-strength concrete, establishing moment continuity for superimposed deck and live loading, and utilizing pier geometry to allow longer spans. Each of these methods is discussed and examples are provided. This report discusses the design and construction of spliced-girder bridges. Design theory, post-tensioning analysis and details, segment-to-segment joint details and examples of recently constructed spliced-girder bridges are given. In recent years the trend toward increased span capacity of girder bridges has continued due to the need for improved safety and fast bridge replacement. Precast concrete members must now span further while minimizing the superstructure depth in order to compete favorably with a new breed of high-performance structural steel I-beams. This report presents four systems for creating continuous spliced concrete I-girders. For continuous large-span precast/prestressed concrete spliced I-girder bridges, the optimum solution is often a haunched girder system. Because of the need to use standard sizes as repetitively as possible and to clear overhead obstructions during shipping, a separate precast haunch block attached to the girder bottom flange is used to form a deeper section for the negative moment zone. This report summarizes an extensive theoretical and experimental research project on the feasibility of splicing a haunch block onto a standard I-girder to form an efficient negative moment zone. Approximate formulas are developed to estimate losses in post-tension spliced girder construction based on NCHRP 18-07. An overview of NCHRP 18-07 is given followed by an explanation of the work done to extend the results of NCHRP 18-07 to post-tensioned construction. A parametric study undertaken to develop the approximate formulas is then discussed. Finally, the formulas are presented and evaluated. The importance of protecting the corrosion sensitive post-tensioning steel is a focus in this research as well. After the collapse of two post-tensioned structures in England and the recent discovery of corroded tendons in several Florida bridges, many owners began to investigate their grouted post-tensioned structures more closely. Numerous investigations found that typical grout mixes, equipment, and procedures used in the past, as well as field inspection procedures, were not adequate to protect the post-tensioning steel. This research seeks to determine what changes, if any, need to be made to the Nebraska Department of Roads' Post-Tensioning Special Provisions to ensure that the full, corrosion-free design life of post-tensioning tendons in Nebraska's bridges will be attained.			
17. Keyword Spliced Girder, Segmental Bridges, Precast, prestressed, post-tensioning, losses, grout.		18. Distribution Statement No Restrictions. This document is available to the public through the National Technical Information Service, Springfield, VA 22161	
19. Security Classification (of this report) Unclassified	20. Security Classification (of this page) Unclassified	21. No. of Pages 177	22. Price

SPLICED I-GIRDER CONCRETE BRIDGE SYSTEM

NDOR Project Number SPR-PL-1(038) P535

Final Report

December 2003

Principal Investigator

Maher K. Tadros

Charles J. Vranek Distinguished Professor of Civil Engineering
University of Nebraska-Lincoln

Amgad Girgis

Research Assistant Professor
University of Nebraska-Lincoln

and

Robert Pearce

Research Assistant
University of Nebraska-Lincoln

Sponsored By

Nebraska Department of Roads (NDOR)

University of Nebraska-Lincoln (UNL)

DISCLAIMER

The contents of this report reflect the views of the authors who are responsible for the facts and the accuracy of the data presented herein. The contents do not necessarily reflect the official views or policies of the Nebraska Department of Roads nor the University of Nebraska-Lincoln. This report does not constitute any standard, specification, or regulation. Trade or manufacturers' names, which may appear in this report, are cited only because they are considered essential to the objectives of the report. The United States (U.S.) government and the State of Nebraska do not endorse products or manufacturers.

ACKNOWLEDGEMENTS

This project was sponsored by the Nebraska Department of Roads (NDOR). The support of Leona Kolbet, Research Coordinator, Lyman Freemon, Bridge Engineer, Sam Fallaha, Assistant Bridge Engineer, and Gale Barnhill, Bridge Research Engineer, all at the NDOR, is gratefully acknowledged. They spent many hours to coordinate this project, discuss its technical direction and inspire the university researchers.

The university team consisted of Dr. Maher K. Tadros, Charles J. Vranek Distinguished Professor of Civil Engineering, Dr. Amgad Girgis, Research Assistant Professor, and Robert Pearce, Research Assistant. Nick Meek and Kelvin Lein from the University of Nebraska Structures Laboratory provided additional assistance.

Full-scale specimen for production and demonstration purposes and technical assistance were provided by Concrete Industries, Lincoln, NE, and Rinker Materials, Omaha, NE. The efforts of the following individuals are particularly appreciated: Mark Lafferty, Dennis Drews, and Buz Hutchinson.

TABLE OF CONTENTS

TECHNICAL REPORT DOCUMENTATION	i
ABSTRACT.....	i
DISCLAIMER	ii
ACKNOWLEDGEMENTS	iii
TABLE OF CONTENTS.....	iv
LIST OF FIGURES	x
LIST OF TABLES.....	xv
CHAPTER 1: INTRODUCTION.....	1
1.1 PROBLEM STATEMENT.....	1
1.2 RESEARCH OBJECTIVES	4
1.3 GOALS AND BENEFITS	9
1.4 SCOPE AND LAYOUT.....	10
CHAPTER 2: EFFECTIVENESS OF I-GIRDER SPLICING ALTERNATIVES.....	13
2.1 INTRODUCTION	13
2.2 BRIDGE ASSUMPTIONS.....	16
2.3 DESIGN CONSIDERATIONS	18
2.4 DESIGN SYSTEMS.....	21
2.4.1 System I: Full Span Segment.....	21
2.4.1.1 Method A: Conventional Deck Reinforcement	22
2.4.1.2 Method B: Threaded Rod Splicing	23
2.4.1.3 Method C: Full Length Post-Tensioning	25

2.4.1.4 Method D: Stitched Splice	26
2.4.1.5 Concrete NU I-Beam Capacities.....	26
2.4.2 System II: Segmental Construction with Constant Cross Section.....	27
2.4.2.1 Concrete NU I-Beam Capacities.....	28
2.4.2.2 System II Discussion and Recommendations	29
2.4.2.3 Improving the Efficiency of Systems I and II.....	30
2.4.3 System III: Segmental Construction with Curved Pier Segment.....	31
2.4.3.1 Concrete NU I-Beam Capacities.....	31
2.4.3.2 System III Discussion and Recommendations.....	32
2.4.4 System IV: Segmental Construction with Two Pier Segment Pieces: A Straight Haunch Block and an NU I-Girder	34
2.4.4.1 Concrete NU I-Beam Capacities.....	35
2.4.4.2 Optimizing the Haunch Block	35
2.4.5 System Comparisons	
2.4.6 Three Span Bridge	
2.5 CONCLUSIONS.....	39
CHAPTER 3: VERTICALLY SEGMENTED PRECAST CONCRETE	
SPLICED I-GIRDER	40
3.1 INTRODUCTION	40
3.2 PROPOSED CONNECTION DETAILS	41
3.3 DESIGN EXAMPLE	44
3.3.1 Construction Sequence.....	44
3.3.2 Prestress Force	45

3.3.3 Shear Forces and Bending Moments	45
3.3.4 Capacities of the Critical Sections	48
3.4 EXPERIMENTAL INVESTIGATIONS	49
3.4.1 Push-Off Tests	50
3.4.1.1 The Sixth Push-Off Specimen	50
3.4.1.1.1 Specimen Configurations	50
3.4.1.1.2 Test Setup and Instrumentations	50
3.4.1.1.3 Observation	53
3.4.1.1.4 Coil Rods Strain Gauge Readings	54
3.4.1.2 Push-Off Tests Results and Discussion	56
3.4.2 The Pull-Out Test	57
3.4.2.1 Test Setup	57
3.4.2.2 Observations	57
3.4.2.3 Pull-Out Test Discussion	57
3.4.3 Full Scale Test	59
3.4.3.1 Specimen Modeling	59
3.4.3.2 Loading and Measurements	59
3.4.3.3 Test Results	60
3.4.3.3.1 Load Deflection	60
3.4.3.3.2 Concrete Strain at Mid-Span	60
3.4.3.3.3 Flexural Reinforcement Strains	60
3.4.3.3.4 Vertical Shear Reinforcement Strains	61
3.4.3.3.5 Horizontal Shear Reinforcement Strains	61

3.4.3.3.6 Crack Pattern.....	62
3.4.3.3.7 Summary and Discussion of the Beam	
Ultimate Capacities.....	69
3.5 DISCUSSION.....	72
3.6 CONCLUSION.....	72
CHAPTER 4: APPROXIMATE FORMULAS FOR PRESTRESSED LOSSES IN	
HIGH-STRENGTH CONCRETE	74
4.1 INTRODUCTION	74
4.1.1 Problem Statement.....	74
4.1.2 Prestressed Losses.....	74
4.1.2.1 Elastic Effect.....	75
4.1.2.2 Shrinkage	76
4.1.2.3 Creep.....	77
4.1.2.4 Relaxation	77
4.2 NCHRP 18-07 PRETENSIONED BRIDGES	77
4.2.1 Background.....	77
4.2.2 Modulus of Elasticity.....	79
4.2.3 Shrinkage	81
4.2.4 Creep.....	83
4.2.5 Relaxation	84
4.2.6 Losses Step by Step	85
4.2.7 Approximate Formulas	87
4.3 SPLICED GIRDER BRIDGES	88

4.4 APPROXIMATE FORMULA DEVELOPMENT	91
4.4.1 Problem Statement	91
4.4.2 Assumptions.....	92
4.4.3 Parametric Study	97
4.4.4 Approximate Formulas	98
4.4.4.1 Formula #1	98
4.4.4.2 Formula #2	101
4.4.4.3 Formula #3	103
4.4.5 Detailed Method and Approximate Formulas Compared	105
4.4.5.1 Skyline Bridge	106
4.4.5.2 Highway-50 Bridge.....	113
4.5 CONCLUSIONS AND SUGGESTED RESEARCH.....	120
CHAPTER 5: POST-TENSIONING QUALITY CONTROL	121
5.1 INTRODUCTION	121
5.1.1 Problem Statement	121
5.1.2 General Post-Tensioned Performance.....	121
5.2 BACKGROUND AND LITERATURE REVIEW	126
5.2.1 Recent Problems	126
5.2.2 The Engineering Community Responds	131
5.3 GROUTING.....	133
5.3.1 Grout for Post-Tensioning Steel Corrosion Prevention	133
5.3.2 Bleed	136
5.3.3 Thixotropic Grout	138

5.3.4 Thixotropic Grout Testing	141
5.3.4.1 Bleed Testing	141
5.3.4.2 Fluidity.....	143
5.3.5 Early History of Thixotropic Grout	144
5.3.6 Thixotropic Grout Mixing.....	147
5.4 INVESTIGATIVE METHODS.....	149
5.4.1 Borescope Inspection	149
5.4.2 Impact Echo Testing	150
5.4.3 Impulse Radar Testing	154
5.4.4 Magnetic Flux Leakage Testing.....	156
5.4.5 High Energy X-Ray (Linear Accelerator) Testing.....	157
5.4.6 Conclusions.....	158
5.5 OTHER PROTECTIVE MEASURES	159
5.5.1 Plastic Duct Systems.....	159
5.5.1.1 Background.....	159
5.5.1.2 Nebraska’s Situation	164
5.5.2 Galvanized/Epoxy Coated Strand	167
5.5.3 Cost Comparison.....	169
5.5.4 The Most Critical Protective Measure – Personnel	171
5.6 CONCLUSIONS AND RECOMMENDATIONS	172
REFERENCES.....	174
APPENDICES	See CD

LIST OF FIGURES

Figure 1.1-1	Pier Segment Deepening Options	2
Figure 1.2-1	Elevation of Connected Haunch Block to Pier Segment	7
Figure 1.2-2	Pier Segment Haunch Block Cross Sections	8
Figure 2.1-1	Splicing Precast Concrete Bridges Flowchart.....	15
Figure 2.2-1	Typical Cross Section	16
Figure 2.3-1	Positive and Negative Moment Section Reinforcement	20
Figure 2.4.1-1	System I Methods	22
Figure 2.4.1.1-1	Method A NU2000 Span Capacities.....	23
Figure 2.4.1.2-1	Method B NU2000 Span Capacities	24
Figure 2.4.1.3-1	Method C NU2000 Span Capacities	25
Figure 2.4.1.5-1	Comparison between System I Methods' Capacities.....	27
Figure 2.4.2-1	System II Layout.....	28
Figure 2.4.2.1-1	System II NU2000 Span Capacities.....	29
Figure 2.4.3-1	System III Layout	31
Figure 2.4.3.1-1	System III NU2000 Span Capacities	32
Figure 2.4.4-1	System IV Layout	34
Figure 2.4.3.1-1	System IV NU2000 Span Capacities	35
Figure 2.4.5-1	Comparison between the Four Systems	37
Figure 3.2-1	Proposed Connection Details	42
Figure 3.2-2	Full Scale Specimen.....	43
Figure 3.3-1	Design Example Elevation and Cross-Sections	46
Figure 3.3-2	Design Example Post-Tensioning Profile.....	47

Figure 3.4.1.1.1-1	The Sixth Push-Off Specimen Details	51
Figure 3.4.1.1.2-1	Push-Off Specimens Test Setup.....	52
Figure 3.4.1.1.3-1	The Sixth Specimen Mode of Failure	54
Figure 3.4.1.1.4-1	HB4T, GD3T and GD1T Strain Gauge Readings	55
Figure 3.4.2.1-1	Pull-Out Specimen Test Setup.....	57
Figure 3.4.2.-1	Pull-Out Specimen Details.....	58
Figure 3.4.3.1-1	Full-Scale Test Concrete Dimensions and Reinforcement Details	63
Figure 3.4.3.2-1	Full-Scale Test Strain Gauge Locations	64
Figure 3.4.3.3.1-1	Full-Scale Test Mid-Span Deflection	65
Figure 3.4.3.3.1-2	Full-Scale Test South LVDT Readings	65
Figure 3.4.3.3.2-1	Full-Scale Test Concrete Strain Gauge Readings.....	66
Figure 3.4.3.3.3-1	Full-Scale Test Longitudinal Reinforcement Strain Gauge Readings.....	66
Figure 3.4.3.3.4-1	Full-Scale Test Vertical Shear Strain Gauge Readings	67
Figure 3.4.3.3.5-1	HS3ST Strain Gauge Readings.....	68
Figure 3.4.3.3.6-1	Crack Patterns	70
Figure 3.4.3.3.7-1	LRFD Equation and Loov’s and Patnaik’s Equation for Horizontal Shear Versus Test Results.....	71
Figure 4.2.2-1	NCHRP 18-07 Modulus of Elasticity Test Results.....	80
Figure 4.2.3-1	NCHRP 18-07 Shrinkage Test Results.....	82
Figure 4.2.4-1	NCHRP 18-07 Creep Coefficient Test Results, Specimens Loaded At 1 Day.....	84

Figure 4.2.6-1	NCHRP 18-07 Plot of Pretensioned Girder Losses	86
Figure 4.3-1	Plot of Two Post-Tensioned Girder Losses Using the Detailed Method	89
Figure 4.4.1-1	Points for Which Approximate Formulas Were Developed	92
Figure 4.4.4.1-1	Comparison of Formula #1 Results to the Detailed Method Results.....	99
Figure 4.4.4.1-2	Data Used in Development of Creep Term of Formula #1.....	101
Figure 4.4.4.2-1	Comparison of Formula #1 Results to the Detailed Method Results.....	102
Figure 4.4.4.2-2	Data Used in Development of Creep Term of Formula #2.....	103
Figure 4.4.4.3-1	Comparison of Formula #3 Results to the Detailed Method Results.....	104
Figure 4.4.4.3-2	Data Used in Development of Creep Term of Formula #3.....	105
Figure 4.4.5.1-1	General Layout of the 198 th -Skyline Dr. Bridge.....	108
Figure 4.4.5.1-2	Construction Sequence of the 198 th -Skyline Dr. Bridge.....	109
Figure 4.4.5.1-3	Pretensioning Scheme of the 198 th -Skyline Dr. Bridge	110
Figure 4.4.5.1-4	Post-Tensioning Details of the 198 th -Skyline Dr. Bridge	111
Figure 4.4.5.2-1	General Layout of the HW50 Bridge.....	115
Figure 4.4.5.2-2	Pretensioning Scheme of the HW50 Bridge	116
Figure 4.4.5.2-3	Post-Tensioning Details of the HW50 Bridge	117
Figure 5.1.2-1	Post-Tensioning Anchorage.....	122
Figure 5.2.1-1	First Distressed Tendon Discovered on the Mid-Bay Bridge.....	127
Figure 5.2.1-2	Mid-Bay’s “Pulled Out” Tendon	128

Figure 5.2.1-3	Anchor Head of Mid-Bay’s Failed Tendon	128
Figure 5.2.1-4	Florida’s Sunshine Skyway Bridge.....	129
Figure 5.2.1-5	Corroded Tendon at Anchorage Sunshine Skyway’s Troubled Pier	129
Figure 5.3.1-1	Bore Scope Photo Showing an UngROUTED Section of Tendon In the Mid-Bay Bridge	133
Figure 5.3.1-2	Initial Reaction Leading to Rust	133
Figure 5.3.1-3	Passivating Film Formed by Good Quality Grout	134
Figure 5.3.1-4	The effect of Chlorides on Steel Corrosion	135
Figure 5.3.1-5	Typical Corrosive Pitting Found in the Sunshine Skyway's Corroded Tendons.....	136
Figure 5.3.2-1	Grout Column with Intermediate Lens Formation.....	136
Figure 5.3.2-2	Interstitial Areas of 7-Wire Strands	137
Figure 5.3.2-3	Bleed in Vertical Tendons	137
Figure 5.3.3-1	Change In Flow with Degree of Thixotropy.....	139
Figure 5.3.3-2	Non-Tixotropic Grout Flow, Backflow, and Proper Venting at Crest of Draped Tendon.....	140
Figure 5.3.4-1	Modified ASTM C 490.....	142
Figure 5.3.4.1-2	Schupack Filter Test Setup	142
Figure 5.3.4.2-2	Mud Balance Test	143
Figure 5.3.5-1	Tendon Section, Grout Penetration Between Strands.....	145
Figure 5.3.6-1	Colloidal Mixer.....	148
Figure 5.4.1-1	Ft. Lauderdale Airport Access Bridge in Florida.....	149

Figure 5.4.2-1	Commercial Impact-Echo System	150
Figure 5.4.2-2	Stress Waves Caused by Impact at a Point	151
Figure 5.4.2-3	The Impact Echo Method.....	152
Figure 5.4.2-4	Examples of Amplitude Spectra From Impact-Echo Tests.....	153
Figure 5.4.3-1	Radar Profile of a Concrete and Rebar Specimen	154
Figure 5.4.3-2	Reflection of the Wave of Intensity “A” Reflection Coefficient “RC” and Dielectric Constants ϵ_1 and ϵ_2	154
Figure 5.4.3-3	Typical Impulse Radar Record	155
Figure 5.4.4-1	Magnetic Flux Leakage Testing Device for Internal Post-Tensioning	156
Figure 5.4.5-1	High Energy X-Ray Testing Device.....	157
Figure 5.5.1.1-1	Dual Duct System Incorporating Polyethylene Ducts in Florida’s Sunshine Skyway.....	159
Figure 5.5.1.1-2	Polyethylene Duct.....	163
Figure 5.5.1.2-1	Detail Showing 2” Concrete Cover Over Duct.....	164
Figure 5.5.1.2-2	Detail Showing Concrete Encasement of Anchorage Region	166
Figure 5.5.2-1	Externally Coated Epoxy Strand.....	167
Figure 5.5.3-1	Post-Tensioning Grout Discharge.....	170

LIST OF TABLES

Table 2.2-1	Bridge Assumptions.....	16
Table 2.2-2	Assumed Effective Prestressing at Each Construction Stage	17
Table 2.3-1	Critical Section Locations.....	18
Table 2.4.4.2-1	Two-Span Bridge NU I-Girder Web Width Modifications for System IV	36
Table 2.4.6-1	Three-Span Bridge NU I-Girder Web Width Modifications for System IV	38
Table 3.3.3-1	Unfactored Shear Force and Bending Moments for Typical Interior Girder	48
Table 3.3.4-1	Critical Sections Shear Force and Bending Moments Capacities	48
Table 3.4.1-1	Push-Off Specimens.....	53
Table 3.4.1.2-1	Summary of Group 1 Specimen’s Capacities	56
Table 3.4.1.2-2	Summary of Group 2 Specimen’s Capacities	56
Table 3.4.3.3.7-1	Summary of the Maximum Load Capacity (P, kips) for the Different Ultimate Capacities	69
Table 4.4.5.1-1	Loss Prediction Comparison, Skyline Bridge.....	112
Table 4.4.5.2-1	Loss Predication Comparison, Highway-50 Bridge	118
Table 5.1.2-1	Federal Highway Administration National Bridge Inventory Data, 1997	124

CHAPTER 1

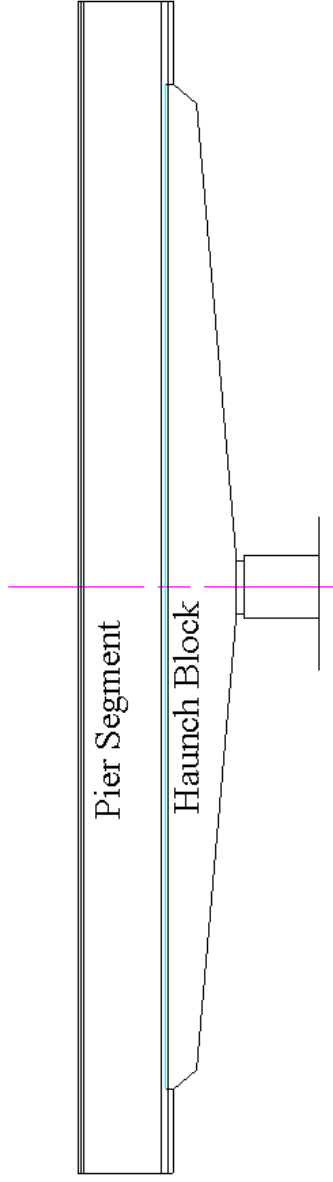
INTRODUCTION

1.1 PROBLEM STATEMENT

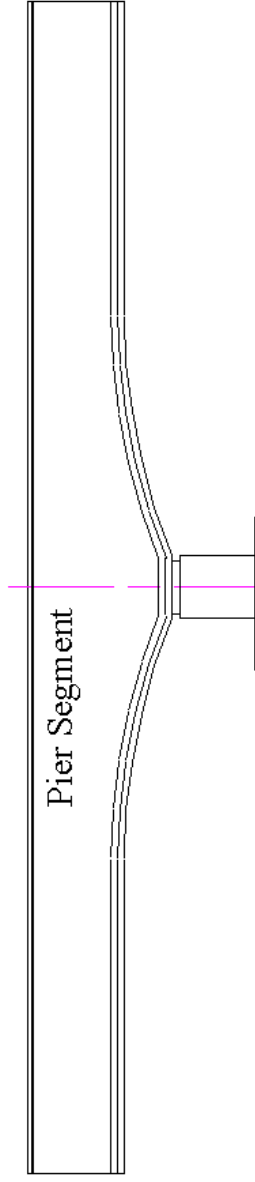
Constructing prestressed concrete bridges exceeding a certain length and/or weight is constrained by the contemporary capacities of precast concrete producers, as well as the shipping capacity limitations of the highways of most states. Thus, all bridges with spans exceeding these limits have to be designed with structural steel plate girders. However, due to various reasons, there has been a national tendency to increase precast concrete bridge spans. This presents a real challenge for researchers, professionals and practitioners in the field to find a technically feasible, economic, and aesthetic solution that allows for extending span capacity.

It is widely known that for continuous, relatively large-span bridges, the critical section is generally at the pier due to large negative moments or large shear forces. Therefore, in order to utilize precast concrete in bridges efficiently, the beam at the pier needs to be deepened. The deepened beam is able to resist the high values of negative moments and shear forces, and creates an optimum overall structural system.

One of the alternatives to deepening the section is adding a composite precast haunch block underneath the pier segment. Through the utilization of a haunched concrete girder, a large number of relatively short, light girders, interconnected using post-tensioned cables, are proven to result in longer-than-usual pre-stressed concrete bridge spans. A one-piece variable depth precast concrete pier segment would be



A) Composite Pier Segment and Precast Haunch Block



B) One Piece Pier Segment

Figure 1.1-1 Pier Segment Deepening Options

economical if standard forms could be used, and if height and weight were within local capabilities. This is, however, not the case.

The haunch block alternative enlarges the span capacity of the precast elements used as bridge girders by allowing for the use of a constant section depth standard girder form. Because it can be fabricated and shipped in smaller sections, this alternative also reduces the cost of the project. Allowing for the complete elimination of false-work (temporary towers) is one of the unique advantages of this system, especially in water-crossing bridges, in addition to keeping enough clearance below the bridge.

The first option utilizes a variable-depth pier segment. However, in the context of large spans, the pier segment is likely to exceed shipping capacities. Please refer to figure 1.1-1 for the two alternatives of deepening the pier segment.

In addition to increasing the span length, this research sought to develop approximate prestress loss formulas for use in post-tensioned spliced girder construction based on recently proposed high-strength concrete prestress loss prediction methods. In 2002, NCHRP project 18-07 resulted in new guidelines for estimating prestress losses in pre-tensioned high-strength concrete bridge girders. The scope of NCHRP 18-07 did not include post-tensioned applications. The design guidelines developed in 18-07 were recently extended to post-tensioned spliced girder applications. Loss prediction in these applications is complex and time-consuming without the use of a computer program. This research project sought to develop approximate formulas for the prediction of these losses.

Given that the previously discussed span lengths would be accomplished by a post-tensioned girder system, the importance of protecting the corrosion sensitive post-tensioning steel is a focus in this research project as well. After the collapse of two post-

tensioned structures in England and the recent discovery of corroded tendons in several Florida bridges, many owners began to investigate their grouted post-tensioned structures more closely. Numerous investigations found that typical grout mixes, equipment, and procedures used in the past, as well as field inspection procedures, were not adequate to protect the post-tensioning steel. This research project seeks to determine what changes, if any, need to be made to the Nebraska Department of Roads' Post-Tensioning Special Provisions to ensure that the full, corrosion-free design life of post-tensioning tendons in Nebraska's bridges will be attained.

1.2 RESEARCH OBJECTIVES

The objectives of this research project are three-fold:

- 1) Develop a cost-effective and aesthetically acceptable haunched concrete girder for continuous spans in excess of 160 feet. The developed system must be adaptable to standardization for various spans up to 300 feet, as well as various girder spacing. It must be usable with the standard NU-1100, 1350, 1600, 1800 and 2000 I-girder sizes already available in Nebraska. Finally, it must provide superstructure span-to-depth ratios comparable to those used for structural steel plate girders.
- 2) Revise the Nebraska Department of Roads' Post-Tensioning Special Provisions in accordance with recent tendon corrosion discoveries, research and recommendations.
- 3) Develop approximate formulas to estimate time-dependent prestress losses in both pre-tensioning and post-tensioning steel based on NCHRP 18-07.

In order to accomplish the objectives stated above the following tasks were performed:

Task 1: Reviewing Recently Constructed Bridges

A collection of recently constructed bridges are described in detail in Chapter 2. These bridges are: Cockshutt Road Bridge, Brantford, ON (1977); Kingston Road Bridge, Scarborough, ON (1977); Annacis Channel East Bridge, Vancouver, B.C. (1984); Umpqua River Bridge, Sutherlin, OR (1970); 128th-Street Bridge, Snohomish, WA (1985); Choctawhatchee Bridge, Walton, FL (1988); Shelby Creek Bridge, Pike County, KY (1989); Provencher Bridge, Winnipeg, MB (1990); Esker Overhead, Skeena District, B.C. (1990); Eddyville–Cline Hill Section, Little Elk Creek Bridges 1-10, Corvallis–Newport Highway (US20), OR (2000); Rock Cut Bridge, WA (1997); US 27–Moore Haven Bridge, FL (1999); and Bow River, Calgary, AB (2002).

Task 2: Establishing the Spliced Girder System

The spliced girder system was established as follows. A two-piece composite pier segment, composed of an NU-I beam and a precast haunch block, were connected together horizontally as shown in Figure 1.1-1A. An eight-inch pocket was created between the two precast pieces to contain all the horizontal shear reinforcement. This pocket was then cast with a flowable concrete mix after installing the confinement reinforcement and the pier segment over the haunch block. Please refer to Figures 1.2-1 and 1.2-2 for the concrete dimensions of the proposed pier segment-haunch block connection. A full-scale specimen with all the proposed concrete dimensions and reinforcement details is described in detail in Chapter 4.

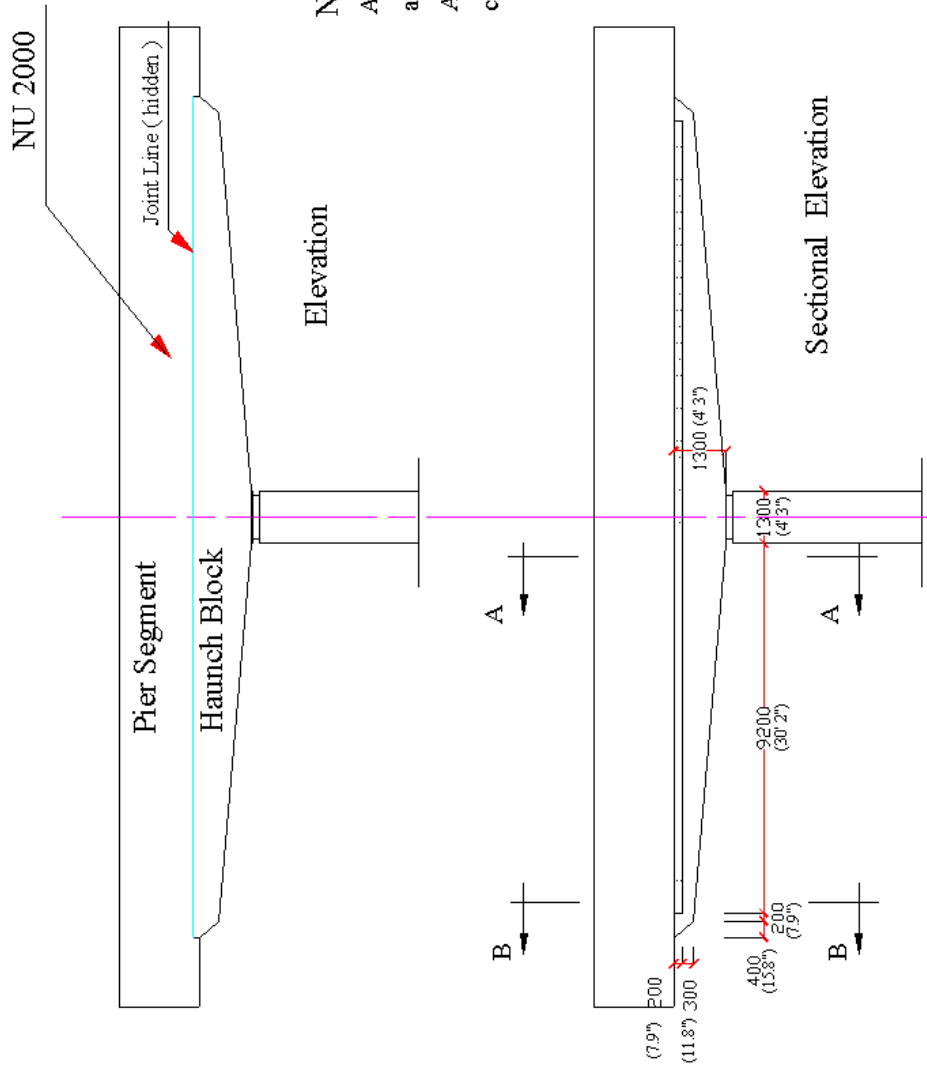
Task 3: Theoretical Design and Detailing

The system selected in task 2 was subjected to a very thorough analysis. A convenient design procedure was developed in order to check for various service loads and strength limits to determine the reinforcement details. A complete design example of a three-span bridge was developed as an example of application of the design procedure.

Task 4: Experimental Verification

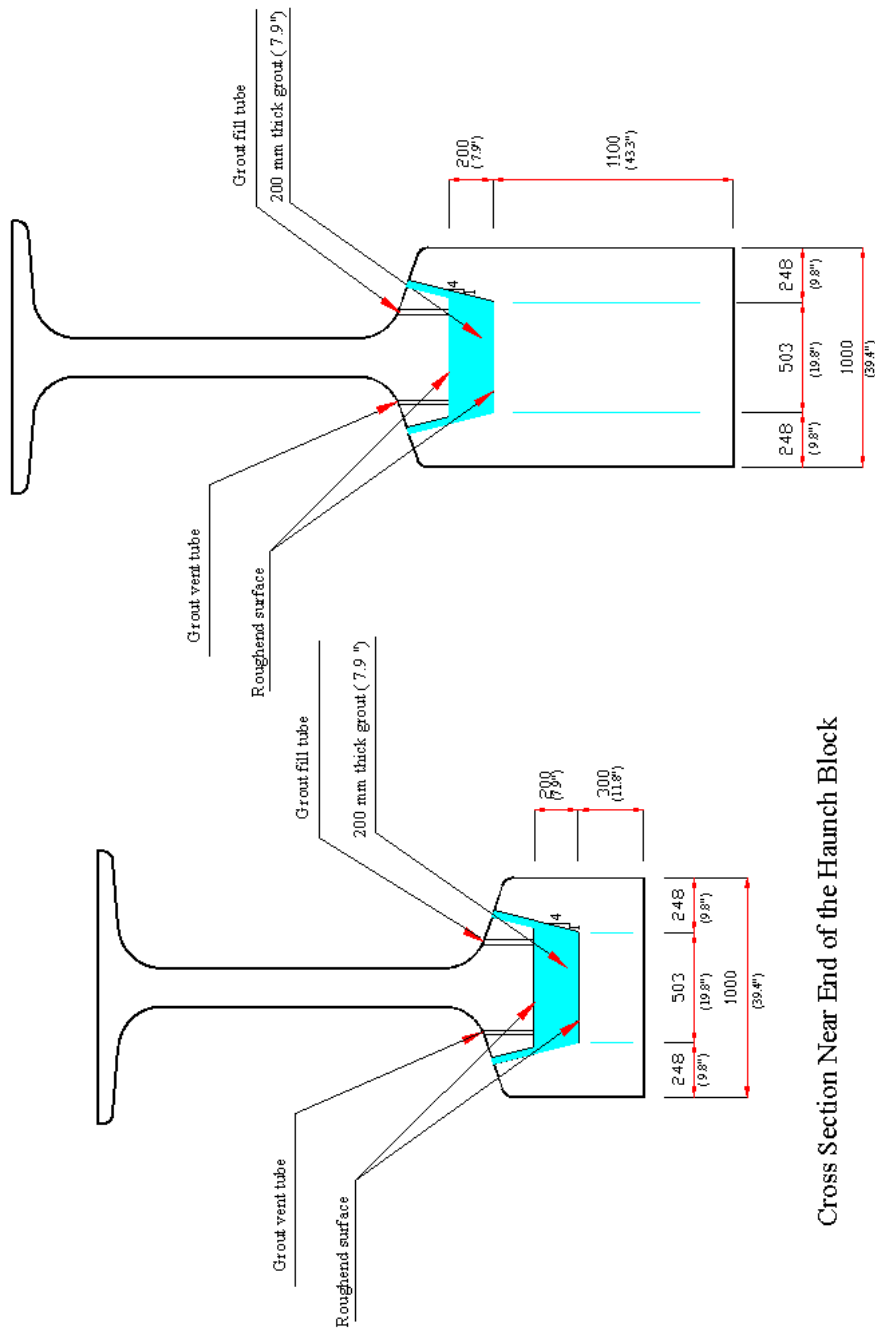
In order to study the capacity of the interface between the haunch block and the pier segment, push-off and pull-out tests were performed. Push-off and pull-out tests were conducted on small-scale members. The push-off specimens consisted of two precast pieces connected together by casting concrete in the pocket created between these pieces. Between the precast concrete and the pocket, there was horizontal shear reinforcement. The push-off specimens were then subjected to vertical force until failure. Each of the pull-out specimens consisted of one precast piece that had the insert hardware, which was pulled until failure. Pull-out and push-off specimens represented the connection behavior between the haunch block and the pier segment. The purpose of these specimens was to estimate the capacity of the interface between the bottom flange components in horizontal shear and verify the developed theory.

A full-scale test was also performed. The specimen consisted of two precast pieces connected together by a horizontal concrete joint. The two precast pieces were an I-beam and a haunch block. The I-beam was an Iowa type A. The haunch block was located at the top of the I-beam. The specimen was simply supported from both ends and was loaded at its mid-span. Iowa type A girder is the shallowest Iowa girders. It has a height of 32 in.



Note:
 All concrete dimensions
 are in hard metric units.
 All other details are in
 customary U.S. units.

Figure 1.2-1 Elevation of Connected Haunch Block to Pier Segment.



Cross Section Near End of the Haunch Block

Cross Section Near Pier

Figure 1.2-2 Pier Segment Haunch Block Cross Sections

Task 5: Tendon Corrosion Literature Review

Literature relevant to the revision of the Nebraska Department of Roads' Post-Tensioning Special Provisions was reviewed. This included case studies of post-tensioned tendon corrosion problems, guides for avoiding these problems in the future, and post-tensioning special provisions from other states.

Task 6: Parametric Study and Formula Development

A prestress loss analysis was performed on a representative sample of post-tensioned spliced girder bridges using the method based on NCHRP 18-07 and modified to include post-tensioning. Formulas were developed based on the parametric study.

Task 7: Revision of Post-Tensioning Special Provisions

The document was revised in accordance with the findings in the literature review.

Task 8: Final Report

A final report that includes the results of tasks 1 through 8 was prepared based on the experimental and analytical results.

1.3 GOALS AND BENEFITS

Several goals and benefits can be achieved by extending bridge spans as follows:

- a- Enhancing safety when shoulder piers are eliminated in overpass applications.
- b- Enhancing hydraulic capacity in bridging waterways.
- c- Minimizing environmental impact on constructed facilities.
- d- Adaptability to Single Point Interchange (SPUI) and similar recent interchange geometries requiring extended spans.

In addition, precast prestressed concrete has generally been shown to offer advantages over steel in terms of low initial cost, construction speed, and maintenance savings.

1.4 SCOPE AND LAYOUT

This study focuses on extending the span capacity of NU-I girder bridges. A total of six chapters are included in this report.

In this chapter, the problem statement, the research objectives, the goals and benefits have been presented.

In Chapter 2, the span capacities of the concrete bridge systems are studied. Four different precast concrete bridge systems are covered. Within the first system, three methods of continuity are covered. Comparisons between the system capacities and the method capacities are performed. Finally, design charts are presented for NU2000 for the four systems.

Chapter 3 analyzes the spliced concrete I-girder bridges using standard haunch block shapes composite with the pier segment. An example of a three-span bridge is using the precast haunch block is given. The experimental investigations are presented in this chapter. The experimental investigations consist of eight push-off specimens, two pull-out specimens and one full-scale test.

Chapter 4 discusses the approximate formulas developed to estimate the losses in post-tension spliced girder construction based on NCHRP 18-07. An overview of NCHRP 18-07 is given followed by an explanation of the work done to extend the results of NCHRP 18-07 to post-tensioned construction. The parametric study undertaken to develop the approximate formulas is then discussed. Finally, the formulas are presented and evaluated.

Chapter 5 addresses post-tensioning quality control. A survey of the general performance of post-tensioned bridge construction is conducted, followed by a review of recent corrosion problems experienced with a few isolated post-tensioned bridges. The chapter also includes an in-depth look at tendon corrosion, grout properties, and thixotropic grout. Various methods used to inspect for grout voids and tendon corrosion are surveyed. A brief look at the positive and negative aspects is included, followed by final conclusions and recommendations.

Appendix A contains the preliminary design charts done for the five Nebraska beams (NU1100 through NU2000) using the four studied bridge systems. Preliminary design charts using the three studied bridge methods within the first system are also presented.

Appendix B contains the material properties used in the push-off specimens, the pull-out specimens and the full-scale test.

Appendix C contains the description of the push-off and the pull-out specimens.

Appendix D contains the strain gauge readings in the push-off specimens.

Appendix E contains the strain gauge readings in the full-scale test.

Appendix F covers full-scale specimen production, shipping and handling.

Appendix G includes parametric study for developing the approximate prestressed formula

Appendix H was written by Dr. Tadros, Dr. Saleh, and Dr. Girgis in a format suitable for publication as a chapter in the PCI Bridge Design Manual. It has already been submitted to PCI. It is expected to be accepted for publication, with possible technical and editorial changes, based on the comments generated in the standard PCI review process. Methods to extend precast concrete bridge spans are discussed. Several

important post-tensing issues are covered. Three examples are covered. The first example is a two-span bridge with two precast beams, post-tensioned in two stages. The second example is also a post-tensioned two-span bridge, with three precast beams. The third example is a post-tensioned single span bridge with three precast beams.

Appendix J is the revised NDOR Post-Tensioning Special Provisions

CHAPTER 2

EFFECTIVENESS OF I-GIRDER SPLICING ALTERNATIVES

2.1 INTRODUCTION

As the trend moves toward extending the span capacities of precast concrete bridges, the need for an optimum system increases. This paper presents four different systems for building concrete NU I-girder bridges (see Figure 2.1-1). Within the first system four different methods are studied, including the advantages and disadvantages of each system. The actual bridge capacity of each system is the least of four different capacities: the ultimate negative moment capacity, the ultimate positive moment capacity, the service III positive moment capacity, and the shear capacity. The capacity of each system is carefully calculated and NU2000 span charts are presented. System capacities are compared, and recommendations for improving the capacity of each system are presented.

A number of prestressed concrete I-girder bridges built in the past several decades have demonstrated the ability of precast, prestressed spliced girder bridges to compete with structural steel plate girder bridges in the 120 foot to more than 300 foot span range. Some states limit the maximum transportable length of a member to 120 feet and the weight to 70 tons. Others, including Pennsylvania, Washington, Nebraska and Florida, have permitted precast girders with lengths up to about 175 feet and weights up to 100 tons to be shipped by truck.

Experience has shown that the simplest and most economical system is when full span-length pieces are installed directly onto their permanent supports as in system I.

When span lengths exceed the maximum shippable length or weight, however, girder segments must be spliced at intermediate locations in the girder away from the piers as in system II through system IV, as shown in Figure 2.1-1.

Bridge designers are often constrained to using standard, readily-available girder types and sizes. They may thus be required to make girders work for spans and spacing beyond their normal capacity. This is especially true in situations where the structural depth must be limited due to clearance requirements and roadway grade constraints.

There are several other ways, however, to extend the span capacity limits of standard products. These include using high strength concrete, establishing moment continuity for superimposed deck and live loading, and utilizing pier geometry to allow longer spans. This paper focuses on establishing moment continuity and girder splicing. The paper presents a unique attempt to integrate and compare the successes and limitations of the main girder splicing approaches utilized throughout the past half century or more.

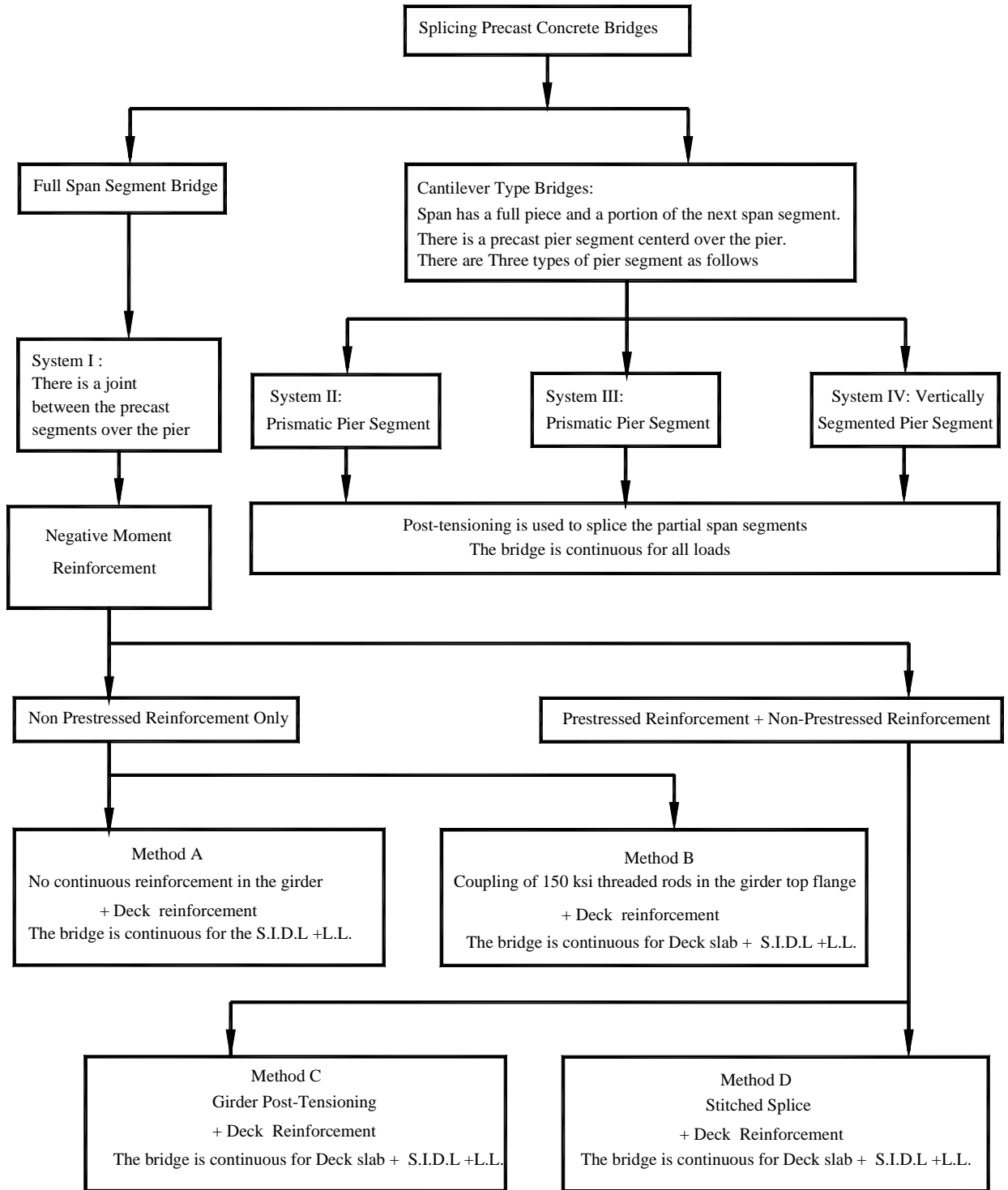


Figure 2.1-1 Splicing Precast Concrete Bridges Flowchart

2.2 BRIDGE ASSUMPTIONS

In order to study the capacities of each system and perform the comparison, assumptions need to be made, as shown in Table 2.2-1.

Table 2.2-1 Bridge Assumptions

Bridge Data	Girder Spacing	8-10-12 ft	See Figure 2.2-1
	Overall Width	46 ft-6 in.	
	Number of Spans	2-3	
	Deck Slab Thickness	8-10 ft girder spacing = 7.5 in. 12 ft girder spacing = 8.0 in.	
Span Data	Two Span Bridge	L-L	
	Three Span Bridge System I Method B	0.85L-L-0.85L	
	Three Span Bridge System IV	0.8L-L-0.8L	
Concrete Data	Precast Concrete	28-days strength	= 8,000 psi
		Release strength	= 5,500 psi
		Unit weight	=150 pcf*
	Cast in Place Concrete	28-days strength	= 4,000 psi
		Unit weight	=150 pcf*
Reinforcement Data	Steel bars	Yield strength	= 60 ksi
		E_s	=29,000 ksi
	Strands: See table 2 for prestress losses Low-Relaxation Strands 0.6 in.	Ultimate strength	= 270 ksi
		E_s	=28,500 ksi
	Threaded Rods	Min. yield stress**	= 120 ksi
		Ultimate stress***	= 150 ksi
Load Data	S.I.D.L.	Future wearing surface	= 25 pcf
		Barrier load	= 0.3 kips/ft
	Live Loads	HL93	
Post-tensioning****	Stages: Applied at one stage	After casting the diaphragm	
	Tendons: 3, 3.75 in. diameter, 15-0.6 in. strands each	Inside duct area > 2.5 strands area	

* 148 pcf for young's modulus calculations and 150 pcf for weight calculations

** Elongation for 20 bar diameter 4% for yield stress

*** Reduction in area is 20% for ultimate stress

**** For initial and time dependent losses, please refer to Table 2.2-2

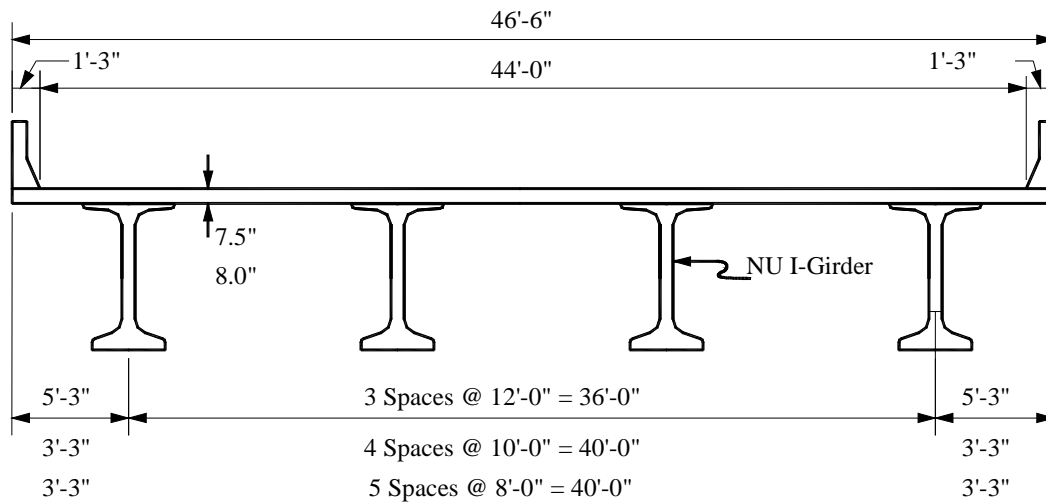


Figure 2 Typical Cross Section

Table 2.2-2 Assumed Effective Prestressing at Each Construction Stage

Construction Stage	Stress in Pretensioning Strand	Stress in Post-Tensioning Strand
Pretensioning Strands	$0.92(0.75)f_{pu}$	---
Post-Tensioning Strands	$0.87(0.75)f_{pu}$	$0.92(0.78)f_{pu}$
Service Loads	$0.82(0.75)f_{pu}$	$0.82(0.78)f_{pu}$

2.3 DESIGN CONSIDERATIONS

Maximum bridge spans are calculated according to the following considerations:

- a. Partial prestressed -Ultimate negative bending moment only
- b. Fully prestressed -Ultimate positive bending moment at 0.4 L
-Girder bottom flange tensile stress (service III)

$$\text{At } 0.4 L = 0.19\sqrt{f'_c}$$

- c. Ultimate shear stress $V_u = \Phi(0.25f'_c b_w d_v)$

For the locations of the critical sections, refer to Table 3

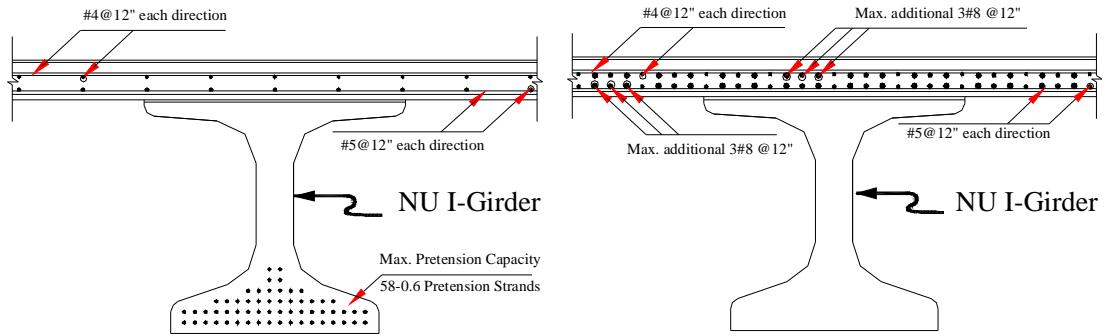
Table 3 Critical Section Locations

Design Criteria	System I	System II	System III	System IV
Negative Moment Section	the face of the 8 in. diaphragm	Pier Center Line	many sections are studied near the pier	
Shear Critical Sections	8 ft-0 in. from the Pier Center Line		many sections are studied near the pier	
Positive Moment section	0.4 L			

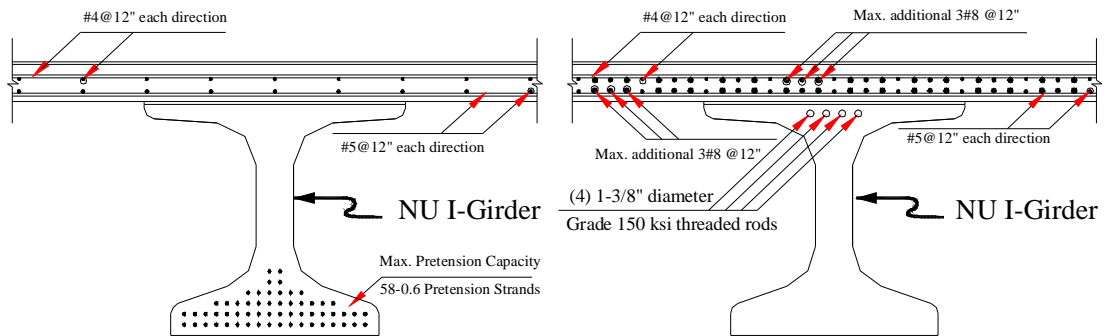
The c/h value is less than or equal 0.4, with additional compression reinforcement as needed. Although the negative moment section is calculated as a cracked section, the structural analysis is calculated using the full concrete section properties.

Deck reinforcement according to the empirical design is # 4 @12 in. at the top in each direction and # 5 @12 in. at the bottom in each direction. Mild reinforcement is

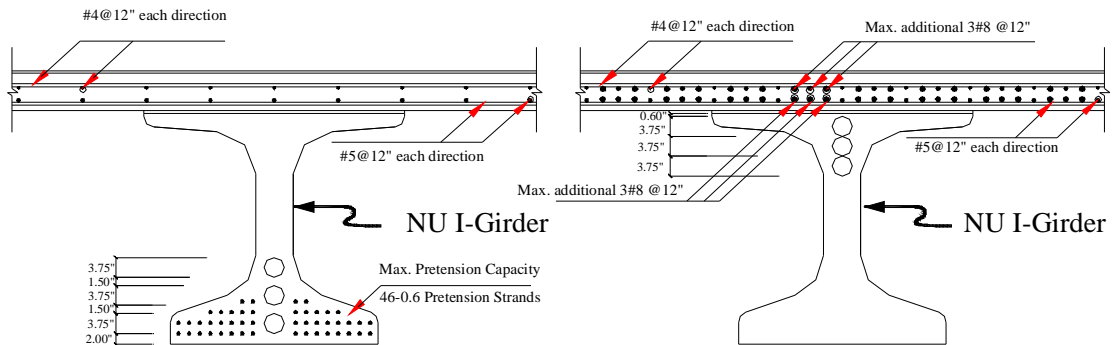
added in the deck slab in the negative moment area as needed. The maximum additional mild reinforcement is a group of 3#8 top and bottom at 12" as shown in figure 2.3-1.



System I, Method A



System I, Method B



System I, Method C and Systems II, III, IV

a) Positive Moment Section
Reinforcement [At 0.4 L]

b) Negative Moment Section
Reinforcement at the Pier

Figure 2.3-1 Positive and Negative Moment Section Reinforcement.

2.4 DESIGN SYSTEMS

Precast prestressed concrete I-girders can be efficiently designed and constructed by utilizing one full precast segment per span and creating continuity over the pier as in system I or using a cantilever type bridge in which the pier segment is centered on the pier as in system II through system IV. Continuity methods in system I efficiently utilize the bridge girder, which leads to a reduction in girder size or an increase in girder spacing, consequently reducing bridge cost. Splicing the girders gives the designer the flexibility to increase the bridge spans more than the maximum length of the precast segments. Another feature of spliced girders is the ability to adapt to a horizontally-curved alignment. By casting the I-girders in appropriately short segment lengths and providing the necessary transverse diaphragms, girder segments may be chorded along a curved alignment. This scheme results in an efficient framing system without sacrificing aesthetics. There are several potential systems for creating continuity and girder splicing as shown in Figure 2.1-1. Each system is studied and its maximum capacity is specified. Each of the following sections is devoted to one of these systems/methods.

2.4.1 System I: Full Span Segment

System I is the easiest and most economical system. However bridges in this system are limited by shipping and handling capacities. The shipping and handling capacity in Nebraska is 160 ft. The precast pieces in this system span between the permanent supports (pier, abutment). Four methods of creating continuity are studied to optimize this system.

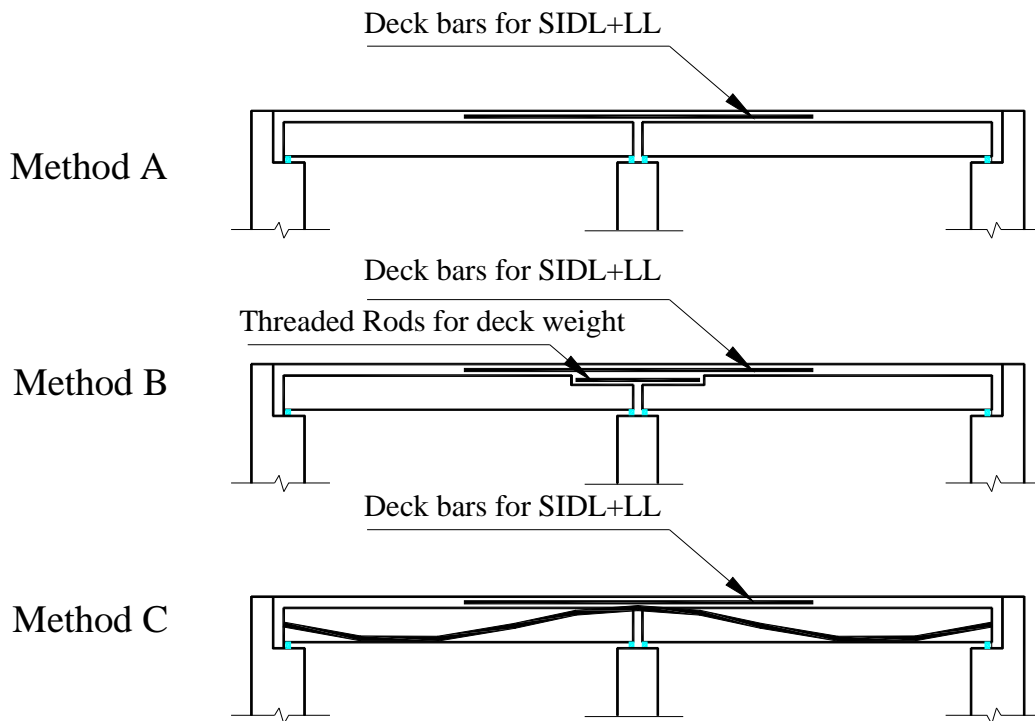


Figure 2.4.1-1. System I Methods

2.4.1.1 Method A: Conventional Deck Reinforcement

This method is the simplest and perhaps the least costly of existing methods. Continuity is created by placing mild reinforcement in the deck over the piers. The girder self-weight and deck slab weight are carried by the simple span precast segments. However, superimposed dead load and live load are carried by the continuous composite girder/slab system. This method does not require extra equipment or a specialized contractor. But the superstructure is continuous only for the superimposed dead loads and live loads, which is approximately only one third of the total loads. Consequently,

method A has small negative moments and relatively high positive moments, leading to a relatively high pretension force which causes high prestress losses and bottom cracking at the piers.

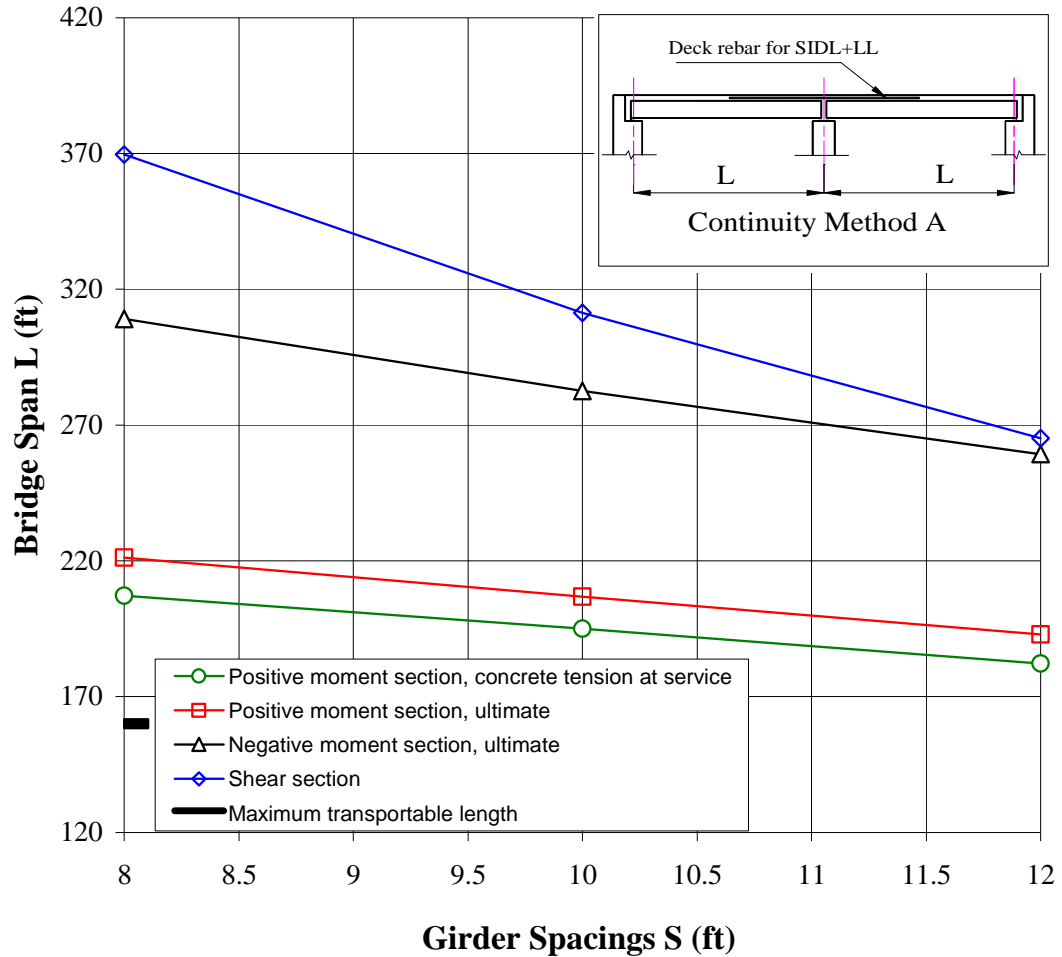


Figure 2.4.1.1-1 Method A NU2000 Span Capacities

2.4.1.2 Method B: Threaded Rod Splicing

In this method, I-girders are fabricated with 150 ksi high strength threaded rods embedded in the top flange. The threaded rods are mechanically spliced in the field at the diaphragms over the piers. The diaphragm concrete is then placed, and the deck slab is cast after the diaphragm gains the required strength. For more details, see Ma et al

(1998). This is a relatively new system. The first bridge using this system has been designed and was scheduled for construction near Clarks, Nebraska in the fall of 2002. As opposed to Method A, this method allows for the superstructure to be continuous for the deck slab in addition to the superimposed dead load and live load, which is almost 70% of the total load. Accordingly, Method B can improve the span capacity of a given girder size by 10 to 15% over Method A. The negative moment created by the deck slab weight, superimposed dead load and live load reduces the need for crack control bottom reinforcement over the piers.

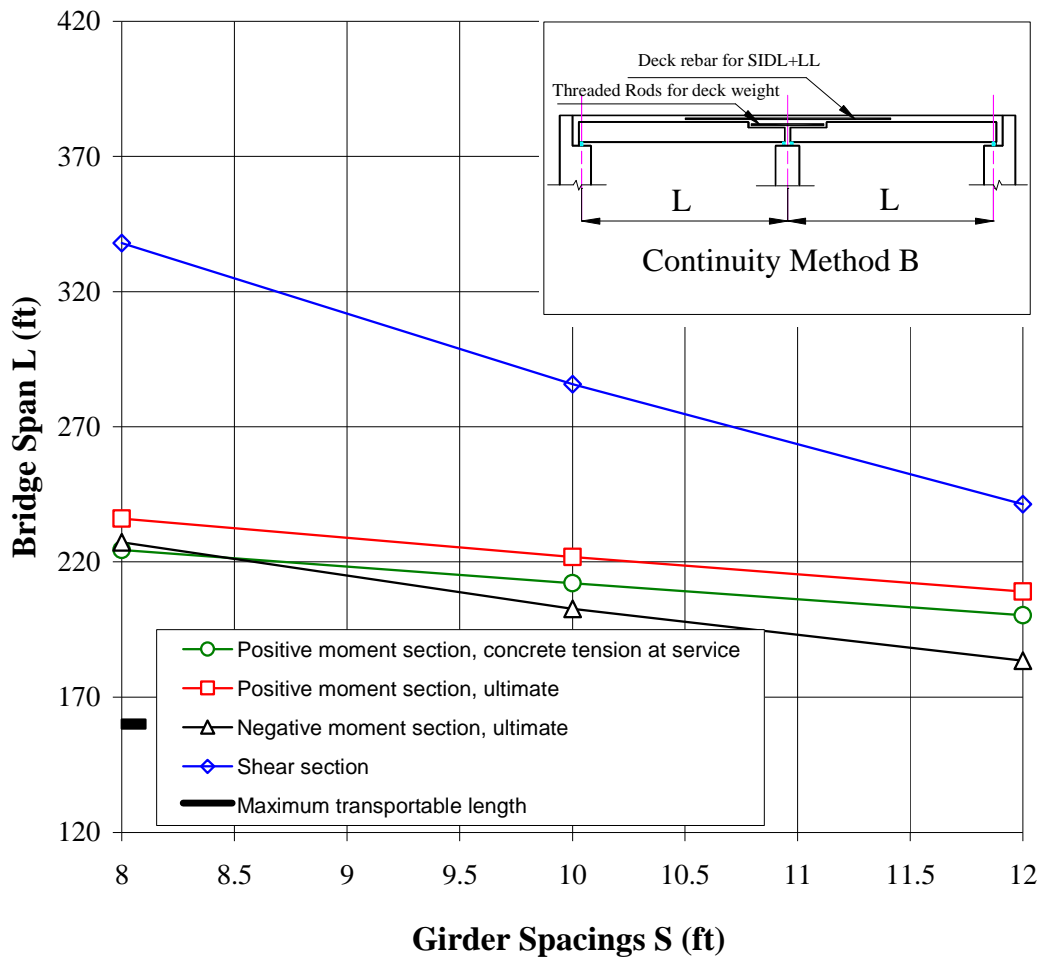


Figure 2.4.1.2-1 Method B NU2000 Span Capacities

2.4.1.3 Method C: Full Length Post-tensioning

This method is more expensive than the previous methods. It requires full-length ducts and usually necessitates widening the girder webs. It also requires end blocks to resist stress cogenerations at the anchorage zones.

Continuity in this method is created through post-tensioning the full length of the bridge. This method, like Method B, allows for the superstructure to be continuous for the deck slab in addition to the superimposed dead load and live load which is almost 70% of the total load. This is an effective method, especially if spliced segmental I-beams are needed for spans longer than the shipping capabilities of single-piece spans.

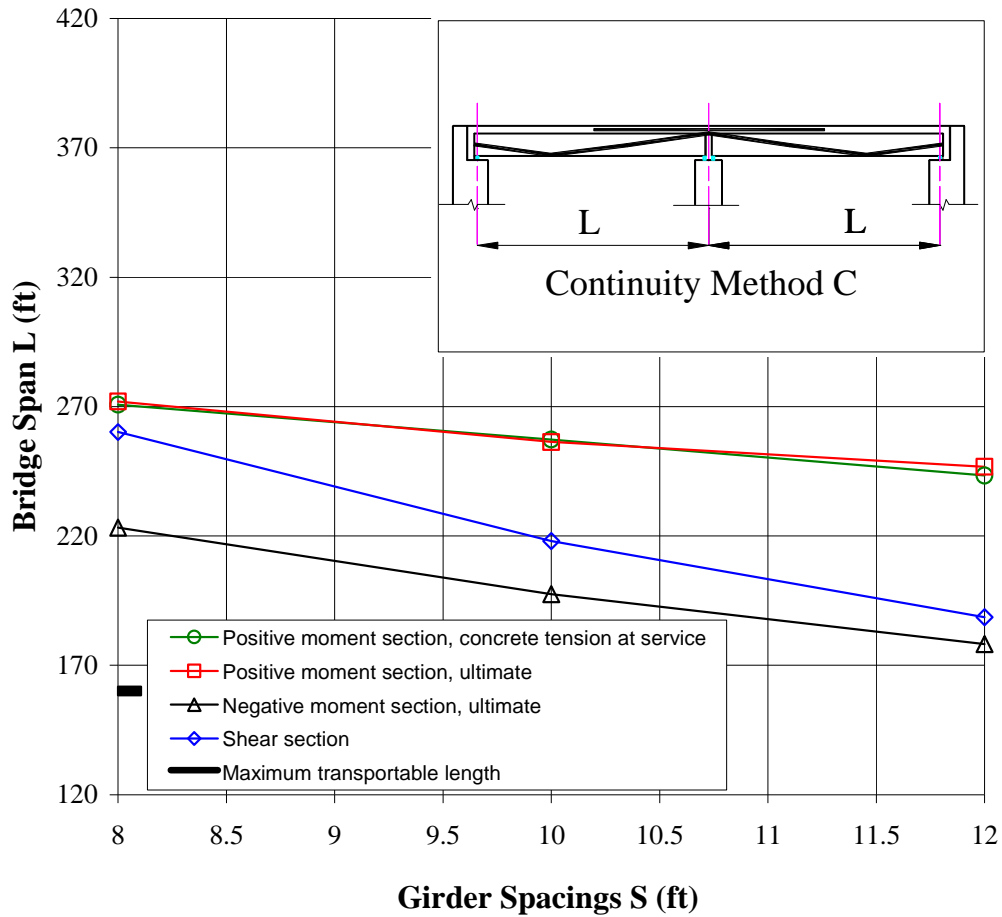


Figure 2.4.1.3-1 Method C NU2000 Span Capacities

2.4.1.4 Method D: Stitched Splice

This type of splicing the girder is not common. In this type of splice, the precast, pretensioned segments are post-tensioned across the splice, using short tendons or threaded bars. It should be noted that precise alignment of the post-tensioning ducts is essential for the effectiveness of the post-tensioning. If proper alignment is not achieved, considerable frictional losses can result, which decreases the effectiveness of the post-tensioning. Oversized ducts are often used to provide some tolerance. In addition, because of the short length of the tendons, anchorage seating losses can be unacceptably large. To reduce anchorage seating losses, the use of threaded bars that are post-tensioned by power wrench is recommended.

End blocks are required at the spliced ends of the girders in order to house the post-tensioning hardware and provide the “end zone” reinforcement to resist concentrated concrete stresses due to post-tensioning forces.

2.4.1.5 Concrete NU I-Beam Capacities

Within the first system, the threaded rod continuity method gives the largest span capacity without changing the web width. The reinforcement steel in the deck slab method, method A, gives a higher capacity than post-tensioning in beams beyond a 10.25 ft girder spacing using NU2000 girders. The reinforcement steel in the deck slab method is mostly controlled by the positive moment concrete tension at service. The threaded rod continuity method is controlled by the ultimate negative moment. Adding a steel plate at the bottom flange of the NU I-girder at the negative moment section can improve the capacity of this system.

Post-tensioning results in a high gap between the capacities of the positive moment section (service and ultimate) and those of the ultimate negative moment and shear. The negative moment capacity controls the design of the NU2000 girder.

For a comparison among the system capacities of methods A, B and C with a 10 ft girder spacing, refer to Figure 2.4.1.5-1.

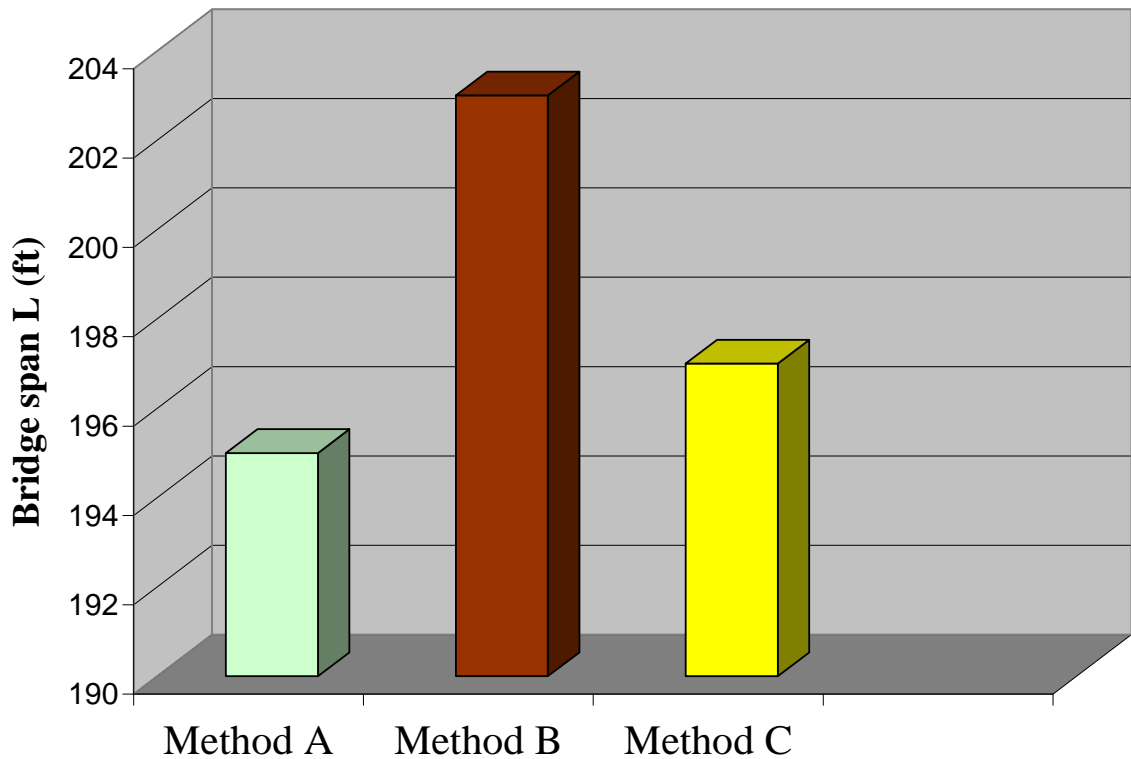


Figure 2.4.1.5-1 Comparison among System I Methods' Capacities

2.4.2 System II: Segmental Construction with Constant Cross Section

The precast pieces used in this system are spliced with post-tensioning tendons away from the pier, as shown in Figure 2.4.2-1. The system allows for larger bridge spans than the maximum transportable concrete precast beams. The field segments are

pretensioned to carry the beam self-weight during shipping and construction and to contribute to the flexure capacity of the positive moment section. The pier segment can have some pretensioning to carry the beam self-weight during shipping and construction, and top convention reinforcement to contribute to the flexure capacity of the negative moment section. All the precast pieces have the standard NU cross-section.

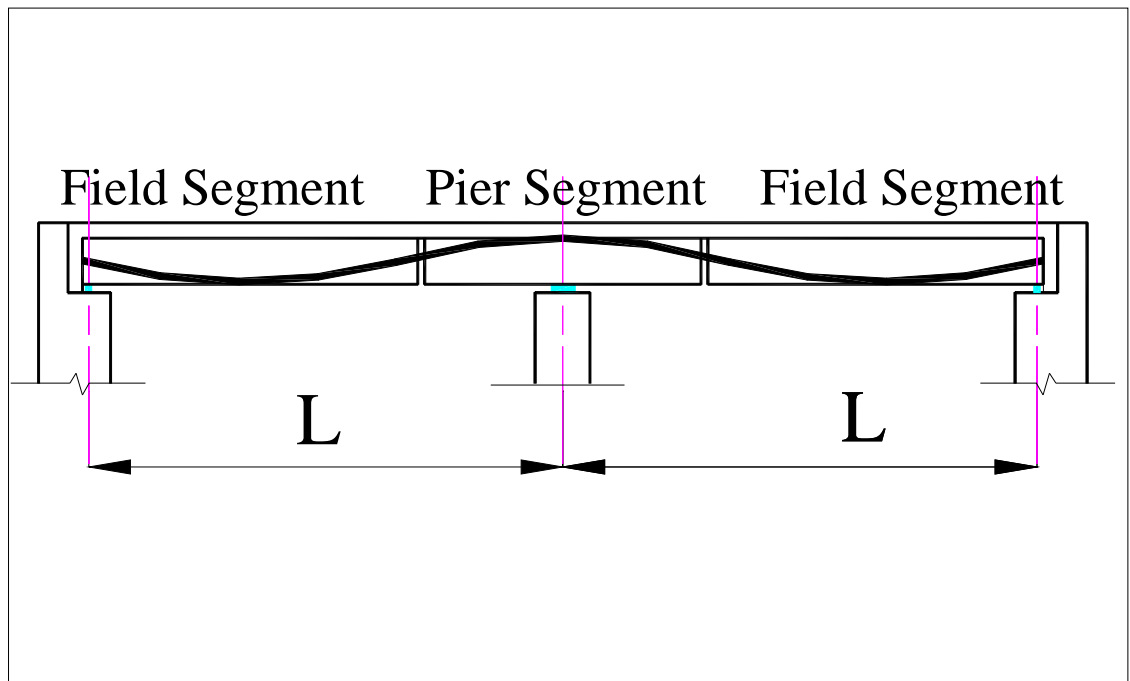


Figure 2.4.2-1 System II layout

2.4.2.1 Concrete NU I-Beam Capacities

As shown in Figure 2.4.2.1-1, the ultimate negative moment capacity controls the design. The maximum segmental span length for this system is higher than the span capacities. Consequently, the system is not optimized for this reason.

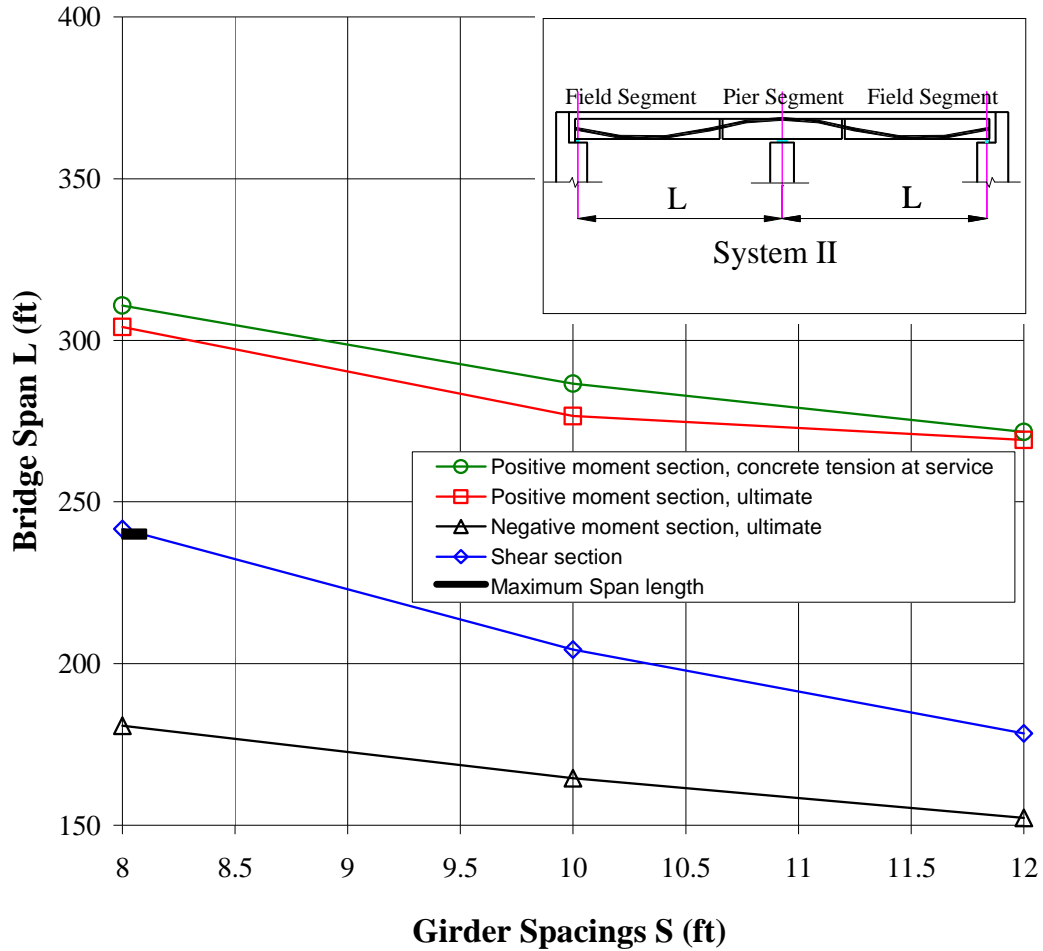


Figure 2.4.2.1-1 System II NU2000 Span Capacities

2.4.2.2 System II Discussion and Recommendations

The positive service tension capacity is close to the positive ultimate moment capacity, indicating that this system is efficient for these design criteria. However, the large difference between the negative and the positive capacities makes this system inefficient overall. See Figure 2.4.2.1-1.

Generally for this system the ultimate shear and the ultimate negative moment capacity are lower than the positive ultimate moment capacity and the tension service capacity, respectively. Significant capacity in the positive region remains unused. For

example, for an NU2000 girder spacing of 10 feet the ultimate positive span capacity is 270 while the ultimate negative capacity limits the span to 165 ft. That is why the pier segment needs to be deepened to optimize the structure as in system III or IV.

2.4.2.3 Improving the Efficiency of Systems I and II

In long-span spliced bridges, the sections over the pier are often subject to high shear and bending moment. In most cases, these sections may limit the span capacities of the system as we see in system II and system I methods B and C. In such cases, designers often use deeper sections at the pier in order to satisfy shear and flexure design requirements. Usually this is done by varying the web depth as in system II or by increasing the thickness of the girder's bottom flange at the pier section. An alternative approach is to increase the web height of the girder and keep the bottom flange unchanged as in system III.

2.4.3 System III: Segmental Construction with Curved Pier Segment

The third system is the first method of deepening the pier segment by using a curved haunched girder. For a two-span bridge, three precast pieces are used in this system: two field segments and a one-piece curved pier segment. This system is the same as system II, with the exception of the pier segment's variable depth. See Kamel (1996).

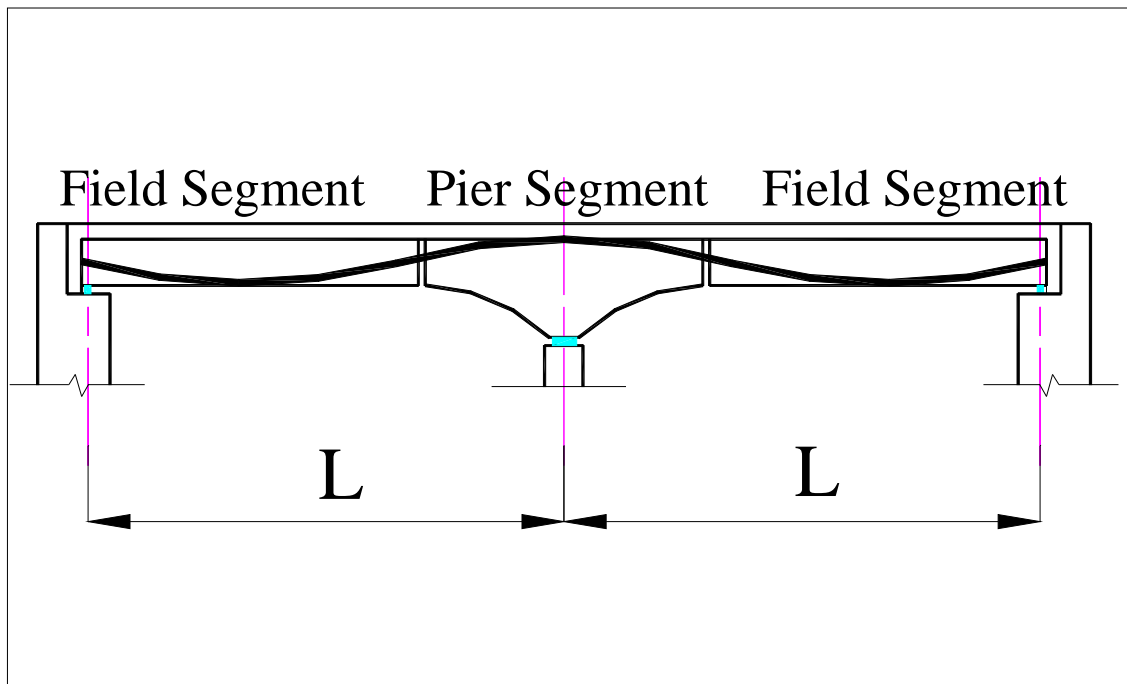


Figure 2.4.3-1 System III Layout

2.4.3.1 Concrete NU I-Beam Capacities

Here we see little improvement from System II. The ultimate negative moment capacity still controls the design. The ultimate shear capacity is improved from system II as can be seen from figure 2.4.3.-1. The maximum segmental span length for this system is much higher than the span capacities.

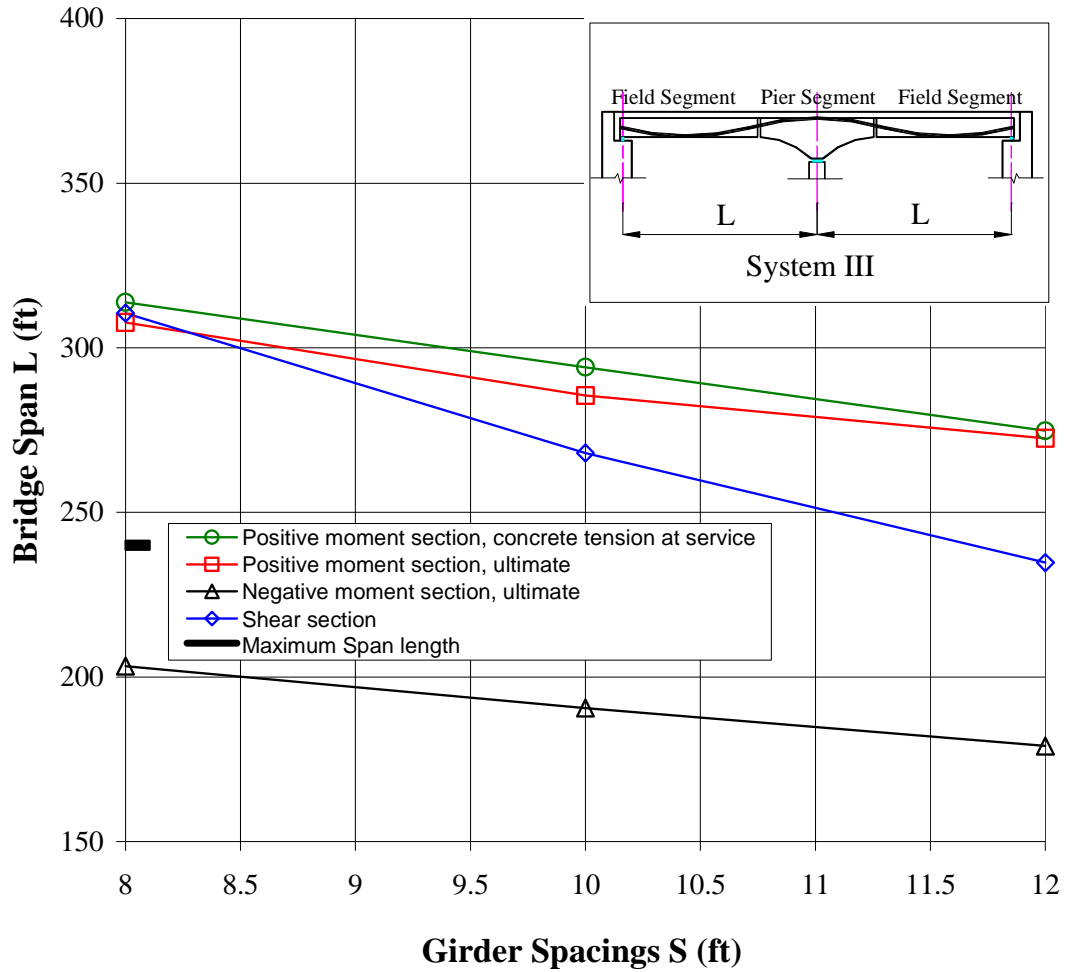


Figure 2.4.3.1-1 System III NU2000 Span Capacities

2.4.3.2 System III Discussion and Recommendations to Improve the System Capacity

For system III, the ultimate negative moment capacity controls the design. The critical section for the ultimate negative moment is found to be three quarters of the distance from the pier center line to the end of the curved portion of the pier segment.

The tension positive service capacity is close to the ultimate positive moment capacity, indicating that this system is efficient for these design criteria. However, the

large difference between the negative and the positive capacities makes this an inefficient system overall. See Figure 2.4.3.1-1 for System III NU2000 span chart.

The maximum segmental span length for this system is higher than the span capacities. Generally for this system the ultimate shear and the ultimate negative moment capacity are lower than the ultimate positive moment capacity and the tension service capacity. Significant capacity remains unused. That is why the pier segment needs to be deepened more so that all the capacities are equal. However if the pier segment was deepened to optimize the system capacities, the height and the weight of the pier segment would be greater than the shipping and handling capacity. It is therefore recommended that a two-piece pier segment be used. This pier segment consists of a straight haunch block and I-girder to optimize the structure, shown as System IV.

2.4.4 System IV: Segmental Construction with Two Pier Segment Pieces: A Straight Haunch Block and an NU I-Girder.

The fourth system is the second method of deepening the pier segment. The system utilizes a two-piece pier segment: a straight haunch block and an NU-I girder. Refer to figure 2.4.4-1. Dividing the pier segment into two pieces allows constructing a deeper pier segment within the allowable shipping and handling capacities.

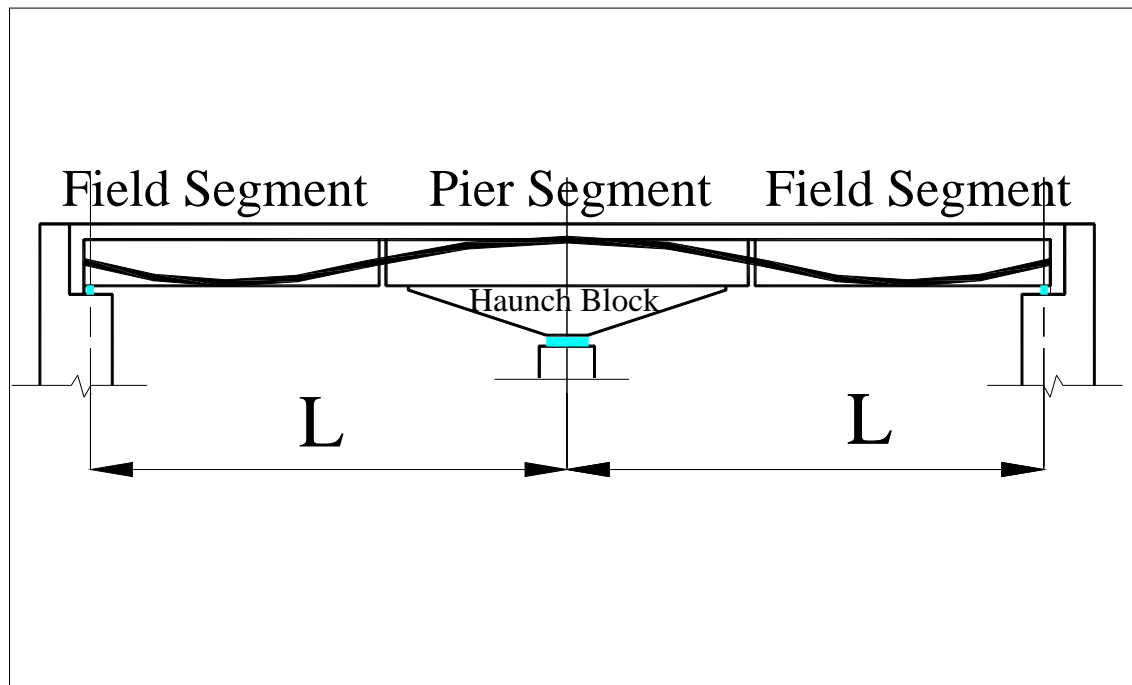


Figure 2.4.4-1 System IV Layout

2.4.4.1 Concrete NU I-Beam Capacities

The ultimate negative moment capacities, the ultimate positive moment capacities, the service III positive moment capacities, and the ultimate shear capacities are almost the same for all girders (with some modification for the web).

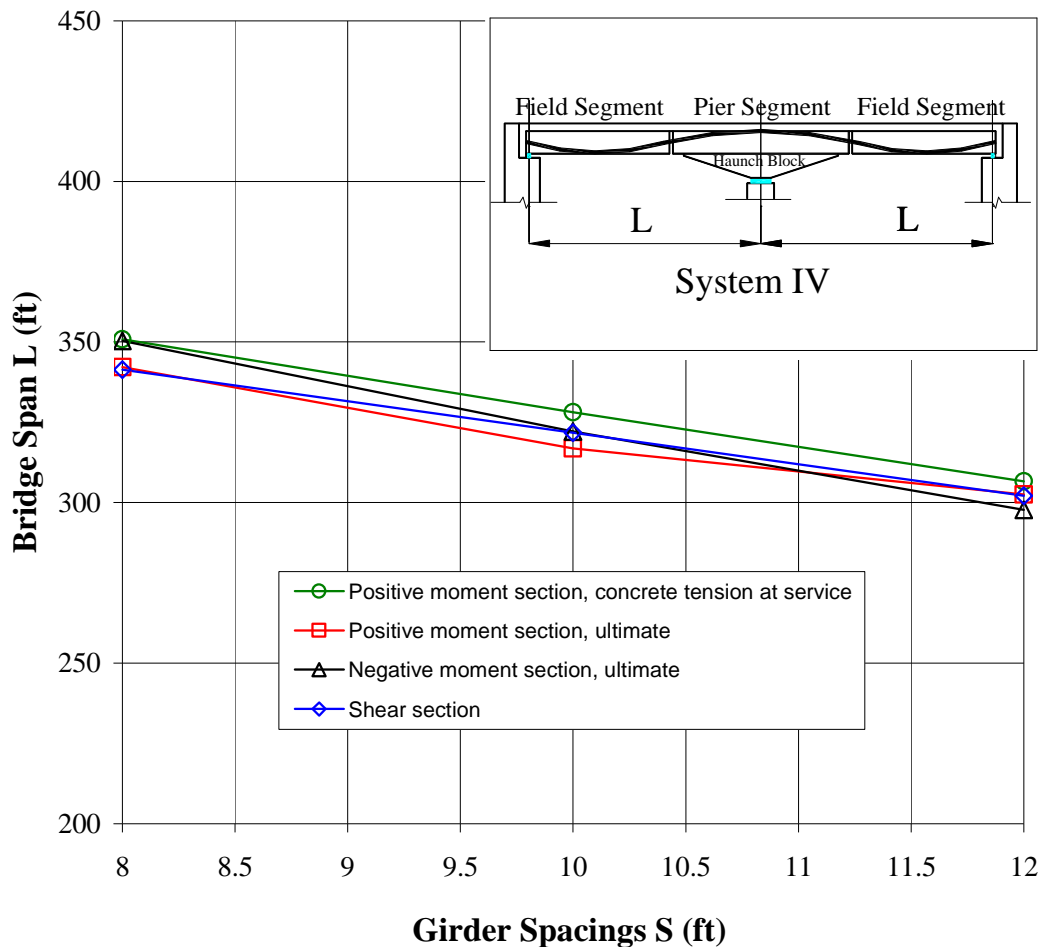


Figure 2.4.4.1-1 System IV NU2000 Span Capacities

2.4.4.2 Optimizing the Haunch Block

The system is most efficient because all the capacities are equal. In order to achieve this goal, a two-piece pier segment is used, with an NU I-girder and a straight

haunch block underneath. Haunch block dimensions of $0.50(L)$ in length and $0.9(h)$ deep were found to be the most efficient haunch block size, equalizing the ultimate negative, the ultimate positive, the service III positive, and the shear capacities with some modifications as shown in Table 2.4.4.2-1.

(Where h is the girder height and L is the span length)

Table 2.4.4.2-1 Two-Span Bridge NU I-Girder Web Width Modifications for System IV

	8 ft Girder Spacing	10 ft Girder Spacing	12 ft Girder Spacing
	Web width (in.)	Web width (in.)	Web width (in.)
NU2000	7.0	7.5	8.0

With minor adjustments for the web width, it is clear that system IV is superior in terms of span capacity, as shown in Figure 2.4.5-1. The maximum segmental span length for shipping is lower than the span capacities for system IV. For this system it is recommended to barge the girder or splice more than one piece together in the field. See Figure 2.4.4.1-1 for System IV NU2000 span chart.

2.4.5 Systems Comparisons

Figure 2.4.5-1 shows a comparison between the four systems using NU2000 and girder spacing of 10 feet. The span capacity of System II is about 16% less than that of system I, because system II has higher negative moment than system I, which controls the design. The span capacity of system III is almost equal to that of system I. However, in system III, the maximum transportable span is higher. System IV is superior in terms of span capacity and provides 60% improvement in span capacity over System I.

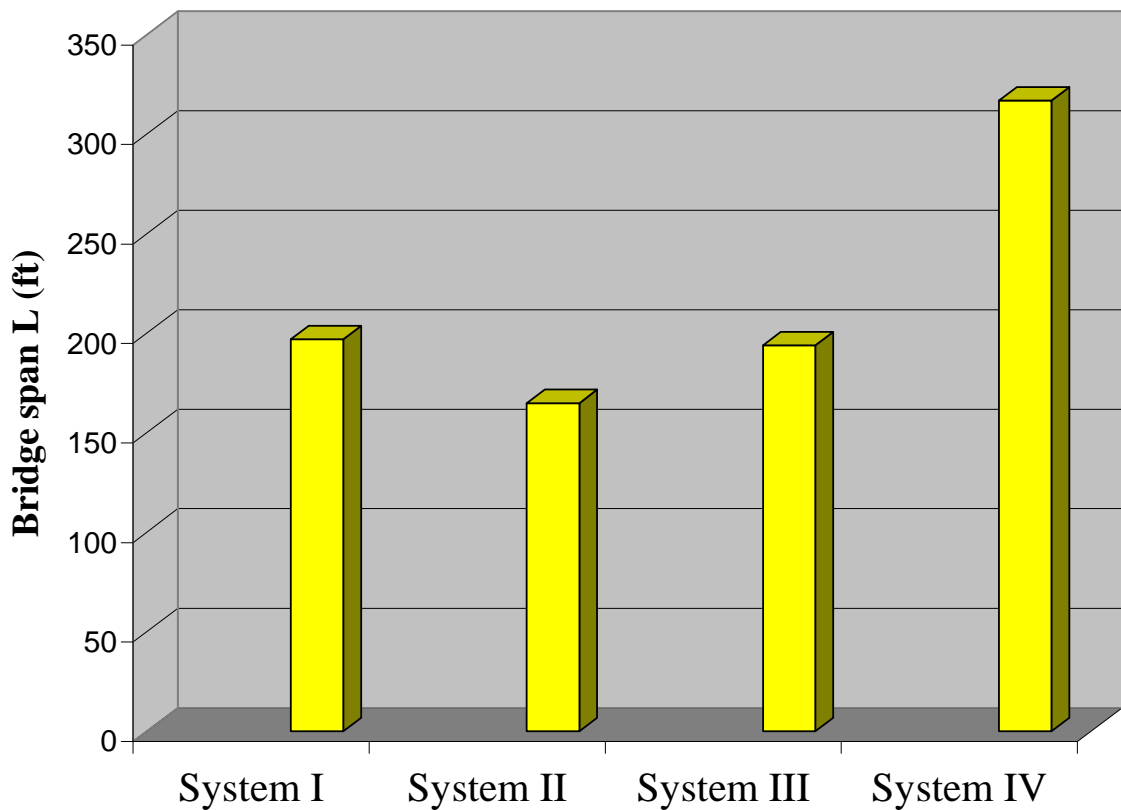


Figure 2.4.5-1 Comparison between the Four Systems' Capacities

2.4.6 Three Span Bridges

For system I method B: The span ratio 0.85L-L-0.85L was found to be the most efficient ratio. This ratio can be calculated easily by multiplying the ratio 0.8 times the percentage of all the loads on the continuous beam which is almost 70%, added to the ratio 1.0, times the percentage of the all loads on the simply supported beam which is almost 30%. The ultimate negative moment controls the design for a girder spacing greater than 8.5 ft. For a girder spacing of 8.5 feet or less, the design is controlled by service III positive moment. Also, the positive service capacity is close to the ultimate service capacity, indicating that this system is efficient. The precast pieces in this system are longer than the maximum transportable length.

For system IV: The span ratio is 0.8L-L-0.8L. The ultimate negative moment capacities, the ultimate positive capacities, the service III positive moment capacities, and the shear capacities are almost equal for all girders, with some modifications for the web, as explained in Table 2.4.6-1.

Table 2.4.6-1 Three-Span Bridge NU I-Girder Web Width Modifications for System IV

	8 ft Girder Spacing	10 ft Girder Spacing	12 ft Girder Spacing
	Web width (in.)	Web width (in.)	Web width (in.)
NU2000	7.0	7.5	8.0

2.5 CONCLUSIONS

When the capacities are far apart, the lower capacity controls the design, leading to under-utilized capacities. The second system has a large gap of up to 130 ft between the span capacities of the positive moment section (service and ultimate) and those of the ultimate negative moment and shear, while the first system has only a 60 ft gap.

The third system has a smaller gap than the second system, reaching 100 ft between the span capacities of the positive moment section (service and ultimate) and those of the ultimate negative moment and shear.

With the suggested haunch block dimensions ($0.5 L$ and $0.9 h$), and using the modifications in table 2.4.4.2-1, the fourth system was found to be the most efficient system. All capacities of the system are equal. The gaps between the capacities that existed in the previous systems were avoided. In conclusion, ranking the four systems according to span capacities, the fourth system received the highest rank, followed by the third, the first, and the second system, in that order.

CHAPTER 3

VERTICALLY SEGMENTED PRECAST CONCRETE SPLICED I-GIRDER

3.1 INTRODUCTION

For continuous span precast prestressed concrete spliced I-girder bridges, the critical location is generally at the pier due to large negative moments or large shear forces. Because of clearance requirements and lower structural forces in the positive moment zone, the optimum overall solution is often a haunched girder system where the standard prismatic girder size is deepened over the pier area to meet the relatively high forces. Also, in the negative moment zone, the bottom flange of the I-beam is much smaller than the deck slab available in the positive moment zone to resist the required compression force component of the applied flexure. Often standard I-beam shapes are produced in depths ranging up to 6 to 8 feet. Because of the need to use the standard sizes as repetitively as possible and to clear overhead obstructions during shipping, one solution is to have a separate precast haunch block and to attach it to the girder bottom flange to form a deeper section for the negative moment zone.

This chapter provides a summary of extensive theoretical and experimental research on the feasibility of splicing a haunch block onto a standard I-girder to form an efficient negative moment zone. The theory and design for the horizontal shear between the haunch block and the pier segment was verified with three types of specimens: small shear specimens, small connector pull-out specimens, and a large beam specimen, representing the pier zone of a continuous span bridge. Reinforcement details of the haunch block, the I-beam and the connection between them were evaluated for

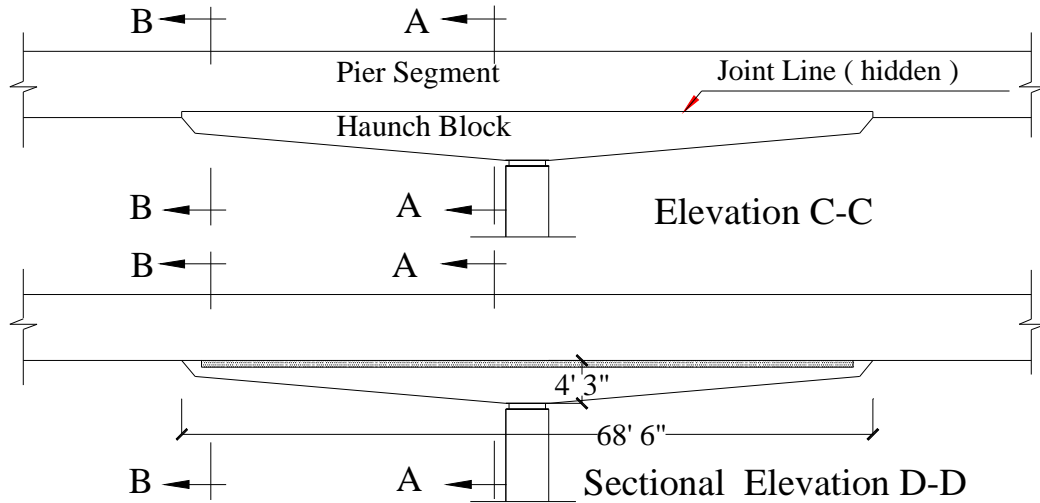
practicality and efficiency. A full-scale specimen, 68.5 ft long by 4 ft wide with a depth varying from 2.25 ft to 4.3 ft, was produced by a precast producer to investigate production and handling issues. The research has confirmed the tremendous potential of this novel system for I-girder spans up to 350 feet, without the need to purchase special forms for non-standard I-beam shapes.

3.2 PROPOSED CONNECTION DETAILS

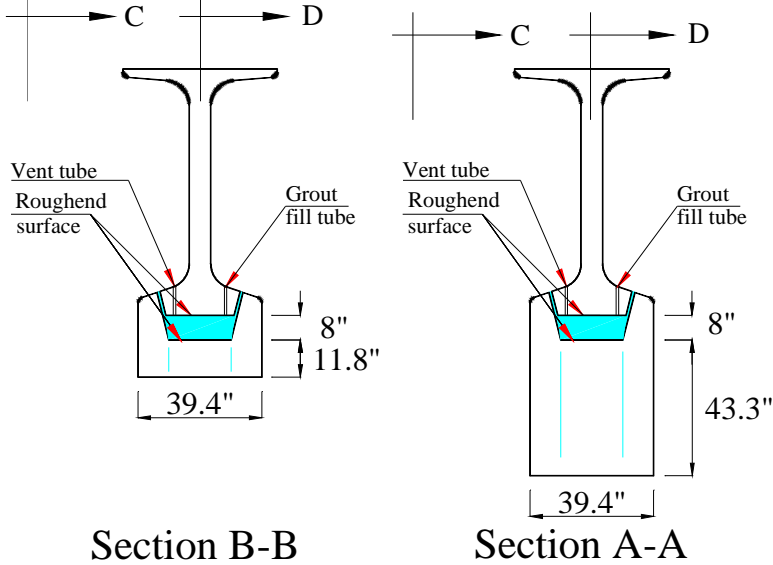
To connect the haunch-block with the pier segment, an 8 in. pocket is created between the two precast elements, which will be filled with a flowable concrete after installing the pier segment. Figure 3.2-1A shows the elevation of the connection. Figure 3.2-1B shows cross sections in the pier segment haunch block connection. Figure 1-C shows the horizontal shear reinforcement details.

The horizontal shear reinforcement was 1-1/4 in. x 36 in. lubricated threaded rods @ 12 in. spacing, each with a welded hex nut that was turned before installing the pier segment such that the extension below the bottom of the I-beam was 8 inches. Each threaded rod was confined in the NU girder by a 24-in. long, 3.5-in. outside diameter spring.

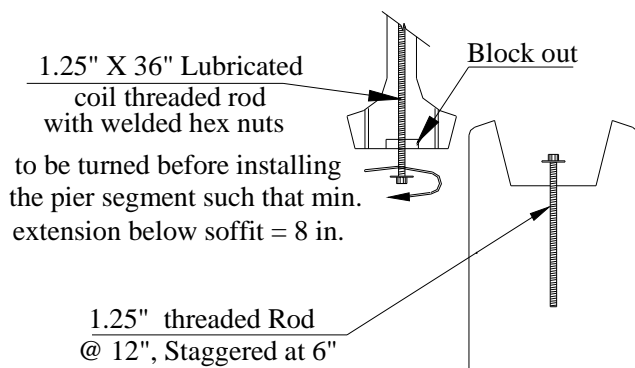
A full-scale specimen was manufactured by two precast producers in Nebraska as shown in Figure 3.2-2. The purpose of manufacturing the specimen is to go through the production process to uncover any potential problems as well as for demonstration purposes. For more details, refer to Appendix F.



A- Elevation of Connected Haunch Block to the Pier Section



B- Concrete Cross-Sections



C- Horizontal Shear Reinforcement Details

Figure 3.2-1 Proposed Connection Details



Figure 3.2-2 Full-Scale Specimen

3.3 DESIGN EXAMPLE

This design example demonstrates the design of a non skew bridge with three spans (240ft-300ft-240 ft) using five NU2000 beams, and two haunch blocks in the girder line, and post-tensioning, as shown in Figure 3.3-2. This example illustrates the design of a typical interior beam at the critical sections in ultimate positive flexure, ultimate negative flexure, LRFD shear, and service III at the positive moment cross section due to prestress, dead and live loading. The superstructure consists of five girder lines spaced at 10'-0" centers, as shown in Figure 3.3-1. The compressive strength of the precast beams is 10 ksi and of the CIP slab is 4 ksi. The beams are designed to act compositely with the 8-in., cast-in-place concrete slab to resist all superimposed dead loads, live loads and impact. An additional ½ in. wearing course is considered an integral part of the 8-in. slab. The design is in accordance with *LRFD Specifications*, 2nd Edition 1998 and Interims 1999 and 2000.

3.3.1 Construction Sequence

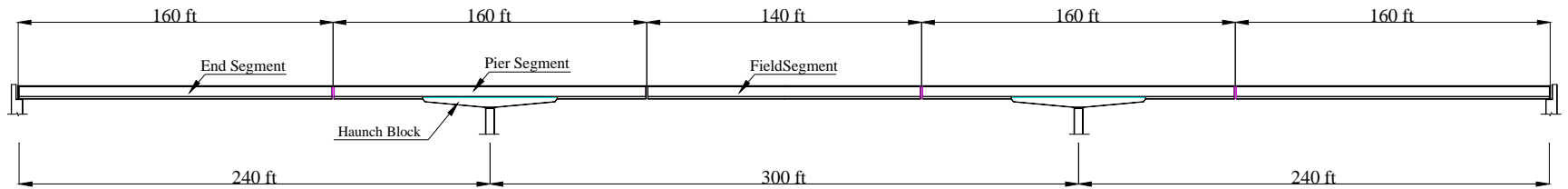
First, each of the haunch blocks is installed over the pier and two temporary supports. The pier segments are then installed over the haunch blocks and the horizontal joint is cast. Then, the field segments are installed and the wet joints between the segments are cast. Post-tensioning is then applied, and the deck slab is cast. Finally, the barriers are installed, the wearing surface cast, and the bridge opened to traffic.

3.3.2 Prestress Force

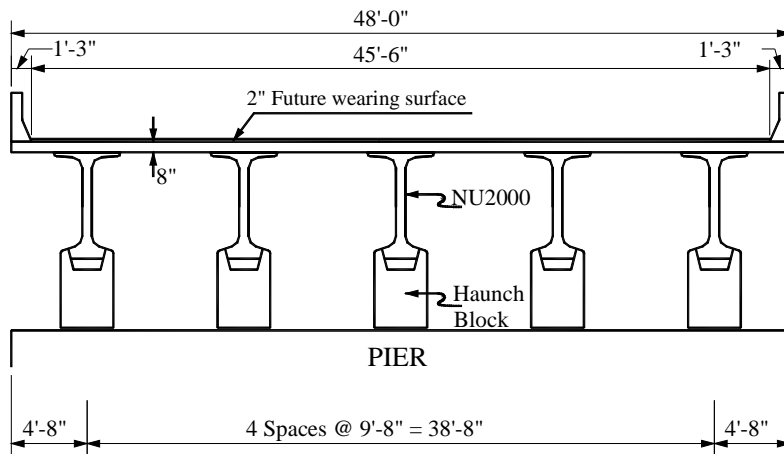
Post-tensioning is applied at only one stage after casting the wet joint between segments. Three 3.75 in., diameter ducts are used in the calculations. Each duct contains 15-0.6 inch strands. The post-tensioning profile is shown in Figure 3.3-2. The pre-tensioning is 46-0.6 inch strands only in the field segments.

3.3.3 Shear Forces and Bending Moments

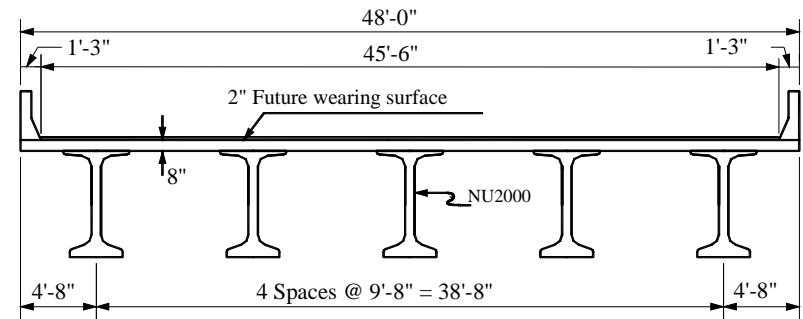
The shear forces and the bending moments due to prestress, dead and live loading are shown in Table 3.3.3-1. The live load distribution factors are calculated based on the LRFD equations without the span upper limit of 240 ft. These distribution factors are calculated based on 10 ft girder spacing and an average span length of 270 ft. The post-tensioning is calculated by dividing the structure into short elements. The post-tensioning effect at each node of an element is then converted to its equivalent nodal force.



Bridge Elevation



Bridge Cross Section at Pier



Bridge Cross Section at Mid-Span

Figure 3.3-1 Design Example Elevation and Cross-Sections

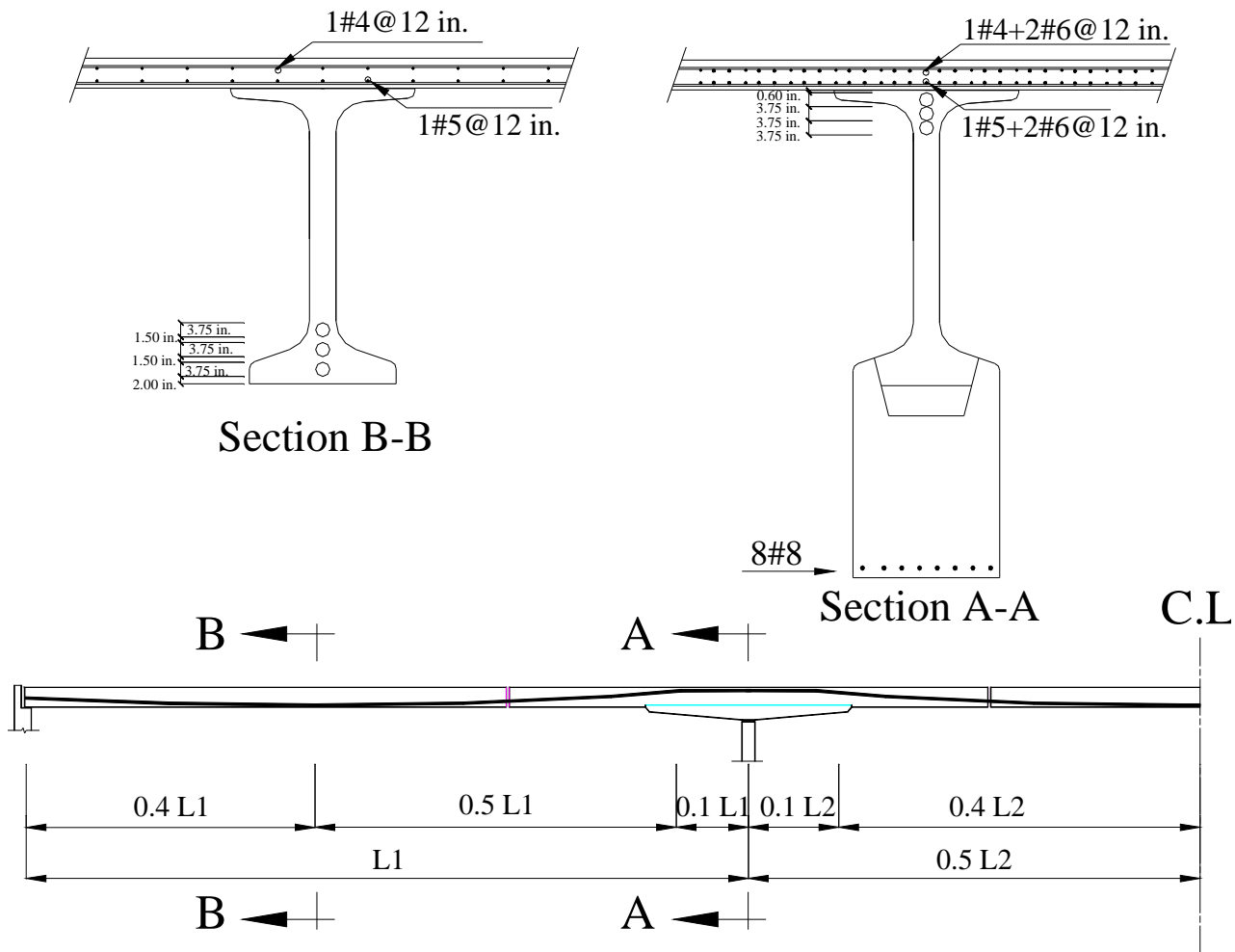


Figure 3.3-2 Design Example Post-Tensioning Profile

Table 3.3.3-1 Unfactored Shear Force and Bending Moments for a Typical Interior Girder

	Positive Bending Moment at 0.4 L (k.ft)	Negative Bending Moment at Haunch Block End (k.ft)	Negative Bending Moment at Pier C.L. (k.ft)	Shear Force at 13 ft from the Pier C.L.* (kips)
Girder Weight	3,552.1	-4,290.5	-9504.1	164.9
Deck Slab	3,248.2	-3,949.5	-8079.66	128.4
Wearing Surface	866.2	-1,053.2	-2154.58	34.3
Barrier	415.8	-505.536	-1034.2	16.4
Live Load	5,401.3	-4,842.79	-7329.72	181.6
Post-Tensioning Total Moment	-3,528.4	6,093.3	11,743.8	-----
Post-Tensioning Secondary Effect	318.6	687.0	797.3	0.0

* The shear force critical section is located at 13 ft from the pier center line at the second span

3.3.4 Capacities of the Critical Sections

The stress at the NU I-beam bottom flange at 0.4 L₁ from the first span is -0.08 ksi tension due to service III. The LRFD allowable tensile stress is 0.6 ksi. The strength limit state design is summarized in Table 3.3.4-1. The horizontal shear is 82 klf at the pier centerline.

Table 3.3.4-1 Critical Sections Shear Force and Bending Moments Capacities

	Positive Bending Moment at 0.4 L (k.ft)	Negative Bending Moment at Haunch Block End (k.ft)	Negative Bending Moment at Pier C.L. (k.ft)	Shear Force at 13 ft from the Pier C.L. (kips)
LRFD Due to Factored Load	19,771.6	-20,986.6	-39,331.3	756.4
Section Capacity (Ø M_n & Ø V_n)	23,700.2	-21,368.0 ^(3,4,5)	-39,952.5 ^(3,4,5)	1428.4*

* The maximum shear capacity is calculated based on the equation $\phi V_n = 0.9 f_c' b_v d_v$

3.4 EXPERIMENTAL INVESTIGATIONS

Three types of tests were done to verify the composite action between the two precast pieces, the haunch block and the I-girder, and to estimate the capacity of the proposed horizontal shear reinforcement details between these two precast pieces. The first type was push-off tests, which were done on two groups of reinforcement. The other two types were the pull out tests and the full scale test.

3.4.1 Push-Off Tests

Seven push-off specimens in two groups with different heights and different numbers of rods were used, as described in Table 3.4.1-1. The first group tested a 1-1/2 in. (38.1 mm) diameter mild steel coil bolt and included two specimens. The second group tested a 1-1/4 in. (31.75 mm) diameter hard steel coil treaded rod and included five specimens.

Each specimen had two precast pieces. An 8 in. (200mm) pocket was created between these two precast pieces, containing part of the horizontal shear reinforcement. The pocket was cast with flowable concrete afterward. The geometry of that pocket had the same dimensions as those proposed in the real system. The first specimen in the first group had double the pocket size [16 in. (400 mm)], and its horizontal shear reinforcement was not staggered as shown in Table 3.4.1-1. Only specimen 6 is explained in detail.

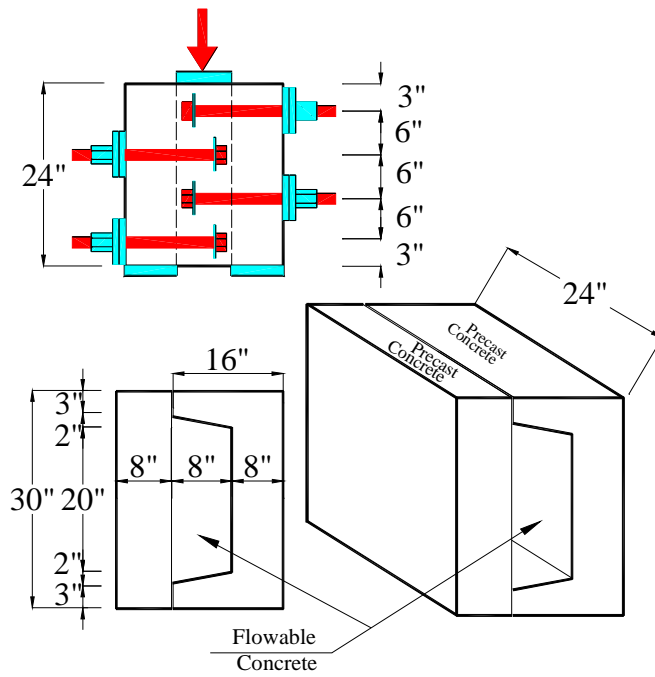
3.4.1.1 The Sixth Push-Off Specimen

3.4.1.1.1 Specimen Configurations

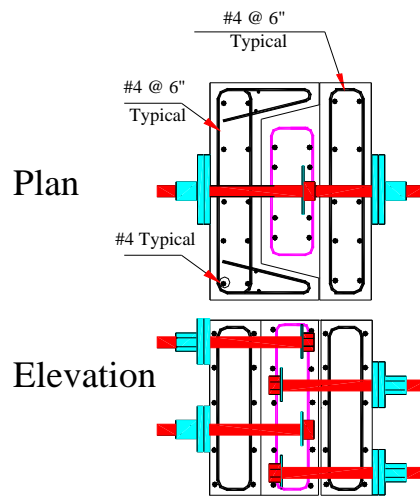
As shown in Figure 3.4.1.1.1-1, the specimen had four threaded rods, two on each of the precast concrete faces. The rods were staggered at the pocket. The thickness of the pocket was 8 in. (200 mm), as in the real system. For reinforcement details, also refer to Figure 3.4.1.1.1-1B. The roughened surface used in this specimen was a plastic roofing sheet which was also proposed for the real system.

3.4.1.1.2 Test Setup and Instrumentations

The push-off specimen was attached to nine steel beams, four 1- $\frac{3}{4}$ in. threaded rods, and two 440 kips hydraulic jacks, as shown in Figure 3.4.1.1.2-1. During the push-off test, each jack pushed one beam, and both of these beams were pushing another crossing beam, which pushed the specimen pocket as one concentrated load. The load was applied and increased incrementally. The pressure gauges and the strain gauges were continuously monitored using a digital data acquisition system through a computer.



A) Concrete Dimensions



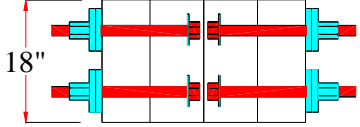
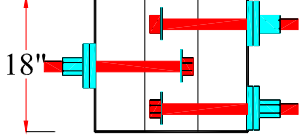
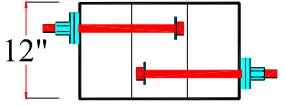
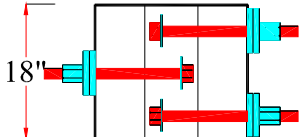
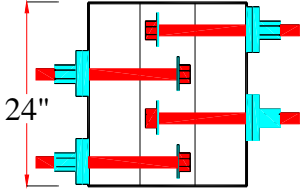
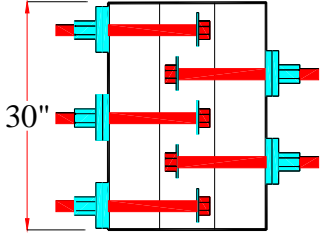
B) Reinforcement Details

Figure 3.4.1.1.1-1 The Sixth Push-Off Specimen Details



Figure 3.4.1.1.2-1 Push-Off Specimens Test-Setup

Table 3.4.1-1 Push-Off Specimens

Push-off test		Number of Rods	Height in. (mm)	Elevation
Group 1 (using mild steel)	Specimen 1	4 bolts, 2 bolts per face	18 (460)	
	Specimen 2	3 bolts	18 (460)	
Group 2	Specimen 3	2	12 (305)	
	Specimen 4	3	18 (460)	
	Specimen 5	4	24 (610)	
	Specimen 6			
Specimen 7	5	30 (762)		

3.4.1.1.3 Observations

At 350 kips, the cracking load, a hair crack developed as a straight line between the haunch block and the pocket concrete. This crack did not get wider until failure. The specimen failed at the load of 633 kips. At failure, the whole pocket settled down by 1.25

inches. The two precast concrete parts opened up from the bottom. There was a small chunk of concrete that failed at the nut location, as shown in Figure 3.4.1.1.3-1. Many diagonal cracks could be observed inside the pocket between the two precast pieces.

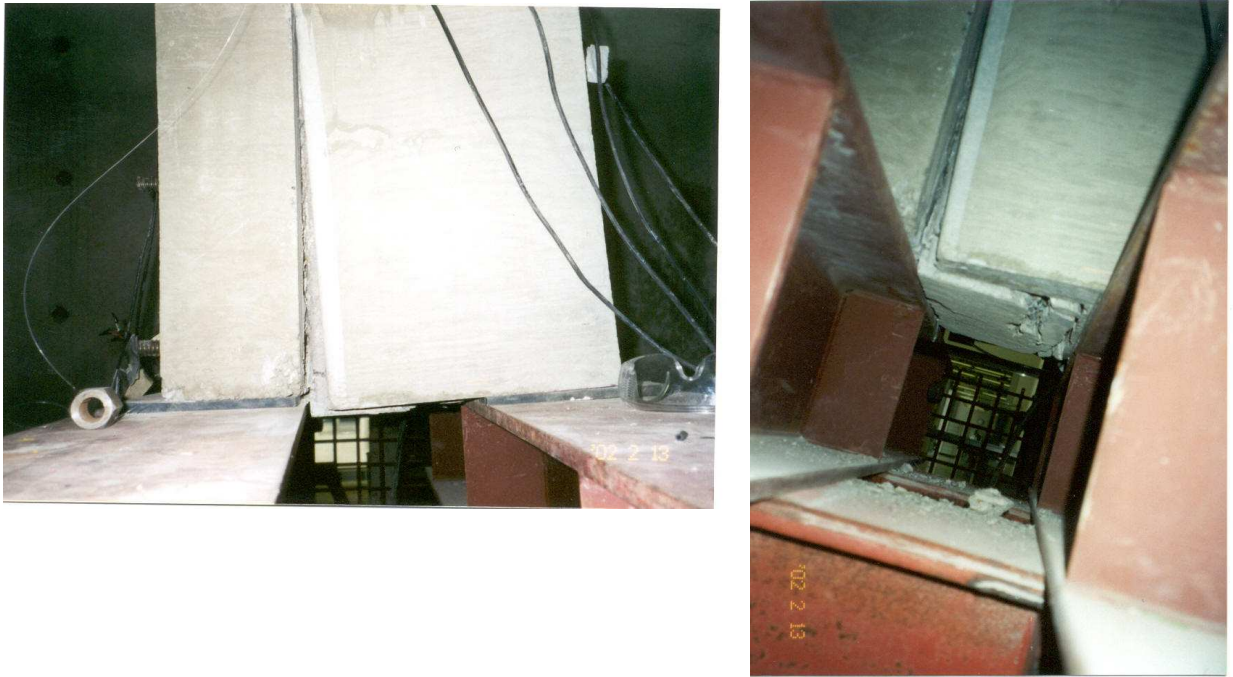
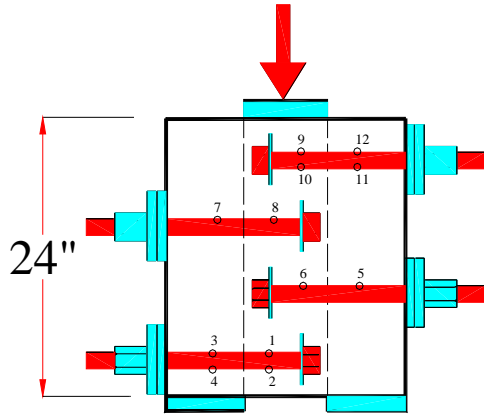


Figure 3.4.1.1.3-1 The Sixth Specimen Mode of Failure

3.4.1.1.4 Coil Rods Strain Gauge Readings

Twelve strain gauges were glued to the four rods. Their locations are shown in Figure 3.4.1.1.4-1. Three strain gauges readings are also shown in the Figure.



- | | | | |
|---------|---------|---------|----------|
| 1. GT1T | 4. GD1B | 7. GD3T | 10. GT4B |
| 2. GT1B | 5. HB2T | 8. GT3T | 11. HB4B |
| 3. GD1T | 6. GT2T | 9. GT4T | 12. HB4T |

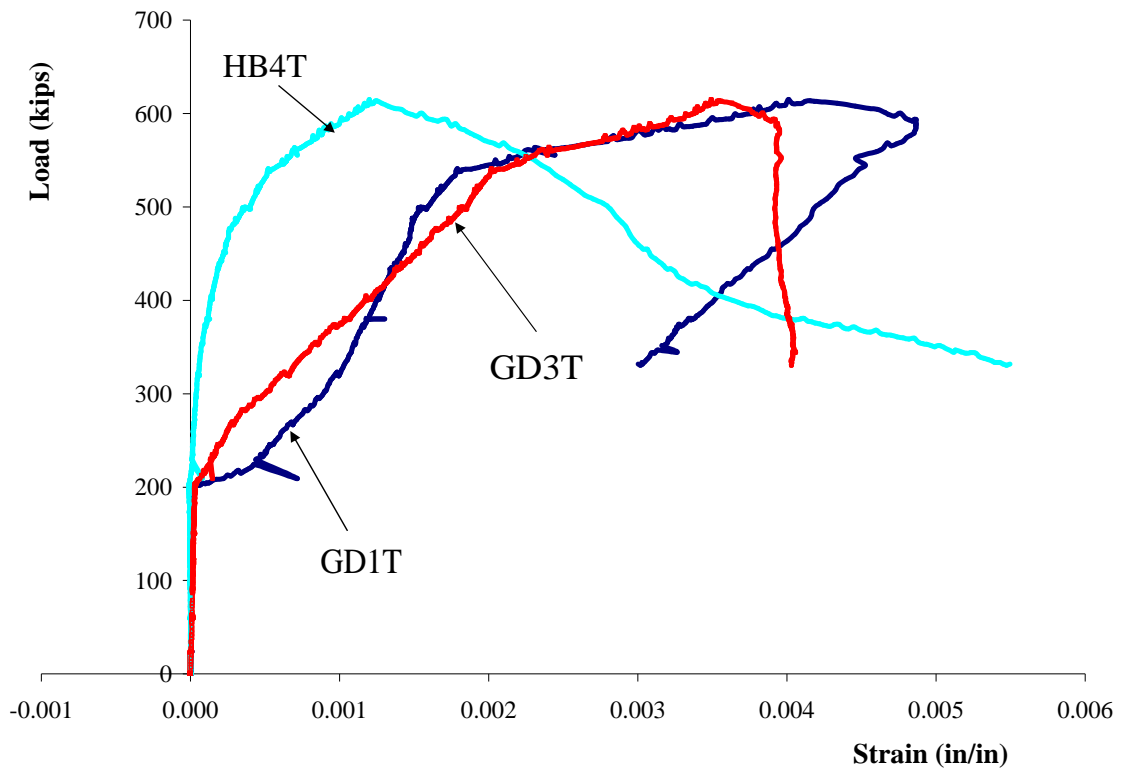


Figure 3.4.1.1.4-1 HB4T, GD3T and GD1T Strain Gauge Readings

3.4.1.2 Push-Off Tests Results and Discussion

It is recommended to use Loov and Patnaik's 1994 equation, since it gives closer failure loads than LRFD equation to the obtained test results as shown in Tables 1 and 2. The yield strength for high strength coil threaded rods should be taken as 0.65 from the ultimate failure capacity.

Table 3.4.1.2-1 Summary of Group 1 Specimen's Capacities (fy = 42.845 ksi, fy = 295.4 MPa)

Specimen ID		Specimen 1	Specimen 2
Failure Load P (kips)		700	558
Cracking Load		550	350
$\rho_s f_y \times 10^3$ (psi)		0.421	0.210
LRFD Equation	$V_n = [0.1A_c + \rho_s A_s f_y] / A_c$	520.6	310.3
	Calculated Failure Load (P kips)	374.85	223.42
Loov's and Patnaik's , (1994) ⁽⁸⁾	$V_n = k\lambda\sqrt{(15 + \rho_v f_y) f_c'}$ & k=0.5	1017.17	731.52
	Calculated Failure Load (P kips)	732.36	526.7

Table 3.4.1.2-2 Summary of Group 2 Specimen's Capacities (fy = 90 ksi =0.65 fpu, fy =620.6 MPa)

Specimen ID		Specimen 3	Specimen 4	Specimen 5	Specimen 6	Specimen 7
Failure Load P (kips)		336.0	422.0	604.0	633.0	806.0
Cracking Load		80.0	170.0	420.0	350	320.0
$\rho_s f_y \times 10^3$ (psi)		0.346	0.229	0.346	0.346	0.275
LRFD Equation	$V_n = [0.1A_c + \rho_s A_s f_y] / A_c$ (psi)	443.5	329.0	443.5	443.5	374.8
	Calculated Failure Load (P kips)	212.9	236.9	425.8	425.8	449.8
Loov's and Patnaik's , (1994) ⁽⁸⁾	$V_n = k\lambda\sqrt{(15 + \rho_v f_y) f_c'}$ (psi) & k=0.5	598.8	494.0	598.8	598.8	538.4
	Calculated Failure Load (P kips)	287.4	355.7	574.8	574.8	646.0

3.4.2 The Pull-Out Test

The NU I-beam bottom flange with the two cuts for the connection was simulated by the pull-out specimen, as shown in Figure 3.4.2-1A section A-A. A 7 in. (175 mm) concrete stem also simulated the web of the post-tensioned NU I-beam as shown in Figure 3.4.2-1. The objective of this test was to estimate the maximum pull-out force using the new system-- the lubricated coil rod.

3.4.2.1 Pull-Out Specimens Test Setup

As shown in Figure 3.4.2.1-1, the test set-up consisted of a coil rod going into the insert and holding a hole jack, 110 kips (489.3 KN), and a load cell.

3.4.2.2 Observations

The three rods were tested. Nothing happened to the specimen until the capacity of the jack was reached. No cracks were observed.

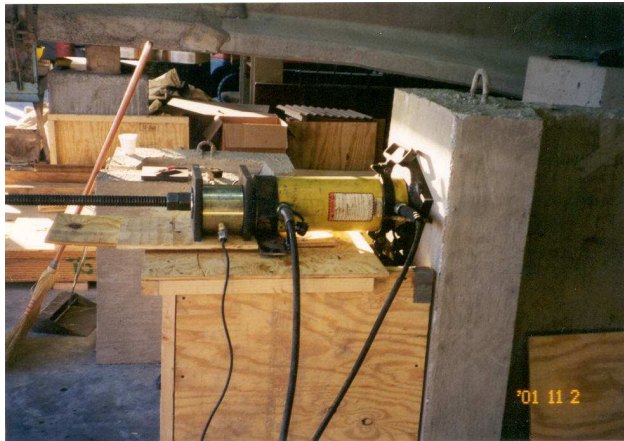
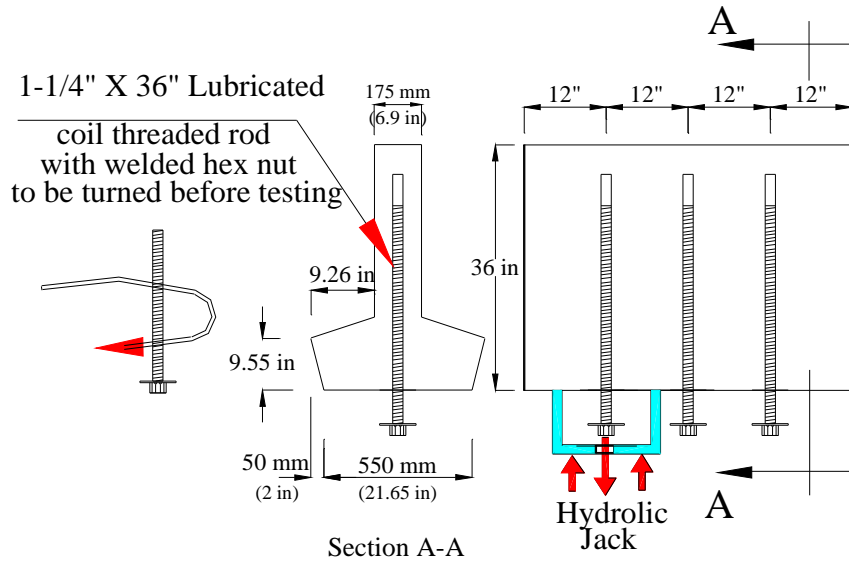


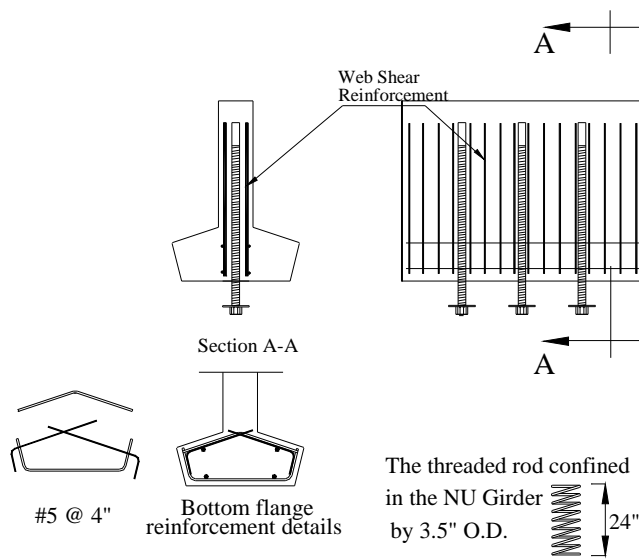
Figure 3.4.2.1-1 Pull-Out Specimens Test Setup

3.4.2.3 Pull-Off Test Discussion

The test results of the pull-out using 1-1/4" lubricated coil rods were satisfactory and larger than 82 k/ft, which is required in the design example.



A- Concrete Dimensions



B- Reinforcement Details

Figure 3.4.2-1 Pull-Out Specimen Details

3.4.3 Full-Scale Test

3.4.3.1 Specimen Modeling

The specimen consisted of two precast pieces connected together by a horizontal concrete joint. The two precast pieces were an I-beam and a haunch block, similar to the real system except that the I-beam was an Iowa type A instead of an NU I-girder. The haunch block was located at the top of the I-beam. The specimen was simply supported from both ends and was loaded at its midpoint, as shown in the longitudinal section in Figure 3.4.3.1-1. The midpoint simulated the pier reaction and the two end-supports simulated the two field segments reactions.

3.4.3.2 Loading and Measurements

Loads were applied at one point load at the mid-span of the specimen. Two oil jacks with capacity of 440 kips each were used. The specimen was loaded to failure due to horizontal shear. During the test, displacements at the mid-span were measured. A total of 20 strain gauges were installed on the reinforcement steel and 4 strain gauges were installed on the concrete to measure the concrete strain at the compression block. From the 20 strain gauges, five strain gauges were installed to measure the bottom flange longitudinal reinforcement strain. Six strain gauges were installed to measure the vertical shear reinforcement strain.

Nine strain gauges were installed to measure the horizontal shear reinforcement strain. Two LVDTs were set up at the specimen ends to measure the slippage between the precast I- girder and the concrete joint. Please see Figure 3.4.3.2-1.

3.4.3.3 Test Results

3.4.3.3.1 Load-Deflection

The load-deflection curve at the mid-span is shown in Figure 3.4.3.3.1-1. The curve shows that the deflection went to a value of 1.15 in. at the maximum load. At failure, the deflection continued to increase with no increase in the load. The estimated deflection was 0.7 inches. The south LVDT did not record a significant movement until failure, and then a displacement of up to 0.3 in. was recorded. The failure happened between the haunch block and the concrete joint. However, some displacement was recorded by the LVDT between the I-girder and the concrete joint. Please refer to Figure 3.4.3.3.1-2. The north LVDT did not record a significant movement, where no failure was observed.

3.4.3.3.2 Concrete Strain at Mid-Span

Four strain gauges were glued at 6 in. south and north of the mid-span, at 1 in. and 2 in. from the top surface of the specimen. The readings of these four strain gauges were very consistent and the average of these readings was almost 0.0015 in. /in., which indicates that there was no flexure concrete compression failure. Please refer to Figure 3.4.3.3.2-1.

3.4.3.3.3 Flexural Reinforcement Strains

Five strain gauges were glued to the longitudinal reinforcement. Two strain gauges were glued to the first layer from the bottom, two strain gauges were glued to the second layer, and one strain gauge was glued to the third layer. The readings of these five

strain gauges were consistent. The three layers were almost at yield at the failure load. Please refer to Figure 3.4.3.3.3-1.

3.4.3.3.4 Vertical Shear Reinforcement Strains

Six strain gauges were glued to the vertical shear reinforcement. Three strain gauges at the south end of the specimen were glued to the bottom I-beam vertical stirrups at 15 in., 30 in. and 45 in. from the edge of the bottom plate at the support. Three strain gauges were glued to the north end of the specimen in the same sequence of the previous strain gauges.

The readings of the south strain gauges are shown in Figure 3.4.3.3.4-1A. The readings of the north strain gauges are shown in Figure 3.4.3.3.4-1B. The reinforcement was far from yielding as it was expected. The north and the south strain gauge readings were consistent, which means that the load was centric and the test setup was perfectly aligned.

3.4.3.3.5 Horizontal Shear Reinforcement Strains

Nine strain gauges were glued to the horizontal shear reinforcement. Two of these strain gauges did not work. Two of the threaded rods (HS3ST and HS5NB) yielded. The first rod mentioned was located right at the beginning of the observed horizontal shear failure. Three strain gauge readings were very close to yielding. Those rods are: HS1ST, HS5SB and HS4NB. The north strain gauge readings were very close to the strain gauges located at the same distance but south of the specimen. One can see this consistency in the two pairs of strain gauges, HS5NB&HS5SB and HS2SB&HS2NB. Please refer to Figure 3.4.3.3.5-1.

3.4.3.3.6 Crack Pattern

Figure 3.4.3.3.6-1 shows the crack patterns developed in the specimen while testing.

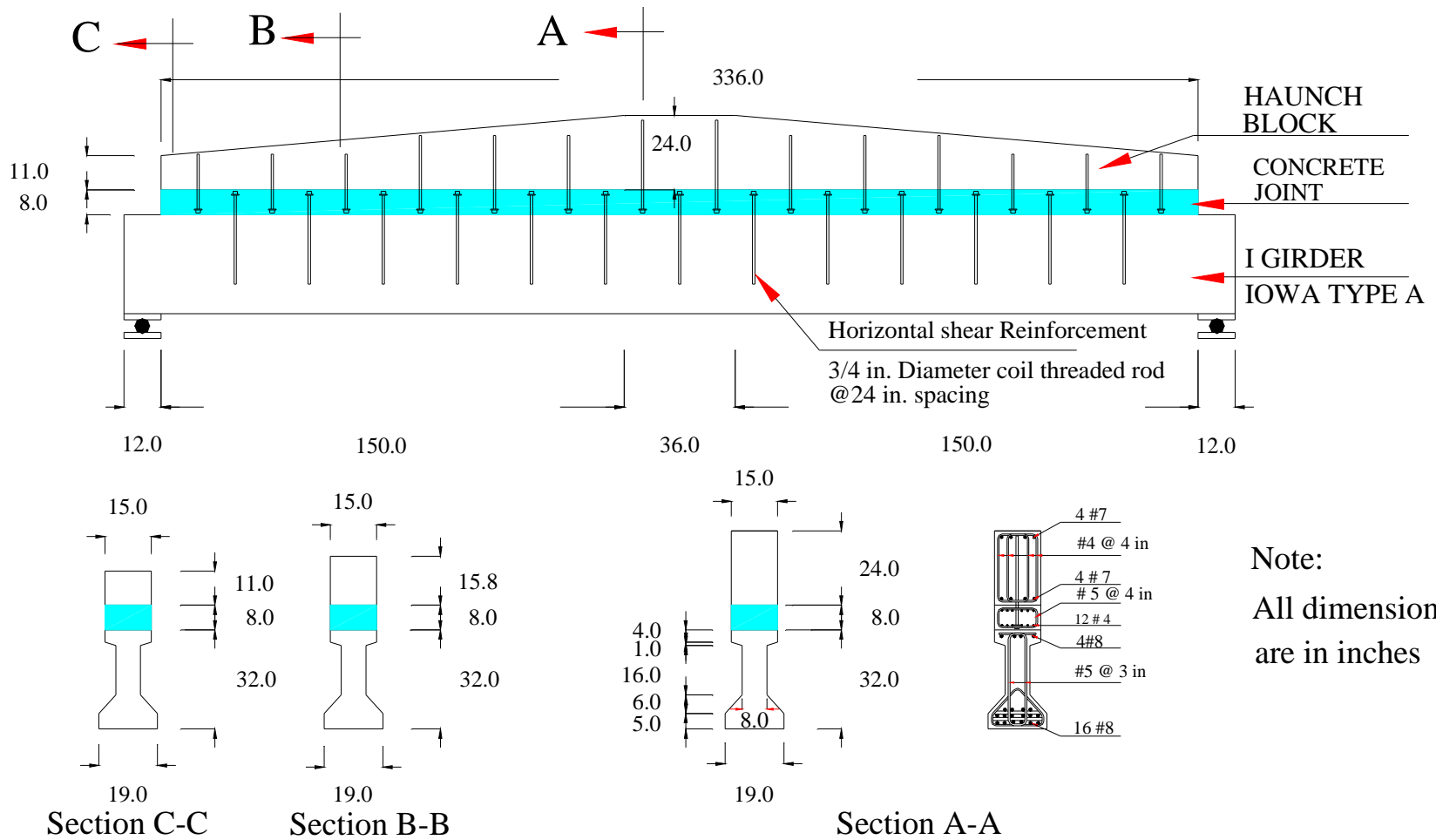


Figure 3.4.3.1-1 Full Scale-Test Concrete Dimensions and Reinforcement Details

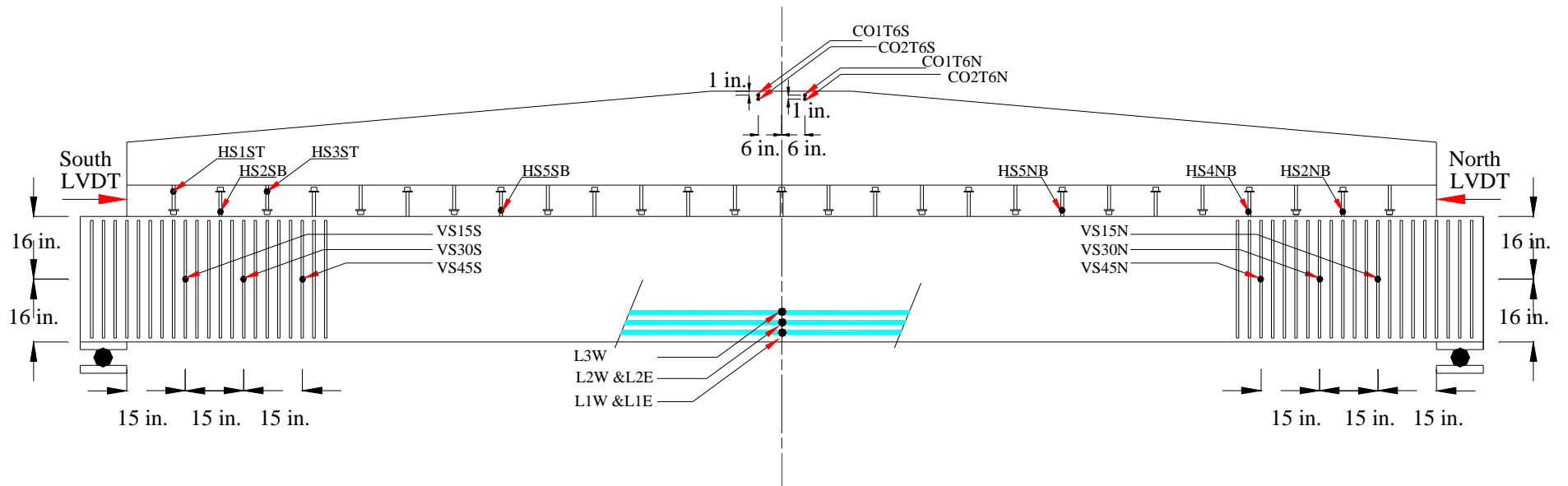


Figure 3.4.3.2-1 Full Scale Test Strain Gauge Locations

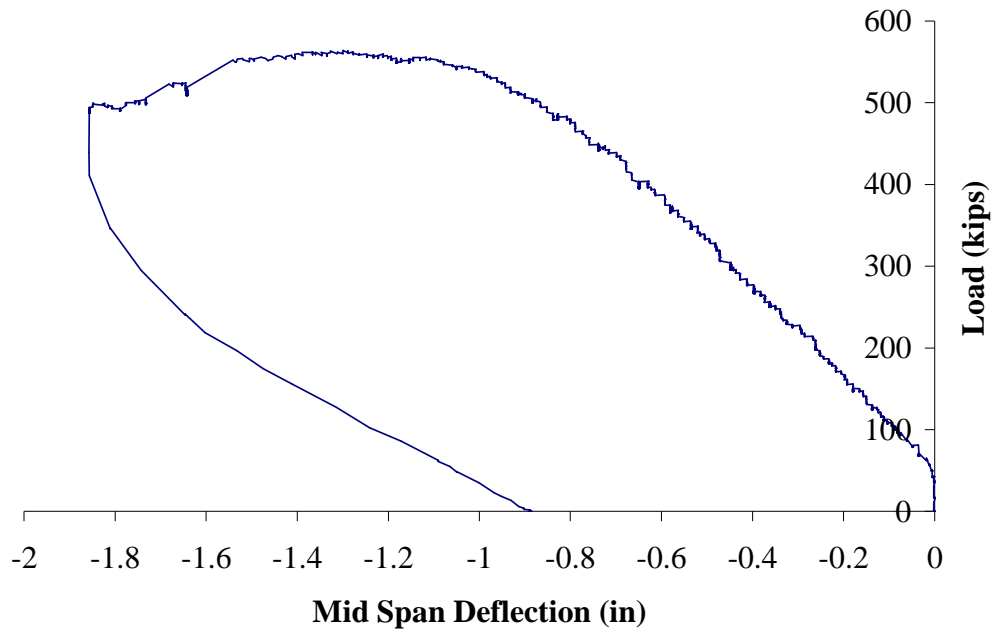


Figure 3.4.3.3.1-1 Full-Scale Test Mid-Span Deflection

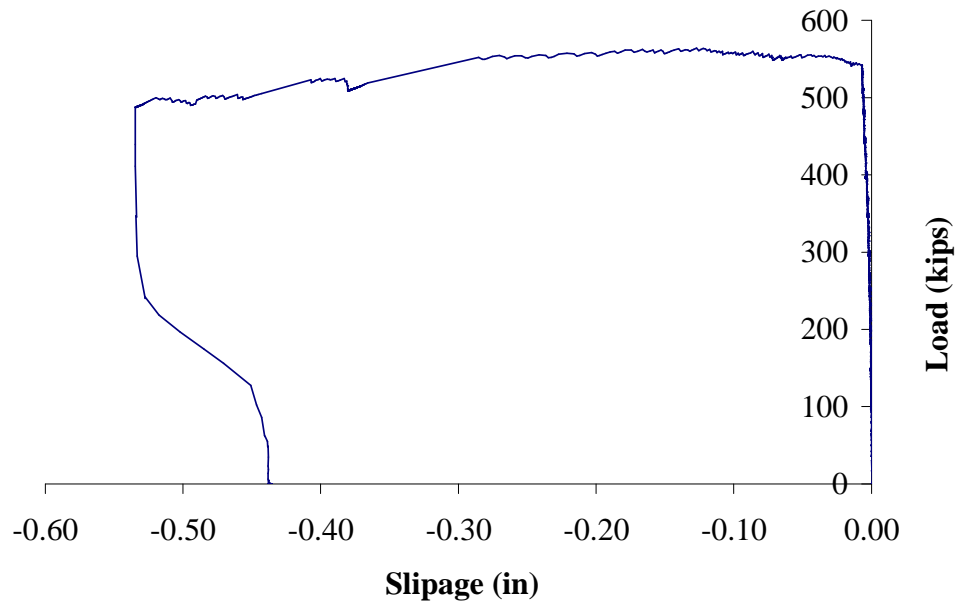


Figure 3.4.3.3.1-2 Full-Scale South LVDT Readings

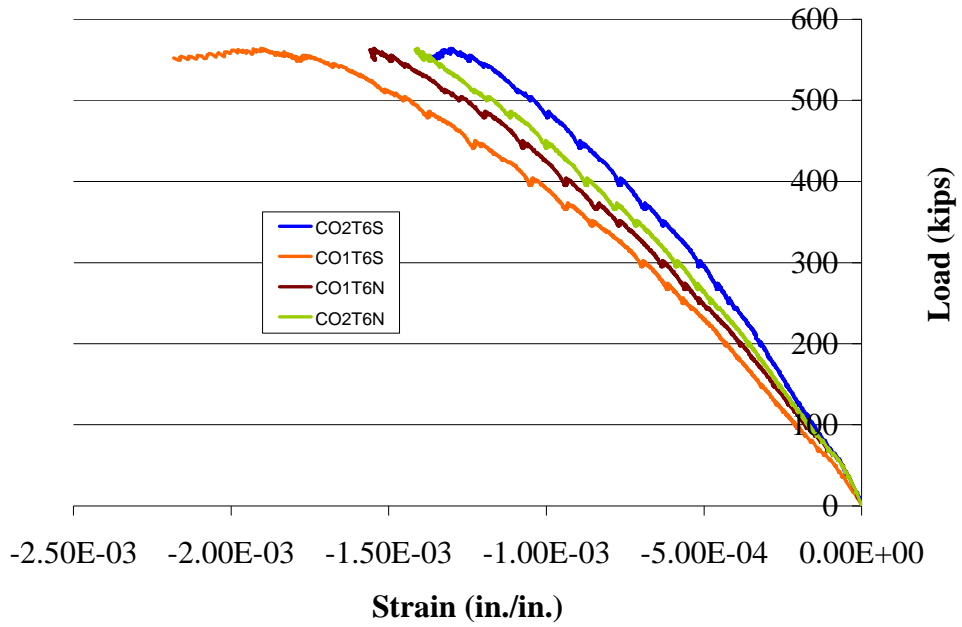


Figure 3.4.3.3.2-1 Full-Scale Test Concrete Strain Gauge Readings

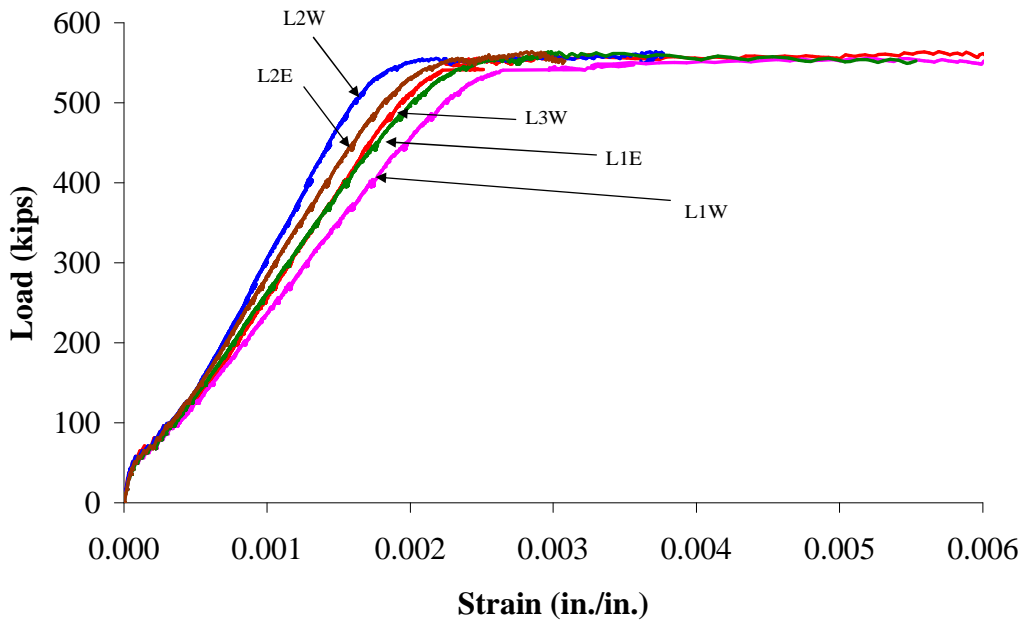
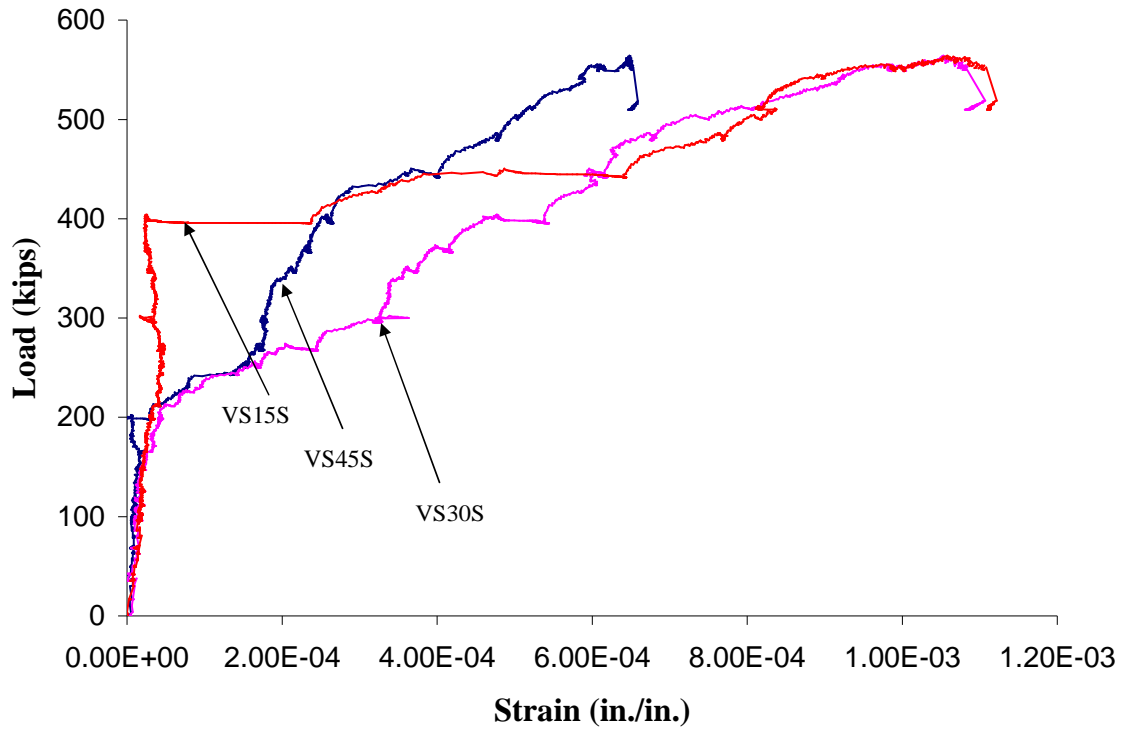
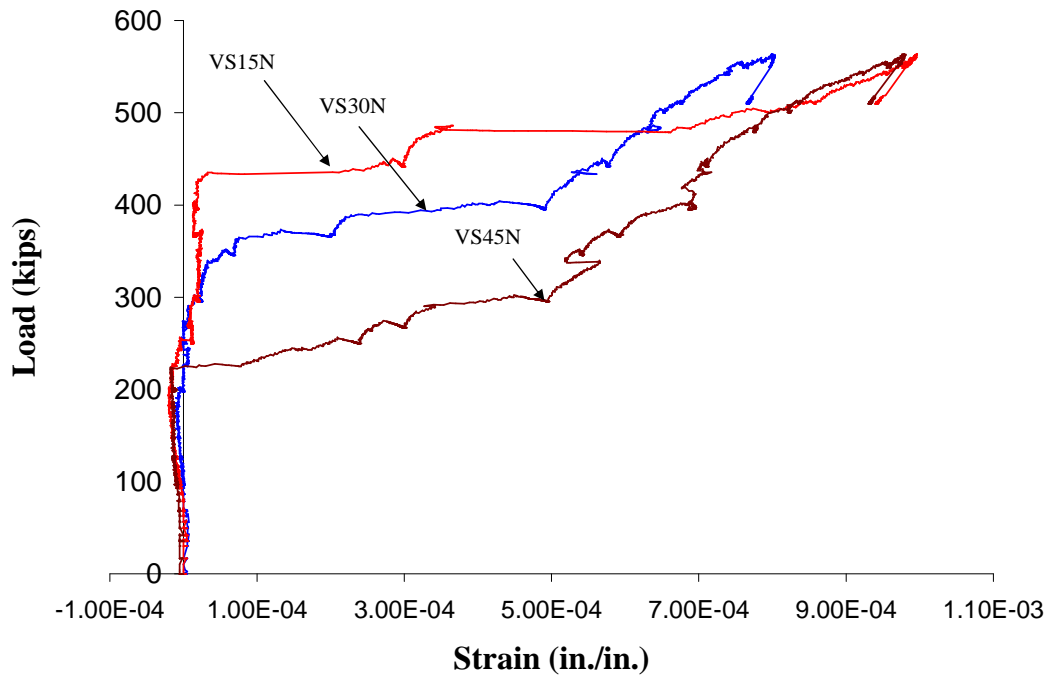


Figure 3.4.3.3.3-1 Full-Scale Test Longitudinal Reinforcement Strain Gauge Readings



A- South Strain Gauge Readings



B- North Strain Gauge Readings

Figure 3.4.3.3.4-1 Vertical Shear Strain Gauge Readings

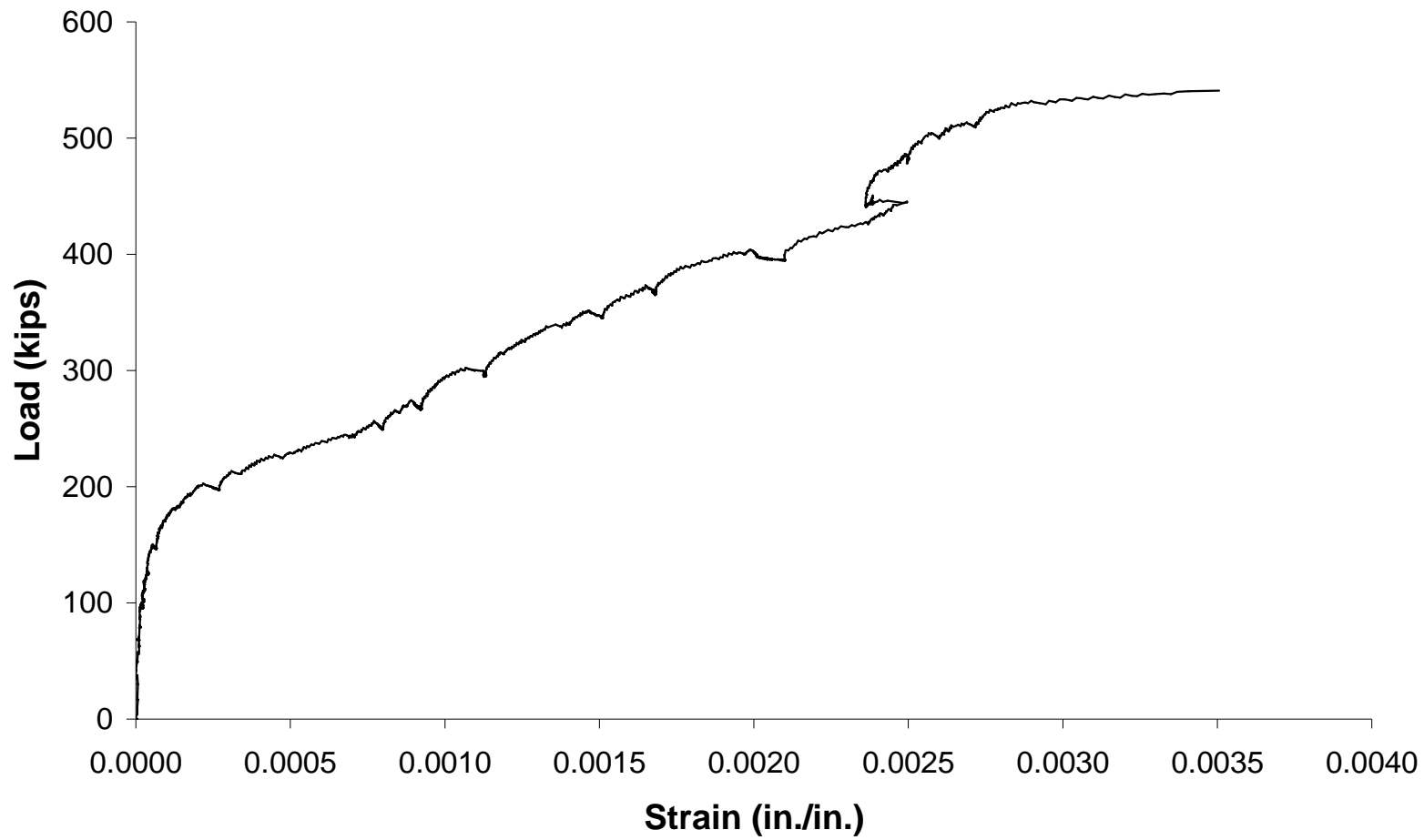


Figure 3.4.3.3.5-1 HS3ST Strain Gauge Readings

3.4.3.3.7 Summary and Discussion of the Beam Ultimate Capacities

It is recommended to use Loov and Patnaik's 1994 equation, since it gives closer failure loads than the LRFD equation to the obtained test results, as shown in Table 7 and Figure 3.4.3.3.7-1.

Table 3.4.3.3.7-1 Summary of the Maximum, Load Capacity (P kips) for Different Ultimate Capacities.

	Point Load Capacity (kips)
Ultimate Flexure Capacity (calculated)	636.40 ⁽¹⁾
Ultimate vertical shear capacity using two branches # 5 @ 3 in. (calculated)	784.85 ⁽²⁾
Ultimate Horizontal Shear Capacity Using the Following two Equations $V_n = k\lambda\sqrt{(15 + \rho_v f_y) f_c'} A_c$ $V_{uh} = \frac{V_u}{d_v} \quad \text{(calculated)}$	545.34 ⁽³⁾
Ultimate Horizontal Shear Capacity Using the Following two Equations $V_n = k\lambda\sqrt{(15 + \rho_v f_y) f_c'} A_c$ $v = \frac{(V)(Q_{cr})}{(I_{cr})(b)} \quad \text{(calculated)}$	519.59 ⁽³⁾
Ultimate Horizontal Shear Capacity Using the Following two Equations $V_n = c A_{cv} + \mu (A_{vf} + P_c)$ $V_{uh} = \frac{V_u}{d_v} \quad \text{(calculated)}$	251.40 ⁽³⁾
Ultimate Horizontal Shear Capacity Using the Following two Equations $V_n = c A_{cv} + \mu (A_{vf} + P_c)$ $v = \frac{(V)(Q_{cr})}{(I_{cr})(b)} \quad \text{(calculated)}$	239.50 ⁽³⁾
Ultimate Horizontal Shear Capacity From the Full Scale Test (observed)	564.00 ⁽⁴⁾

⁽¹⁾ The critical section for flexural capacity is at mid span

⁽²⁾ The vertical shear capacity due to only the I-beam capacity

⁽³⁾ The critical section for horizontal shear is at 61.8 in. from the support or 55.8 in. from the end of the base plate

⁽⁴⁾ The horizontal shear failure happened at almost 5 ft from the support.

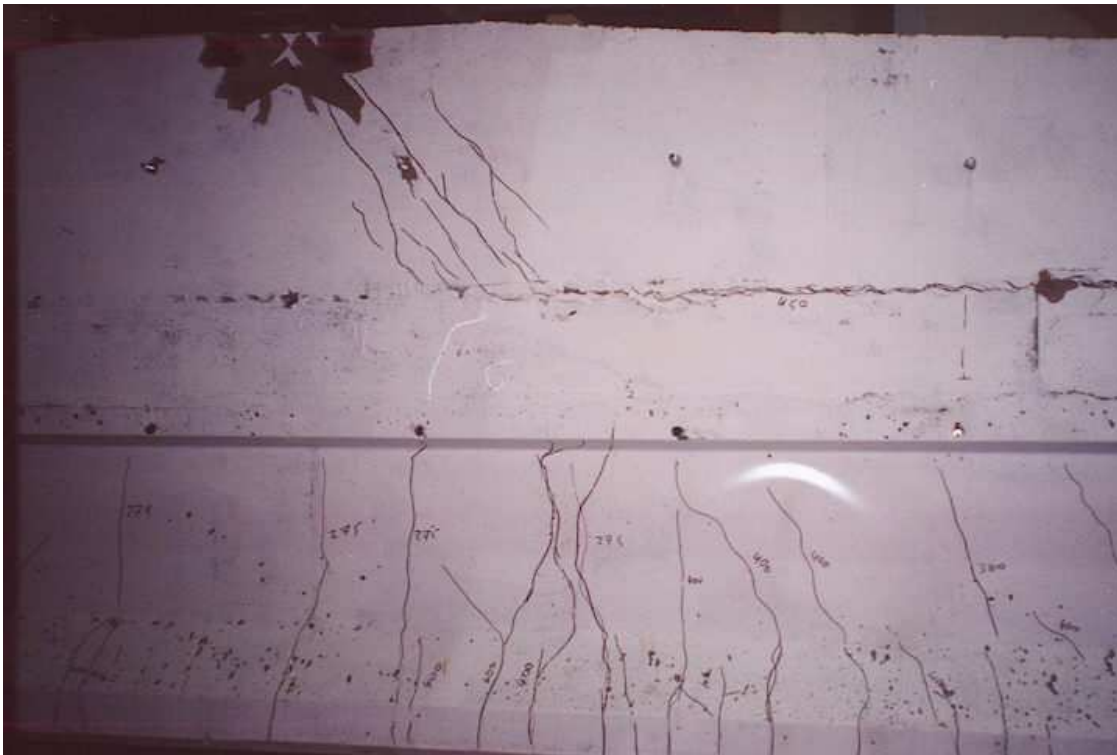


Figure 3.4.3.3.6-1 Crack Patterns

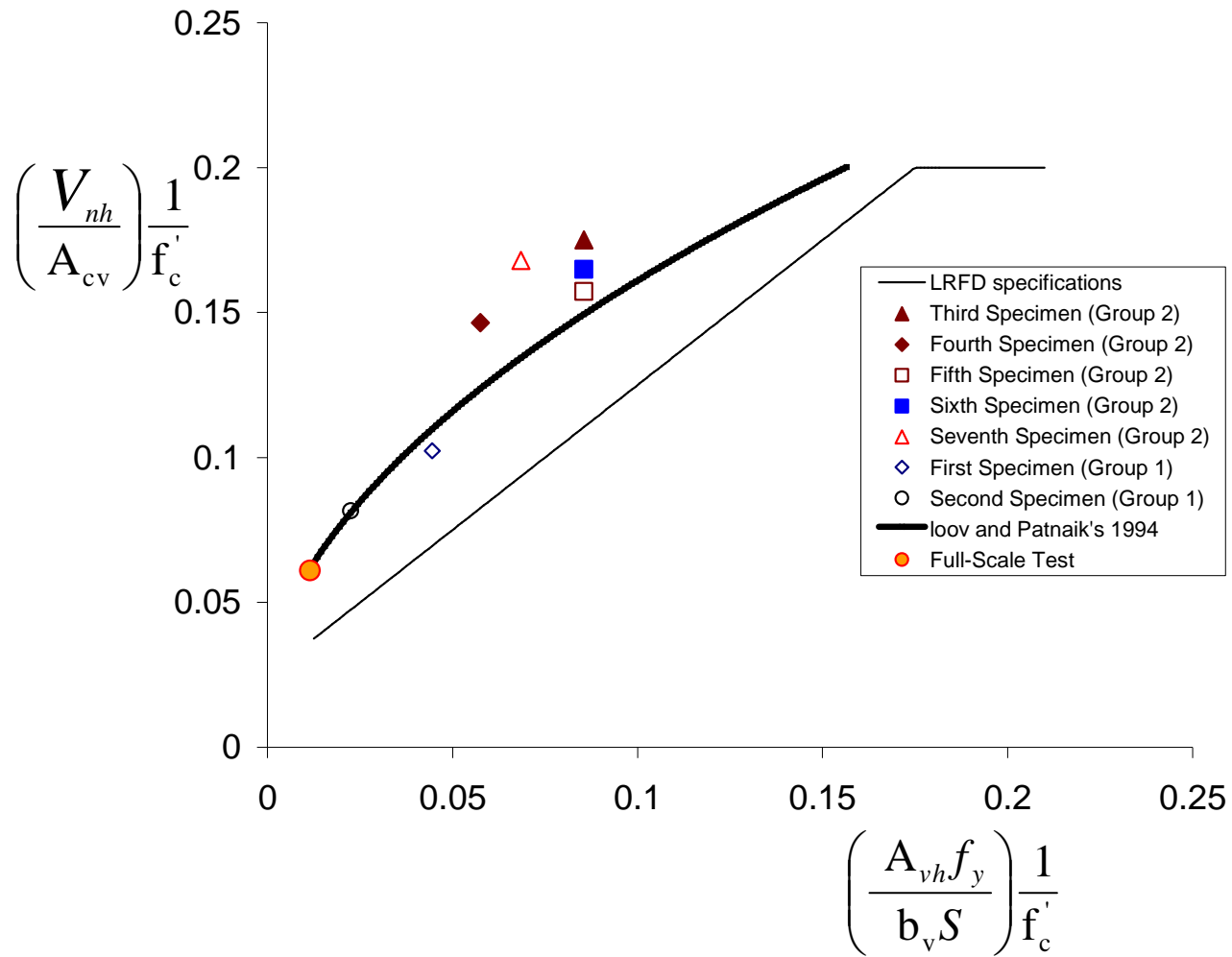


Figure 3.4.3.3.7-1 LRFD Equation and Loov and Patnaik's equation for Horizontal Shear Strength Versus Test Results

3.5 DISCUSSION

This paper introduces a cost-effective and aesthetically appealing revolution in extending precast concrete bridge spans. Through extensive theoretical and experimental research, it has been shown for the first time that connecting a haunch block to a standard I-girder in the pier segment results in extending the spans of prestressed concrete bridges to up to 350 ft, while meeting the limitations of shipping and handling capacities. This approach efficiently substitutes for a customized, deepened pier segment while optimizing the negative and the positive moment capacities.

The presented innovative horizontal shear reinforcement uses 1-1/4 in. lubricated coil threaded rods, inserted in the form before casting the concrete, and then later turned to protrude 8 in. into the pocket. The reinforcement allows for utilization of standard forms, which enhances the cost efficiency of the proposed system.

The proposed system was progressively tested using seven push-off specimens, a pull-out specimen, and a full-scale specimen. Based on the experimental results, Looov and Patnaik's 1994 equation is recommended over the AASHTO LRFD, as the latter was found to be unnecessarily conservative as shown in Figure 3.4.3.3.7-1.

3.6 CONCLUSIONS

Through the utilization of a segmental haunched concrete girder system, a large number of relatively short, light girders, interconnected using post tensioned cables, are proven to result in longer-than-usual pre-stressed concrete bridge spans. This alternative enlarges the span capacity of the precast bridge girders. In other words, it increases the span-to-depth ratio for the girder. It can also reduce the cost of the project because it is

possible to completely eliminate the false-work (temporary towers). This is one of the advantageous features of this system, especially in water-crossing bridges.

This system is more cost-effective than the traditional solution of deepening the pier segment for several reasons. It allows for the use of beams of less height and/or weight. It also allows for more spacing between beams, and thus fewer beams can be used. As far as aesthetics and clearance are concerned, this system allows for the utilization of girders of less height. This results in more clearance below the bridge and more pleasing aesthetics.

CHAPTER 4

APPROXIMATE FORMULAS FOR PRESTRESSED LOSSES IN HIGH-STRENGTH CONCRETE

4.1 INTRODUCTION

4.1.1 Problem Statement

The primary purpose of calculating losses in prestressing is to accurately predict the stress and deformation in concrete members under service conditions. In 2002, National Cooperative Highway Research Program project 18-07 (Tadros et. al.) resulted in new guidelines for estimating prestress losses in pre-tensioned high-strength concrete bridge girders. In recent months, the guidelines developed in NCHRP 18-07 have been expanded to include post-tensioned spliced girder applications as well. The purpose of this research project is to develop approximate formulas to estimate prestress losses in high-strength concrete post-tension spliced girder applications based on the guidelines developed in NCHRP 18-07.

4.1.2 Prestressed Losses

Loss of prestress is the reduction of tensile stress in prestressing strands due to contraction of the concrete around the strands, relaxation of stress within the strands and external factors which reduce the total initial force before it is applied to the concrete. Prestress loss in pre-tensioned girders is the summation of elastic effects, shrinkage, creep and relaxation losses. Formulas currently used by various codes to determine the concrete modulus of elasticity, shrinkage and creep have been empirically established

based primarily on data for normal-strength concrete with compressive strength up to 6.0ksi (Al-Omaishi).

4.1.2.1 Elastic Effects

Elastic effects are stress gains or losses in the prestressing steel that occur when an applied load causes a shortening or lengthening of the steel such that the force exerted on the concrete member by the steel changes. This results in the shortening or lengthening of the concrete member and an accompanying elastic gain or loss in the steel. Elastic effects affect concrete stress throughout the life of a prestressed element. In a spliced girder bridge with two stage post-tensioning, elastic effects are introduced during the following events.

- 1) At transfer, elastic effects consist of a loss due to pre-tensioning force and a gain due to member self weight.
- 2) During first stage post-tensioning, they result in a loss in the pre-tensioning steel.
- 3) During deck placement, they consist of gains in both the pre-tensioning and first stage post-tensioning steel.
- 4) During second stage post-tensioning, they include losses in both pre-tensioning and first stage post-tensioning steel.
- 5) Finally, elastic effects at the application of superimposed dead loads and live loads consist of gains in the pre-tensioning steel and both stages of the post-tensioning steel.

Elastic effects are different in high-strength concrete as compared with normal strength concrete due to high strength concrete's higher modulus of elasticity. The modulus of elasticity, E , of a material is defined as the change of stress with respect to strain in the linear elastic range – a material's stiffness. Concrete is an elastoplastic material and therefore has a modulus of elasticity, E_c , that varies non-linearly with stress. It is approximated as a linear value by drawing a line on the stress-strain curve from the origin to the point on the curve located at $f'_c/2$, i.e. the secant modulus at $f'_c/2$. Accurately approximating the value of the modulus of elasticity of concrete allows for prediction of a component's initial camber and elastic prestress gains and losses. Variables influencing E_c include cement paste stiffness, porosity and composition of the boundary zone between the paste and aggregates, aggregate stiffness, and concrete constituent proportions.

4.1.2.2 Shrinkage

Shrinkage loss is a long-term loss caused by concrete's natural tendency to shrink over time due to loss of water. It is caused primarily by shrinkage of the cement paste and depends on a number of variables including the concrete strength, stiffness and proportion of aggregates, ambient conditions, and size and shape of the specimen. It continues throughout the service life of the bridge. Shrinkage strain of HSC can be different than normal concrete.

4.1.2.3 Creep

Creep loss is a long-term loss caused by concrete's slow plastic deformation under prolonged stress. It depends on a number of variables including the level of stress, duration of loading, strength and age of the concrete, humidity, amount of steel reinforcement, cement paste content, w/cm ratio, aggregate proportions and properties, and type of curing. It continues throughout the service life of the bridge. Creep in high-strength concrete is generally less than in normal-strength concrete.

4.1.2.4 Relaxation

When a strand is stressed and held at a constant strain, the stress in the strand decreases with time. This decrease in stress is called the intrinsic relaxation loss. The most commonly used type of prestressing steel on the market today is the low-relaxation strand.

The predecessor of the low relaxation strand was the stress relieved strand. Low relaxation strands undergo an extra production step of controlled heating to about 660^oF and then cooling while under tension. This reduces relaxation loss to about 25% of that of its predecessor. Due to wide-spread use of low relaxation strands, relaxation effects are far less significant than in the past.

4.2 NCHRP PROJECT 18-07

4.2.1 Background

NCHRP project 18-07 dealt primarily with time dependent loss prediction in high-strength pre-tensioned girders. It involved testing conducted using concrete mixes from 4 different states – Nebraska, New Hampshire, Texas and Washington. Three high

strength concrete mixes and one deck mix were tested from each state for a total of 16 mixes. The modulus of elasticity, strength, shrinkage, and creep specimens were tested. Components of prestress loss unaffected by concrete strength, for example strand relaxation before transfer and post-tensioning losses like friction and wobble, were not addressed in 18-07.

In this project, a more accurate equation for calculating the modulus of elasticity of concrete was developed. Proposed formulas for estimating shrinkage and creep were developed as well based on extensive test data. Calculation of relaxation in low-relaxation strands was simplified to a single loss value.

A total of seven girders were instrumented in the four participating states. The method developed in NCHRP 18-07 was verified by comparing its predicted results with the loss measured in these girders. In addition to this verification, prestress loss data obtained from other tests were compared to those estimated by the proposed method to assess the method's reliability. Prestress loss measurements were reported for tests on 31 pretensioned concrete girders in 7 states ranging in age from 200 days to 28 years. They represented a wide range of environmental conditions, material properties and construction practices. The girders had I and box sections and had spans ranging from 45 to 152 feet. The methods for calculating prestress loss developed in NCHRP 18-07 were proven to be reasonably conservative and accurate. It gives better correlation with tests than the AASHTO LRFD Refined Method and the PCI-BDM method.

4.2.2 Modulus of Elasticity

NCHRP 18-07 included E_c laboratory tests of a set of three 4" x 8" cylinders for each state's three HSC mixes and each state's deck mix, a total of 16 mixes, at 1, 3, 7, 14,

28, 56, 90, 128 and 256 days. A total of 108 cylinders were tested in the laboratory. E_c field testing included 18 cylinders from each plant. The concrete in the cylinders was the same as the mix selected for each state's instrumented girders. They were cured under the same conditions as the girders. The resulting equation includes a variable to account for the effect of local aggregate stiffness on E_c , K_1 , as well as a variable to allow upper or lower bound modulus of elasticity values to be calculated, K_2 . K_1 varies from 0.975 for the softest aggregate (Nebraska) to 1.359 for the hardest aggregate (Texas). In Nebraska, K_2 varies from 0.788 for a lower bound value to 1.211 for an upper bound value. The equation also accounts for the variability of concrete density with varying strength. A detailed example of loss calculation in a post-tensioned girder using the NCHRP 18-07 modulus of elasticity formula is included in the appendices of this report.

The following are the NCHRP 18-07 proposed modulus of elasticity equations:

$$E_c = 33,000K_1K_2w_c^{1.5}\sqrt{f'_c} \quad (\text{ksi}) \quad (4.2.2-1)$$

$$w_c = 0.140 + f'_c/1000 \quad (\text{kcf}) \quad (4.2.2-2)$$

where: K_1 is a factor to account for local aggregate stiffness, K_2 is a factor allowing for an upper or lower bound modulus of elasticity calculation, w_c is the density of concrete in kips per cubic foot and f'_c is the 28 day concrete strength.

The following chart is a summary of NCHRP 18-07 modulus of elasticity test results and compares current prediction methods with the proposed method.

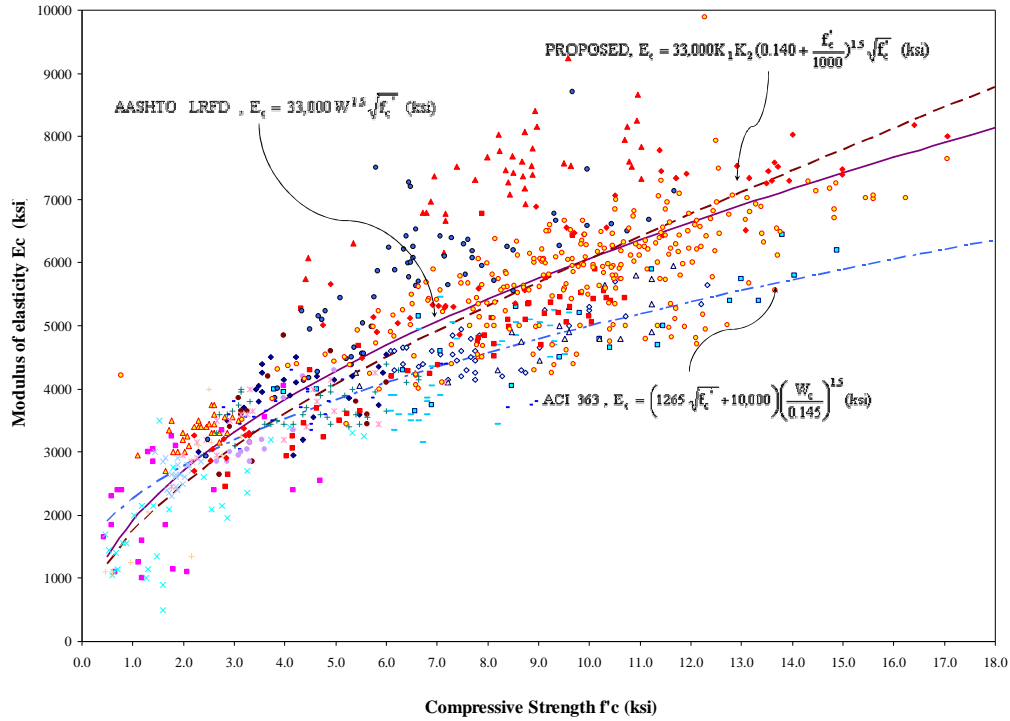


Figure 4.2.2-1 NCHRP 18-07 Modulus of Elasticity Test Results

Another major point made in NCHRP 18-07 relevant to elastic effects is that when external loads, including initial prestress just before transfer and post-tensioning loads, are introduced to a *transformed* section, the elastic effects are automatically accounted for. That is to say, when the change in concrete stress due to external loading is calculated using the transformed section rather than the net or gross sections, elastic effects need not be considered.

There are two options for calculating elastic loss or gain due to various loadings. The first option involves using an iterative net section analysis. Using this option with gross section properties to approximate net section properties is the common practice at present. The second and preferred option involves using a non-iterative transformed section analysis. Using the second option for calculating elastic gains or losses

eliminates the need to account for elastic effects by iteration. For a further explanation see Hennessey et. al.

4.2.3 Shrinkage

NCHRP 18-07 tested twelve laboratory shrinkage specimens in each of the four states. Three specimens were tested for each of the state's three high-strength girder mixes and three specimens were tested for each state's deck mix for a total of 16 mixes. One of the high-strength mixes from each state was the same as the one used in that state's instrumented bridge girders. A total of 48 shrinkage specimens were tested in the lab.

In addition to the laboratory testing, 3 specimens were made from the same materials as Nebraska's girders and monitored in the field. They were subjected to the same curing and environmental conditions as the bridge girders.

The NCHRP 18-07 proposed shrinkage strain formula includes factors to account for the age of the member, the volume-to-surface ratio of the member, humidity and concrete strength. A detailed example of loss calculation in a post-tensioned girder using the NCHRP 18-07 shrinkage strain formula is included in the appendices of this report.

The following is the NCHRP 18-07 proposed shrinkage strain formula:

$$\epsilon_{sh} = 480 \times 10^{-6} k_{td} k_s k_{hs} k_f \quad (4.2.3-1)$$

$$k_{td} = \frac{t}{61 - 4f'_{ci} + t} \quad (4.2.3-2)$$

$$k_s = \frac{1064 - 94 \left(\frac{V}{S} \right)}{735} \quad (4.2.3-3)$$

$$k_{hs} = 2 - 0.0143(H) \quad (4.2.3-4)$$

$$k_f = \frac{5}{1 + f'_{ci}} \quad (4.2.3-5)$$

where: k_{td} is the time development correction factor, k_{cs} is the size factor, k_{hs} is the humidity correction factor for shrinkage, k_f is the concrete strength correction factor, t is the time in days, f'_{ci} is the concrete strength at release, V/S is the volume to surface ratio and H is the average annual ambient relative humidity in %.

The following graph shows a summary of shrinkage test data from NCHRP 18-07 and compares current and proposed shrinkage prediction methods. Notice the significantly lower shrinkage values predicted using the proposed method.

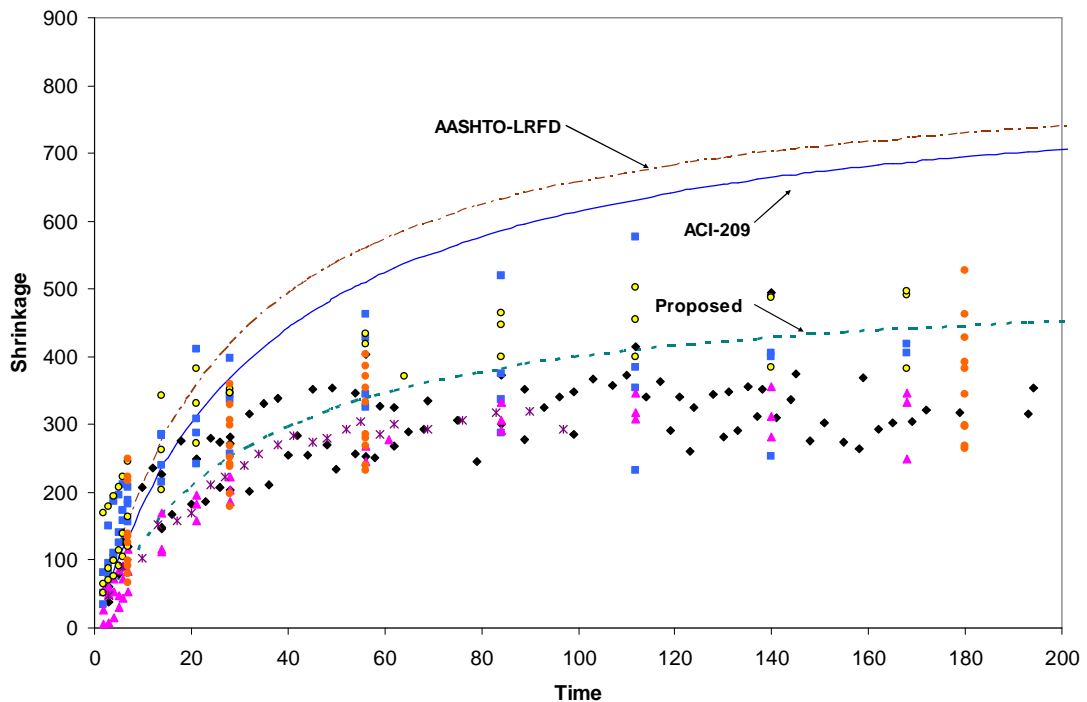


Figure 4.2.3-1 NCHRP 18-07 Shrinkage Test Results

4.2.4 Creep

NCHRP 18-07 included laboratory creep tests on all 12 high-strength mixes. Four 4" x 4" x 24" specimens were tested for each mix. Three specimens were loaded at one day and one specimen was loaded at 56 days. A total of 48 creep tests were conducted.

The NCHRP 18-07 proposed creep factor formula includes factors to account for the age of the member, the loading age of the member, humidity, volume-to-surface ratio and concrete strength. The time development factor is the same as used in the shrinkage formula, as is the size factor and concrete strength factor. The humidity factor is different, however.

The following is the NCHRP 18-07 proposed creep factor formula:

$$\Psi = 1.90k_{td}k_{la}k_s k_{hc}k_f \quad (4.2.4-1)$$

$$k_{td} = \frac{t}{61 - 4f'_{ci} + t} \quad (4.2.4-2)$$

$$k_{la} = t_i^{-0.118} \quad (4.2.4-3)$$

$$k_{hc} = 1.56 - 0.008H \quad (4.2.4-4)$$

$$k_s = \frac{1064 - 94V/S}{735} \quad (4.2.4-5)$$

$$k_f = \frac{5}{1 + f'_{ci}} \quad (4.2.4-6)$$

where: k_{td} is the time development correction factor, k_{la} is the loading age factor, k_s is the size factor, k_{hc} is the humidity correction factor for creep, k_f is the concrete strength

correction factor, t is the time in days, f'_{ci} is the concrete strength at release, V/S is the volume to surface ratio and H is the average annual ambient relative humidity in %.

The following graph shows a summary of creep coefficient test data from NCHRP 18-07 and compares current and proposed creep prediction methods.

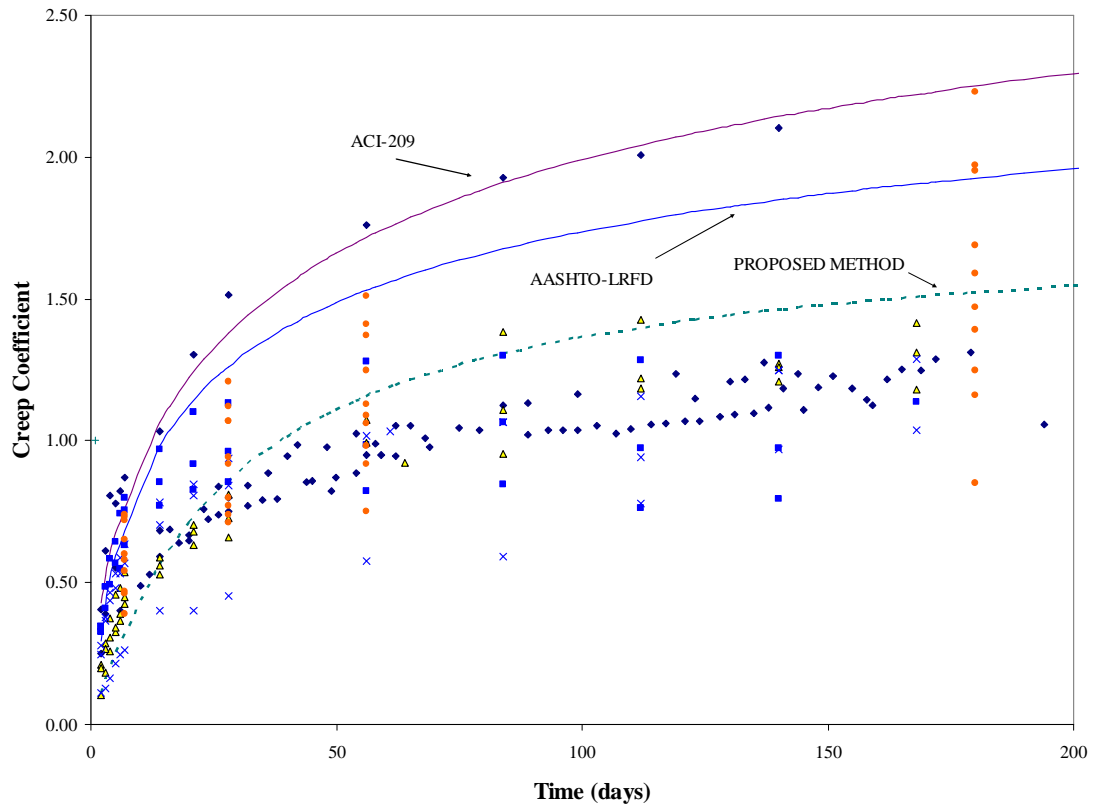


Figure 4.2.4-1 NCHRP 18-07 Creep Coefficient Test Results, Specimens Loaded at 1 Day

4.2.5 Relaxation

Stress loss due to relaxation of prestressing strands, Δf_{pRE} , tensioned initially to f_{pi} can be estimated as follows:

$$\Delta f_{pRE} = \psi K L_r \quad (4.2.5-1)$$

where:

ψ = relaxation reduction factor that reflects the fact that actual relaxation will be less than the intrinsic relaxation due to the steady decrease in strand stress due to shrinkage and creep losses:

$$= 1 - 3[(SH + CR_c)/f_{po}]$$

f_{po} = effective stress in prestressing strands, ksi

L_r = intrinsic (constant-length) relaxation loss without accounting for member shortening due to creep and shrinkage:

$$= [\log(24t)/45][f_{pi}/f_{py} - 0.55] f_{pi}$$

t = time for which relaxation loss is calculated, days

f_{pi} = initial stress at the beginning of relaxation loss period, ksi

f_{py} = yield strength of strands, ksi

These values typically range from 1.8 to 3.0ksi. It is a relatively small component of prestressed loss and is assumed in NCHRP 18-07 to be 2.4ksi for the detailed method and 2.5 ksi for the approximate formula.

4.2.6 Losses Step By Step

Figure 4.2.6-1 is plot taken from NCHRP 18-07 of stress versus time in the strands in a pretensioned concrete girder. It shows the losses and gains occurring at various stages in its life from jacking to final time. A step by step description follows the plot.

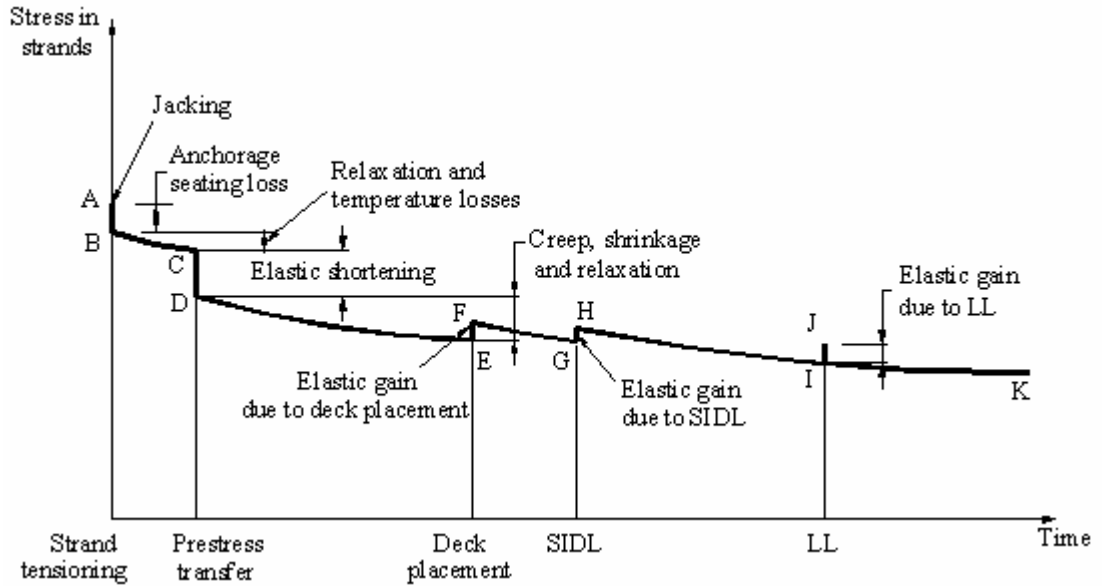


Figure 4.2.6-1 NCHRP 18-07 Plot of Pretensioned Girder Losses

- 1) Jacking (points A to B): Loss due to prestressing bed anchorage seating. This component was not considered in NCHRP 18-07.
- 2) Tensioning to prestress transfer (points B to C): Losses due to relaxation and temperature change from that of the bare strand to the temperature of the strand embedded in concrete. This component was not considered in NCHRP 18-07.
- 3) Prestress transfer (points C to D): Instantaneous prestress loss due to prestressing force and self weight.
- 4) Prestress transfer to deck placement (points D to E): Prestress loss due to shrinkage and creep of girder concrete and relaxation of prestressing strands.
- 5) Deck placement (points E to F): Instantaneous prestress gain due to deck weight on the non-composite section.

- 6) Deck placement to superimposed dead load (points F to G): Prestress loss due to shrinkage and creep of girder concrete and relaxation of prestressing strands.
- 7) Superimposed dead load (points G to H): Instantaneous prestress gain due to superimposed dead load on the composite section.
- 8) Superimposed dead load to final time (points H to K): Prestressed loss due to shrinkage and creep of girder concrete and relaxation of prestressing strands.
- 9) Live load (points I to J): Instantaneous prestress gain due to live load on the composite section.

4.2.7 Approximate Formula

NCHRP project 18-07 also included a simplified derivation and a parametric study of prestress losses in pretensioned high-strength girders for the development of an approximate formula to predict long term losses, i.e. creep, shrinkage and relaxation. The derivation and results of the parametric study are given in NCHRP 18-07.

The formula, as given in equation (4.2.7-1), includes three terms. The first is the creep term, the second is the shrinkage term and the third is the relaxation term. The approximate method proved to be almost as accurate as the NCHRP 18-07 detailed method and much simpler. The final form of the approximate formula is as follows:

$$\Delta f_{pLT} = 10.0 \frac{f_{pi} A_{ps}}{A_g} \gamma_h \gamma_{st} + 12.0 \gamma_h \gamma_{st} + 2.5 \quad (4.2.7-1)$$

$$\gamma_h = 1.7 - 0.01H = \text{correction factor for humidity} \quad (4.2.7-2)$$

$$\gamma_{st} = \frac{5}{1 + f'_{ci}} = \text{correction factor for concrete strength} \quad (4.2.7-3)$$

A_{ps} = area of prestressing steel

A_g = gross section area

where: γ_h is the correction factor for humidity, γ_{st} is the correction factor for concrete strength, A_{ps} is the area of prestressing steel, A_g is the gross section area, H is the average annual ambient relative humidity in % and f'_{ci} is the concrete strength at release.

Notice the humidity factor in the approximate formula is different than the humidity factors used in the creep and shrinkage formulas. This approximate formula was the starting point for the development of the post-tensioned spliced girder bridge approximate formulas.

4.3 SPLICED GIRDER BRIDGES

The next step to continue the work done in NCHRP 18-07 was to extend its applicability to post-tensioned spliced girder construction. A method was developed for this task using loss formulas from NCHRP 18-07. Henceforth, this method will be referred to as the “Detailed Method.” Adding post-tensioning greatly complicates the analysis. Figure 4.3-1 is a plot taken from a bridge analyzed using the detailed method. There are three stages of prestressing steel represented: 1) pretensioning, 2) first stage post-tensioning and 3) second stage post-tensioning. A step by step description follows the plot.

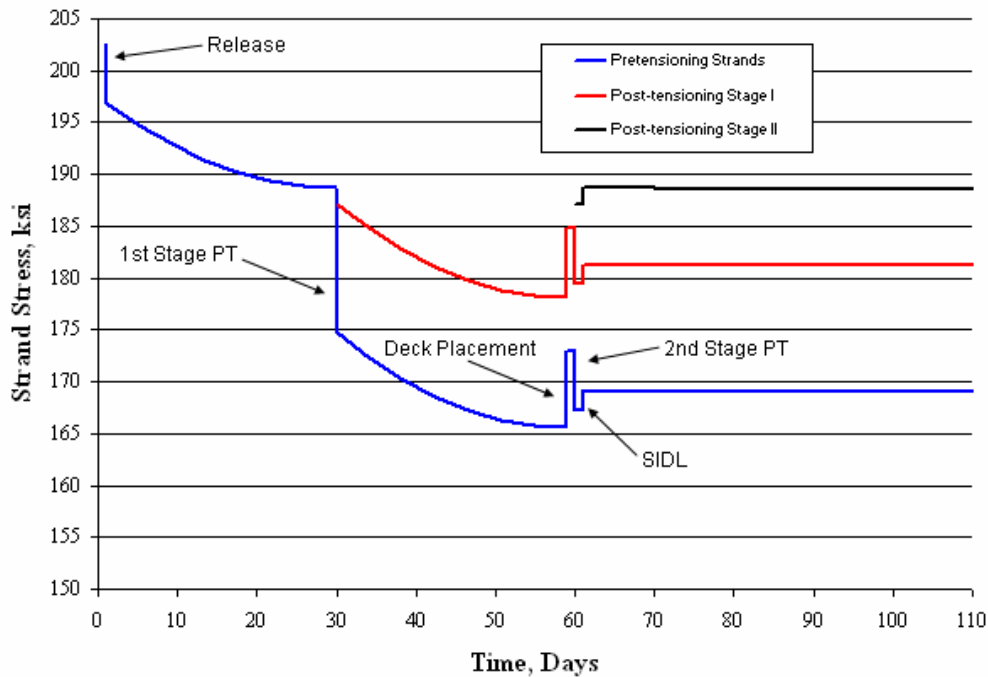


Figure 4.3-1 Plot of Two-Stage Post-Tensioned Girder Losses Using The Detailed Method

The following is a step by step description of the losses in the figure above. It includes all of the prestressing steels.

- 1) Prestress release/transfer (1 day): Instantaneous loss in pretensioning steel due to pretensioning force and self weight
- 2) Release to first stage post-tensioning (1 to 30 days): Loss in pretensioning steel due to shrinkage and creep of girder concrete and relaxation of strands.
- 3) First stage post-tensioning (30 days): Instantaneous loss in pretensioning steel due to elastic shortening caused by first stage post-tensioning.
- 4) First stage post-tensioning to deck placement (30 days to 60 days): Loss in pretensioning and first stage post-tensioning steel due to shrinkage and creep of girder concrete and relaxation of strands.

- 5) Deck placement (60 days): Instantaneous gain in pretensioning and first stage post-tensioning steel due to deck weight on the non-composite section.
- 6) Second stage post-tensioning (60 days): Instantaneous loss in pretensioning and first stage post-tensioning steel due to elastic shortening caused by second stage post-tensioning.
- 7) Superimposed dead load (60 days): Instantaneous gain in pretensioning, first stage post-tensioning and second stage post-tensioning steels due to superimposed dead load on the composite section.
- 8) Superimposed dead load to final time (60 days to 20,000 days): Loss in all prestressing steels due to shrinkage and creep of girder concrete and relaxation of strands.
- 9) Live load: Instantaneous gain in all prestressing steels due to live load on the composite section.

In the above plot, first stage post-tensioning is assumed to occur at 30 days. Deck placement, second stage post-tensioning, and superimposed dead loading are all assumed to occur at the same time, in this case at 60 days. This is a reasonable assumption made to simplify the calculations. The section is assumed to behave as a composite with post-tensioning steel immediately after each post-tensioning event, i.e. the grout is assumed to cure immediately. The deck is assumed to be fully cured at the time of second stage post-tensioning. This will result in slightly unconservative elastic shortening values due to second stage post-tensioning and slightly unconservative creep values from the time of second stage post-tensioning until the time when the deck actually reaches its 28 day compressive strength.

The first two stages of losses shown in Figure 4.2.1-1, the NCHRP 18-07 plot of pretensioned girder losses, are not shown in Figure 4.3-1 – the Detailed Method. These stages are 1) pretensioning loss due to stressing bed anchorage seating and 2) pretensioning loss due to relaxation and temperature change from that of the bare strand to the temperature of the strand embedded in concrete. Neither of these components were considered in NCHRP 18-07.

4.4 APPROXIMATE FORMULA DEVELOPMENT

4.4.1 Problem Statement

Given the cumbersome task of calculating losses in post-tension spliced girders using the detailed method, even with a spreadsheet designed for the task, the desire arose to develop approximate formulas to estimate the losses quickly and reasonably conservatively. As a first step in this process, three formulas were desired.

- 1) A formula to estimate losses in the pretensioning steel at the time of first stage post-tensioning
- 2) A formula to estimate losses in the pretensioning steel at final time
- 3) A formula to estimate losses in the first stage post-tensioning steel at final time

These formulas apply only to one stage post-tensioned bridges and focus on long term losses. Additional formulas to predict losses in bridges with two stage post-tensioning are desirable as well. However, that would not benefit Nebraska's current situation. Nebraska currently specifies only one stage of post-tensioning. Figure 4.4.1-1

shows graphically the locations at which formulas were developed. The numbers on the graph correspond to numbers 1), 2) and 3) above.

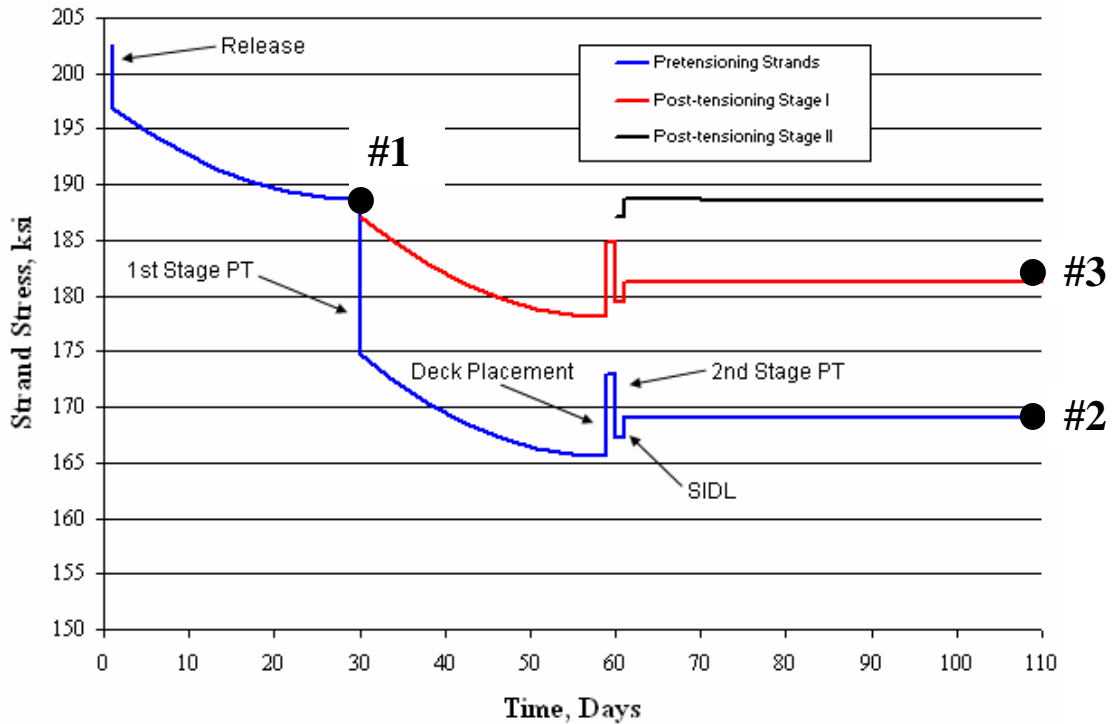


Figure 4.4.1-1 Points For Which Approximate Formulas Were Developed

A parametric study was conducted to look at loss in a large number of bridges. To this end, a spreadsheet was developed to quickly design bridges within the boundaries described in the “Assumptions” section of this report.

4.4.2 Assumptions

The primary assumption governing the development of the formulas for losses at final time was the following: overestimating prestressed loss is conservative for loss in both prestressing steels. The primary governing service conditions during the service life of the bridge are compression in the bottom flange over the pier, tension in the top flange

over the pier and tension in the bottom flange at 0.4L. Overestimating losses will give larger compression values over the pier and larger tension values at 0.4L

The primary assumption governing the development of the formula for pretensioning losses at the time of first stage post-tensioning was the following: underestimating prestressed loss is conservative. The primary governing service condition here is compression in the bottom flange at 0.4L due to pre-tensioning and post-tensioning. Underestimating losses will give larger compression values at this location and is therefore conservative. The remainder of the assumptions that follow are based on these two.

As with the detailed method, the approximate formulas were developed to find the losses at the section of maximum prestressing steel eccentricity. On a two span bridge this is at 0.4L.

The level of pre-tensioning was determined based on an allowable bottom fiber tensile stress limit of $0.19\sqrt{f'_c}$ due to 150% of the girder self weight, M_g , to account for additional forces during construction and transportation. The level of post-tensioning was determined based on required AASHTO service load stress limits.

Only NU shapes were considered. Spans ranged from 80ft to 220ft.

The pre-tensioning steel jacking stress is held constant in this study at 202.5ksi. The area of pre-tensioning steel varies. Initial stress transfer most often occurs about 16 hours after the cement in the concrete mix begins to hydrate. This time is assumed to be 1 day.

A parabolic post-tensioning tendon profile was assumed with the first parabola extending from 0.0L to 0.4L, the second parabola extending from 0.4L to 0.9L and the third parabola extending from 0.9L to 1.0L.

Another factor influencing girder creep is the time at which the post-tensioning is applied. A younger concrete with a lower f'_c will creep more than a more fully hydrated concrete. Therefore the time of post-tensioning is conservatively assumed to be 30 days after the precast section is cast. This allows for a very optimistic construction schedule.

The amount of time that passes before deck placement also affects creep. The weight of the deck, as well as shrinkage of the deck concrete, will reduce the compressive stress at the prestressing steel locations in the positive region. Therefore the time of deck placement is conservatively assumed to be 6 months after the section is cast. This placement time is on the high side but is not unreasonable.

The 160ft transportation limit was ignored. This will cause an overestimation of pretensioning steel, resulting in conservative creep values.

Only two span post-tensioning systems with one precast segment per span and a splice joint over the pier were considered. In a multi-span post-tensioned bridge, the level of prestressing in the positive section is greater than is required in that section. The level of post-tensioning is governed, not by the tensile stress limit in the positive region, but by the tensile stress limit over the pier. The level of pre-tensioning steel in the positive region is governed by the transportation requirement. The girders end up with more total prestressing than is required to meet the tensile stress limit at 0.4L. This is not true of a single span post-tensioned bridge in which the total level of prestressing is governed only by the maximum positive moment at service load. This means that developing the approximate formulas based on the creep at 0.4L in a two span bridge will be more conservative than based on the creep at mid-span in a one span bridge.

The V/S ratios for the NU1100PT to NU2000PT girders range from 3.25 to 3.30 respectively. Girder shrinkage is a function of the V/S ratio. Smaller V/S ratios increase

shrinkage due to greater concrete exposure and long term moisture evaporation. A V/S ratio of 3.25 was selected.

Span length, deck thickness, girder spacing, and barrier selection were also considered. The issue here is DL/LL ratio. A higher DL/LL ratio will reduce the concrete compressive stress at prestressing steel locations in the positive region while a lower DL/LL ratio will increase this stress. Short spans, thin deck slabs, close girder spacings, and light weight barriers (New Jersey as opposed to open rail) reduce the DL/LL ratio. Barrier loads were ignored and girder spacing was set at 10'-0".

In calculating the prestressing required for transportation and construction purposes, the transformed section at 28 days was used.

Cracking was not allowed in the girder over the pier under live load.

The moments due to secondary post-tensioning effects at the pier location range from a minimum of about 3% to a maximum of about 10% of the primary moment. One of these values were assumed for each stress limit checked. The most conservative value for the given stress limit was selected. For example, when checking tensile stress over the pier, 3% was selected as the conservative value. A small value for this stress check would require more post-tensioning steel.

An equal number of strands were assumed present in each duct. A maximum of four ducts were used. A maximum of 15 – 0.6" diameter strands were used per duct. The location of the centroid of the top and bottom ducts were a minimum of 4" from the surface of the concrete. Tendons were spaced 5.25" apart. For a few sections using 12 ksi concrete, the section could handle stress from more than 4 – 15 strand tendons, allowing a longer span. In these few instances, it was assumed that each duct could accommodate more than 15 strands. The most extreme case was an NU2000 spanning

220ft with 18 strands per duct. This is not totally correct but will have little effect on the final results. Transformed section properties will be affected slightly, as will friction losses. But the effects will not be of consequence.

Effective deck width used to calculate composite section properties over the pier is per AASHTO LRFD Art. 4.6.2.6.1.

Live load calculations are based on HL-93 loading as per AASHTO LRFD Specifications, Article 3.6.

Strength limit states were checked at 0.4L and over the pier for the most extreme cases. Tensile stress over the pier usually governed since cracking was not allowed at this location.

Duct spacing was held constant at 5.25". Duct location was varied to meet AASHTO tensile and compressive stress limits.

Post-tensioning is applied when splice joint concrete reaches 6000psi (lower than $f'_c=8000$ psi). The splice joint over the pier is monolithic with the diaphragm at that location. These approximate equations were developed assuming a compressive stress limit of $0.6f'_c$ and a tensile stress limit of $0.19\sqrt{f'_c}$ in the I-section over the pier at the time of post-tensioning. This would create a tensile and compressive stress limit problem at the splice joint if there were no diaphragm over the pier. But with the diaphragm present, the stress in the splice joint due to post-tensioning is much less than would be the case if only the I-section was taking the force. Therefore, these equations are valid only if the splice joint over the pier is monolithic with the diaphragm at that location. If there were splice joints somewhere in the span, stress limits due to post-tensioning would need to be checked there as well.

The assumption that will most quickly be “unassumed” for the purpose of expanding the usefulness of the equations is the constant 70% humidity.

A girder spacing and deck width were assumed such that the interior girder loading controlled the design.

A deck thickness of 7.0” was assumed. This is less than the Nebraska Department of Roads BOPP Manual minimum of 8.0” for a 10’ deck spacing. The 8.0” value given in the BOPP Manual includes the half inch wearing surface, so the minimum effective thickness allowed by NDOR for our spacing is 7.5”. The AASHTO LRFC specifications allows a minimum effective thickness of 7.0”. This smaller value allows less load sharing between girders and results in a more conservative girder design.

Concrete strengths ranging from 8ksi to 12ksi were tested. Concrete strength at release was assumed to be $0.8f_c$. Live load moments for the various sections and span lengths were obtained using ConSpan.

4.4.3 Parametric Study

The parametric study was conducted. A spreadsheet was developed to quickly design each bridge within the guidelines of the assumptions above. Appendix G describes the steps in the design of each bridge including determination of losses using the Detailed Method.

4.4.4 Approximate Formulas

The parametric study led to the development of three approximate formulas for estimating prestressed losses. The NCHRP 18-07 approximate formula was the model for each of these.

4.4.4.1 Formula #1

The first formula developed was to predict time dependent prestress losses in the pretensioning steel at the time of post-tensioning, i.e. during the first period, as shown in Figure 4.4.1-1. The key assumption in the development of this formula is that underestimating prestressed losses is conservative. This is the opposite of what was assumed for the other two formulas. The reason this is conservative is that the stress limits investigated at this point in the construction process are due to stress from pretensioning and post-tensioning steel, not from dead or live loads. If we underestimate the loss then we overestimate the stress due to prestressing, giving conservative results.

$$\Delta f_{pLTI} = 2.0 \frac{f_{pi} A_p}{A_g} \gamma_h \gamma_{st} + 5.5 \gamma_h \gamma_{st} + 1.0 \quad (4.4.4.1-1)$$

$$\gamma_h = 1.7 - 0.01H \quad (4.4.4.1-2)$$

$$\gamma_{st} = \frac{5}{1 + f'_{ci}} \quad (4.4.4.1-3)$$

where: γ_h is the correction factor for humidity, γ_{st} is the correction factor for concrete strength, f_{pi} is the stress in the pretensioning steel at release, A_p is the area of the pretensioning steel, A_g is the gross section area, H is the average annual ambient humidity and f'_{ci} is the concrete release strength.

Notice the similarities between Formula #1 and the NCHRP 18-07 approximate formula, equation 4.2.7-1. Both have three terms, a creep term, a shrinkage term and a relaxation term. In both, the creep term consists of a multiplier, the level of prestressing and factors to correct for humidity and concrete strength. In both formulas, the shrinkage term consists of a multiplier and factors to correct for humidity and strength. In both, the relaxation term is assumed to be a constant. And in both, the strength and humidity correction factors are identical.

Also notice the differences between Formula #1 and the NCHRP formula. The creep multiplier in the NCHRP formula is 5 times as large as the creep multiplier in this formula, 10.0 as opposed to 2.0. This is expected. The NCHRP formula predicts creep at final time where as Formula #1 predicts creep at the time of post-tensioning, which is anywhere from 30 to 120 days or so. Less creep will have occurred at this time.

Also, the NCHRP formula is used to predict creep in girders with much larger amounts of pretensioning steel. Most of the prestressing that happens in spliced girder construction comes in the form of post-tensioning. This means that the level of pretensioning in girders used in spliced girder bridges will be much lower. For both these reasons, it makes sense that the multiplier on the creep term in this formula would be much smaller

Detailed Δf_{pLT} (ksi)	Approx Δf_{pLT} (ksi)	Ratio of Approx to Detailed
5.5	5.1	0.93
5.8	5.3	0.92
5.9	5.5	0.93
5.6	5.4	0.96
5.7	5.5	0.97
6.5	5.8	0.90
5.3	5.3	1.00
6.1	5.6	0.92
6.1	5.7	0.94
5.7	5.6	0.97
6.3	5.8	0.92
6.3	5.9	0.94
5.9	5.7	0.97
6.5	6.0	0.93
6.4	6.1	0.96
5.8	4.6	0.80
6.0	4.9	0.82
6.4	5.2	0.81
6.6	5.3	0.80
6.3	5.2	0.83

**Figure 4.4.4.1-1
Comparison of Formula
#1 Results to Detailed
Method Results**

than the creep term in the NCHRP 18-07 formula.

The shrinkage multiplier in the NCHRP formula, 12.0, is about twice as large as the shrinkage multiplier in this formula, 5.5. This is expected as well since more shrinkage will occur by final time than by first stage post-tensioning.

And finally, the relaxation term here is 1.0ksi as compared with 2.5ksi in NCHRP. This too is expected.

This approximate formula was accurate to within 1.3ksi for all the bridges included in the parametric study. Loss values ranged from 6.6ksi to 5.3ksi. A difference of 1.3ksi is an error of 20%. This sounds large, but when the small values of prestress loss at this point in the life of the girder are considered, 20% or 1.3ksi is a reasonable error. Figure 4.4.4.1-2 is a sample of the data used in developing Formula #1. The 1.397 factor shown on the chart was the starting point for the 2.0 factor that ended up being the creep term multiplier. The idea here is that the creep term multiplier, 2.0, times the correction factors for both strength and humidity, γ_{st} and γ_h , will give a value close to 1.397.

The shrinkage term was a slightly different animal. Although shrinkage values vary due to a number of factors, the differences are small enough that the shrinkage can be approximately represented as a constant value for a given humidity and concrete strength.

Relaxation was found to be about 1.0ksi during the first period.

Losses/gains due to deck shrinkage must also be considered. Deck shrinkage causes prestress gains most of the time, but the gains (and occasionally losses) are so small that a term in the approximate formula to account for them could not be justified.

Therefore, adjustments are made to the formula's various terms instead. In this way, deck shrinkage is considered by the formula, even though there is not a term to specifically address its effects. The final loss prediction results are the real issue.

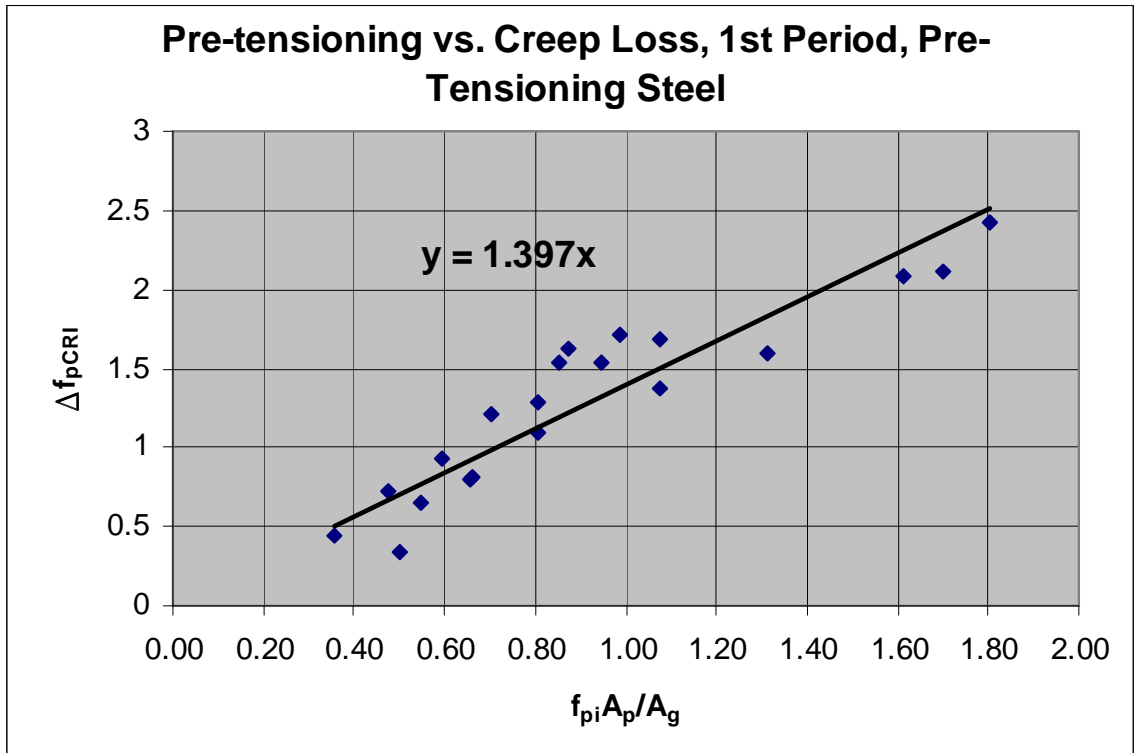


Figure 4.4.4.1-2 Data Used in Development of Creep Term of Formula #1

4.4.4.2 Formula #2

The second formula developed was to predict time dependent prestress losses in the pretensioning steel at final time, assumed to be 20,000 days, as shown in Figure 4.4.1-

1. The key assumption made with this and the next approximate formula is that overestimating prestressed losses is conservative.

$$\Delta f_{pLT} = 8.4 \frac{f_{pi} A_p + 0.7 f_{pu} A_l}{A_g} \gamma_h \gamma_{st}' + 12.6 \gamma_h \gamma_{st} + 2.4 \quad (4.4.4.2-1)$$

$$\gamma_h = 1.7 - 0.01H \quad (4.4.4.2-2)$$

$$\gamma_{st} = \frac{5}{1 + f'_{ci}} \quad (4.4.4.2-3)$$

$$\gamma'_{st} = \left(\frac{8}{f'_c} \right)^{1.65} \quad (4.4.4.2-4)$$

where: γ_h is the correction factor for humidity, γ'_{st} is the correction factor for concrete strength in the creep term, γ_{st} is the correction factor for concrete strength in the shrinkage term, f_{pi} is the stress in the pretensioning steel at release, A_p is the area of the pretensioning steel, f_{pu} is the tensile strength of the post-tensioning steel, A_1 is the area of the post-tensioning steel (see appendices for a notation explanation), A_g is the gross section area, H is the average annual ambient humidity, f'_c is the 28 day concrete strength and f'_{ci} is the concrete release strength.

As with the NCHRP 18-07 approximate formula and the first spliced girder approximate formula, this formula has creep, shrinkage and relaxation terms. Other similarities are present as well.

There are significant differences, however. The creep term in Formula #2 involves total prestressing, not just pretensioning. Also the creep term also contains a different correction factor for concrete strength than in the NCHRP formula or Formula

Δf_{pLT} (ksi)		Ratio of Approx to Detailed
Detailed	Approx	Detailed
23.1	23.2	1.00
27.0	27.0	1.00
29.3	31.2	1.07
26.8	27.4	1.02
29.5	31.7	1.08
32.1	34.8	1.08
25.4	26.1	1.03
28.6	29.7	1.04
31.1	33.0	1.06
27.0	28.6	1.06
31.1	32.5	1.04
31.8	34.4	1.08
29.5	31.3	1.06
33.1	34.9	1.05
32.5	36.7	1.13
25.2	26.4	1.05
26.1	27.2	1.04
28.4	29.1	1.03
28.1	29.9	1.06
28.5	28.7	1.00

**Figure 4.4.4.2-1
Comparison of Formula #2
to the Detailed Method**

#1. This factor reflects the fact that creep loss in post-tensioned girders at final time is generally less than in pretensioned girders with the same amount of total prestressing since most of the prestressing is applied after the concrete has reached a higher strength.

As shown in Figure 4.4.4.2-1, Formula #2 was accurate to within 8% of the Detailed Method in 95% of the bridges investigated. The largest difference within these 95% is 2.6ksi. Figure 4.4.4.2-2 is a sample of the data used in developing Formula #2.

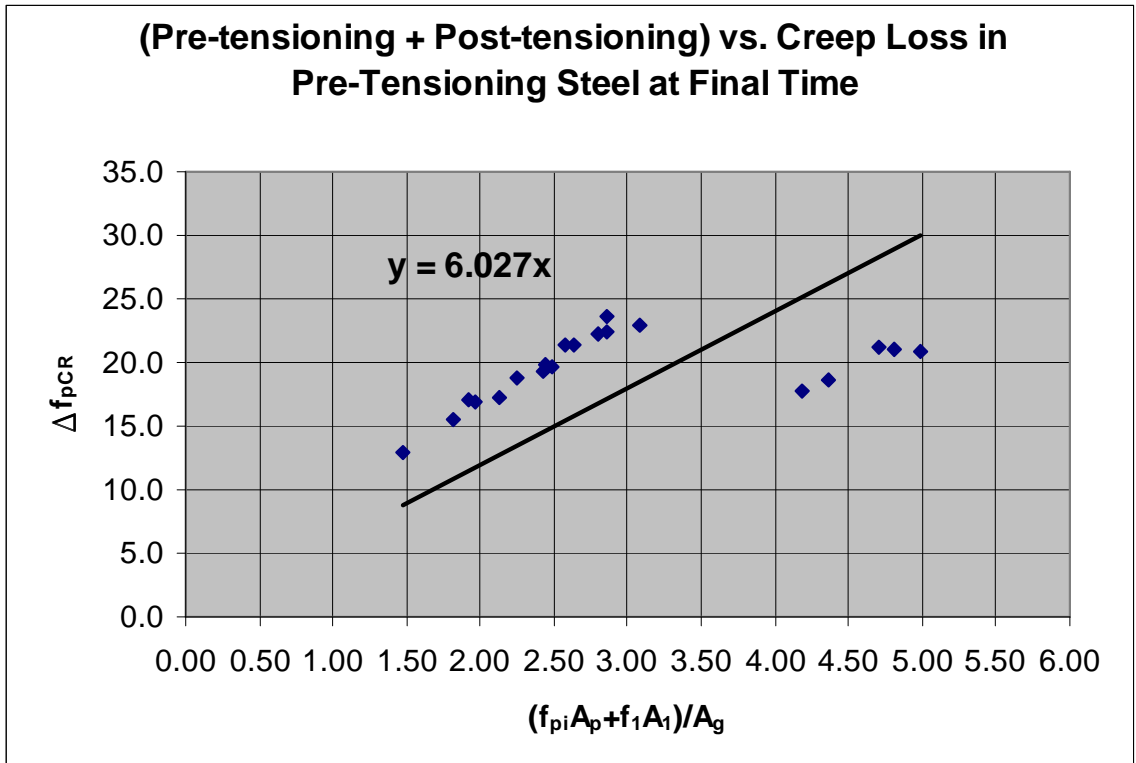


Figure 4.4.4.2-2 Data Used in Development of Creep Term in Formula #2

4.4.4.3 Formula #3

The third formula developed was to predict time dependent prestress losses in the post-tensioning steel at final time as shown in Figure 4.4.1-1.

$$\Delta f_{ILT} = 7.2 \frac{f_{pi} A_p + 0.7 f_{pu} A_l}{A_g} \gamma_h \gamma_{st}' + 7.7 \gamma_h \gamma_{st}' + 5.9 \quad (4.4.4.3-1)$$

$$\gamma_h = 1.7 - 0.01H \quad (4.4.4.3-2)$$

$$\gamma_{st}' = \frac{5}{1 + f_{ci}'} \quad (4.4.4.3-3)$$

$$\gamma_{st}' = \left(\frac{8}{f_c'} \right)^{1.65} \quad (4.4.4.3-4)$$

where: variables are the same as in Formula #2 above.

The most notable difference in Formula #3 is the larger relaxation term. In pre-tensioning steel, significant relaxation occurs between the time of stressing and the time of release. This relaxation is not of consequence to designers who are only interested in the stress in the strand at the time of release and in the losses that follow. The precaster is responsible for making sure the stress at release is that specified by the designer.

With post-tensioning steel, however, these losses have to be accounted for in design. Relaxation losses are considered from the time of jacking to final time. These increased loss values are the cause for the larger relaxation term.

As shown in Figure 4.4.4.3-1, Formula #3 was

Δf_{ILT} (ksi)		Ratio Approx to
Detailed	Approx	Detailed
22.1	22.1	1.00
25.5	25.5	1.00
27.8	29.3	1.05
25.5	25.8	1.01
28.1	29.7	1.06
29.9	32.5	1.09
24.5	24.7	1.01
26.8	27.9	1.04
29.1	30.8	1.06
25.7	27.0	1.05
28.9	30.4	1.05
29.7	32.1	1.08
27.8	29.3	1.05
30.7	32.5	1.06
30.4	34.1	1.12
24.7	25.7	1.04
25.1	26.4	1.05
26.5	28.1	1.06
26.3	28.8	1.10
26.5	27.7	1.05

**Figure 4.4.4.3-1
Comparison of Formula
#3 to the Detailed Method**

accurate to within 10% of the Detailed Method in 95% of the bridges investigated. The largest difference within these 95% is 2.7ksi. Figure 4.4.4.3-2 is a sample of the data used in developing Formula #3.

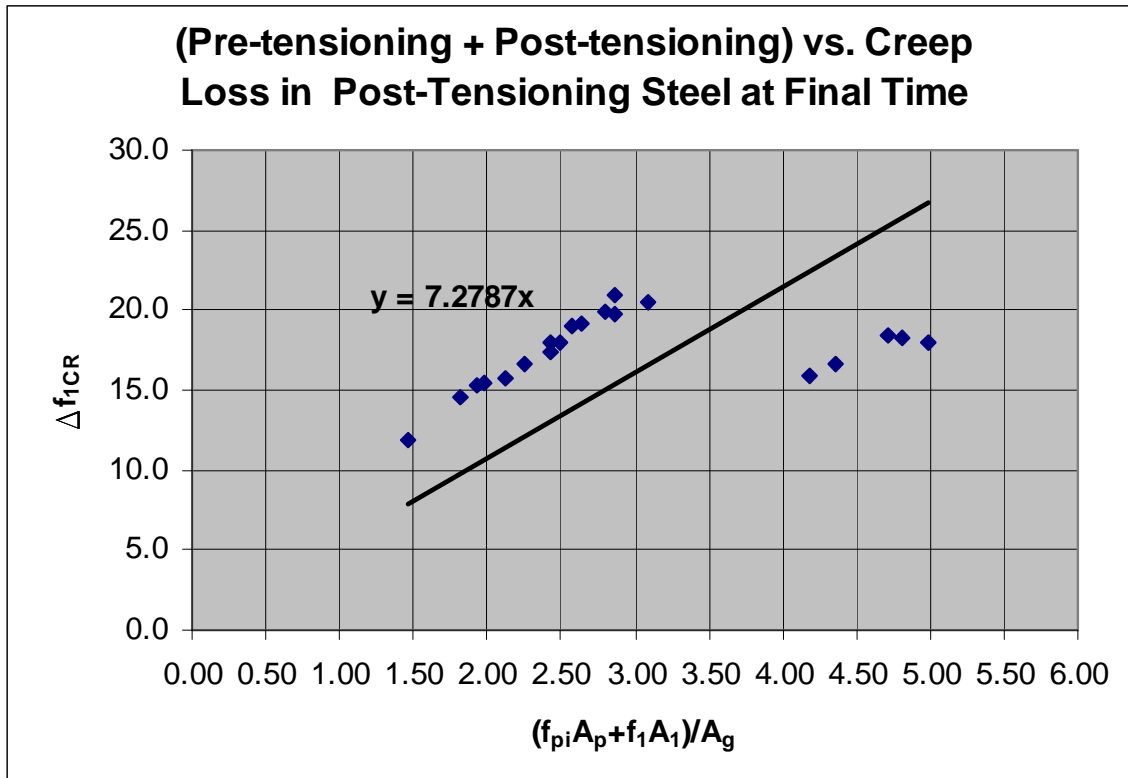


Figure 4.4.4.3-2 Data Used in Development of Creep Term in Formula #3

4.4.5 Detailed Method and Approximate Formulas Compared

Having developed approximate formulas to predict time dependent losses in spliced post-tensioned bridges, we now compare the losses predicted using these formulas versus those predicted using the Detailed Method from which they were developed. The following two numerical examples are single stage post-tensioned bridges designed in the state of Nebraska. One is a single span structure and the other is two-span.

4.4.5.1 Skyline Bridge

The 198th – Skyline Dr. Bridge in Omaha, NE is a 63 000 mm (206 ft - 8.3 in) long, 17 686 mm (58 ft – 0.3 in) wide single-span bridge. NU2000PT Nebraska I-girders were used in its construction. Girder depth was 2000 mm (6 ft - 6.6 in) and web width was 175 mm (6.9 in). The bridge cross section consisted of 7 girders spaced at 2550 mm (8 ft-4.4 in), a composite 200 mm (8 in.) cast-in-place concrete slab and three girder segments per girder line with two splice joints per segment as shown in Figure 4.4.5.1-1. The end segments were each 8 750 mm (28 ft – 8.5 in) long and the field segment was 45 000 mm (149 ft – 3.3 in) long. The release strength of the precast girders is 7.5ksi, their 28 day compressive strength is 10 ksi. The 28 day compressive strength of the CIP slab is 4.3 ksi. The design live load is HL-93.

In the field segment, forty two 0.6in diameter pretensioning strands were released at 202.5ksi. For pretensioning and post-tensioning details see Figures 4.4.5.1-3 and Figure 4.4.5.1-4 respectively. Three post-tensioning tendons, each with 15-0.6 in diameter strands, run through each girder line. Jacking stress was 202.8ksi.

The construction stages were as follows and are also shown in Figure 4.4.5.1-2.

- Stage 1: Fabrication of precast girder segments.
- Stage 2: Erection of precast girder segments on temporary towers and abutments.
- Stage 3: Construction of splice joints.
- Stage 4: Post-tensioning and removal of the temporary towers.
- Stage 5: Placement of deck slab.

Stage 6: Construction of barriers

Additional Detailed Method input values are as follows. Relative humidity is 70%. Age at release is 1 day, age at post-tensioning is 30 days, age at deck placement is 60 days and age at final is 20,000 days.

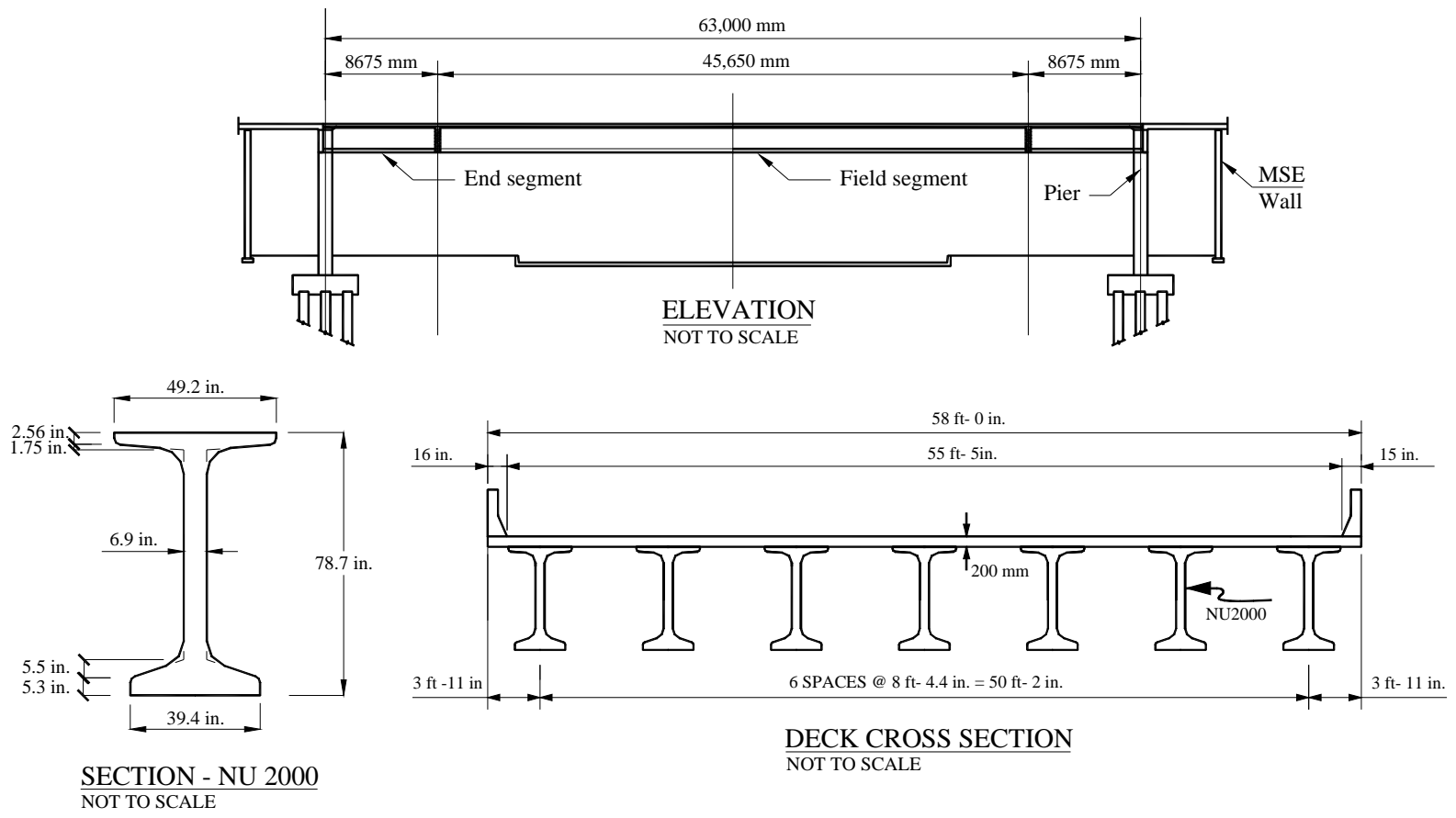


Figure 4.4.5.1-1 General Layout of the 198th – Skyline Dr. Bridge

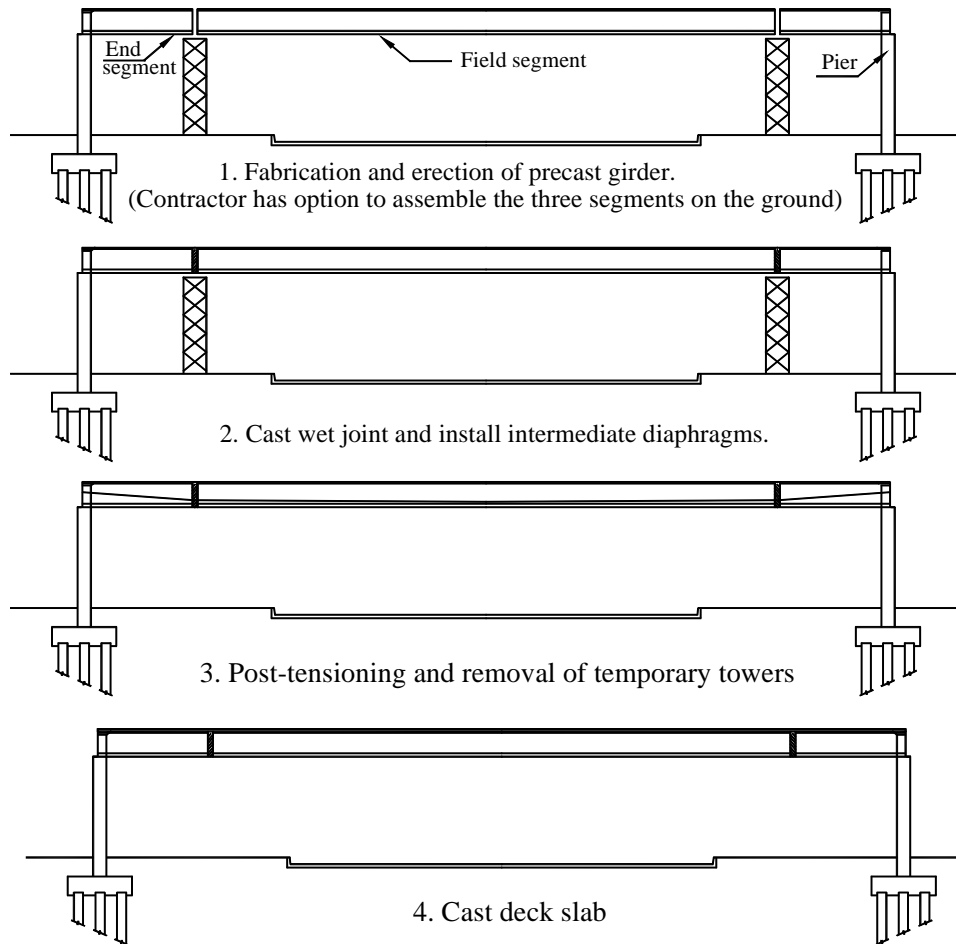


Figure 4.4.5.1-2 Construction Sequence of the 198th – Skyline Dr. Bridge

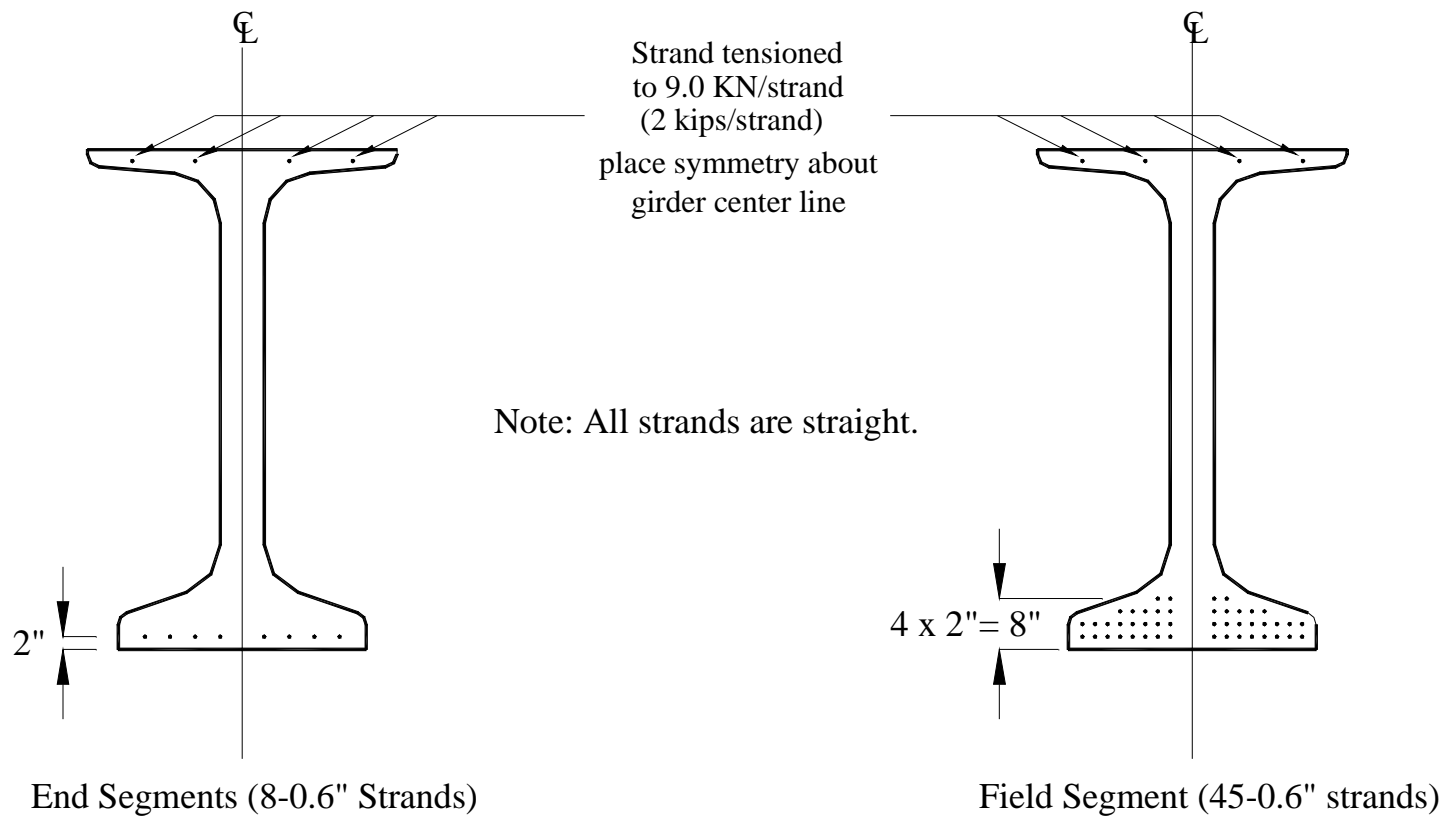
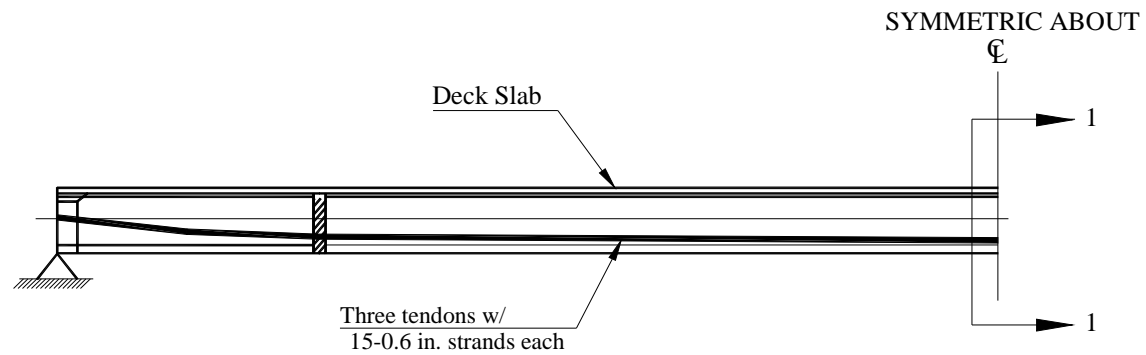
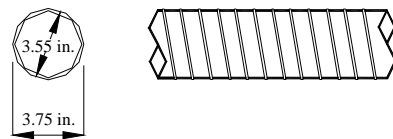


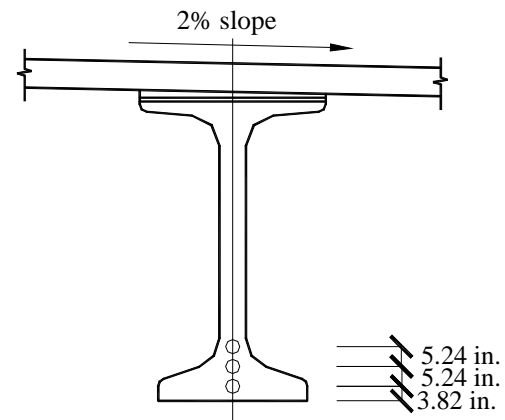
Figure 4.4.5.1-3 Pre-tensioning Scheme of the 198th – Skyline Dr. Bridge



POST-TENSIONING TENDON LAYOUT
NOT TO SCALE



DUCT DETAIL
NOT TO SCALE



SECTION 1-1 AT MID-SPAN
NOT TO SCALE

Figure 4.4.5.1-4 Post-tensioning Details of 198th – Skyline Dr. Bridge

The following is a time dependent loss comparison between the Detailed Method and Approximate Formulas.

	Detailed Method Loss (ksi)	Approximate Formula Loss (ksi)	Approximate Formula / Detailed Method Ratio
Formula #1 Pretensioning Loss At Time of Post-Tensioning	8.17	6.44	0.788
Formula #2 Pretensioning Loss At Final Time	27.08	31.65	1.169
Formula #3 Post-Tensioning Loss At Final Time	23.76	29.18	1.228

Table 4.4.5.1-1 Loss Prediction Comparison, Skyline Bridge

From the results above we see that the approximate formulas conservatively predicted time dependent prestress loss in the pretensioning and post-tensioning steel in the Skyline Bridge. The level of conservatism reflects the fact that these formulas were developed based on a parametric study that did not include one span bridges. Formula #1 conservatively underestimated loss by 1.73ksi, or 21.2%. Formula #2 overestimated losses by 16.9% and Formula #3 overestimated losses by 22.8%.

4.4.5.2 Highway-50 Bridge

The Highway-50 bridge is located on Highway 50 in Sarpy County, Nebraska and was constructed in 2000. It is a two-span bridge with each span measuring 37 800 mm – 37 800 mm (124 ft – 124 ft) and a total width of 30,580 mm (100 ft – 4 in) as shown in Figure 4.4.5.2-1. NU1350PT Nebraska I-girders were used in construction with 10 girder lines spaced at 3 100 mm (10 ft-2 in) each. Girder depth is 1350 mm (4 ft – 5 1/8 in) and web width was 175 mm (6.9 in). A composite 200 mm (8 in.) cast-in-place concrete slab was used. Two girder segments per girder line span between the abutments and the pier. The release strength of the precast girders was 5.5ksi and their 28 day compressive strength was 8ksi. The 28 day compressive strength of the CIP slab was 5 ksi. The design live load was HL-93.

Twenty four ½” diameter pretensioning strands were released at 202.5ksi. Pretensioning details are shown in Figure 4.4.5.2-2. Two post-tensioning tendons, each with 15-0.6in diameter strands, run through each girder line. Jacking stress was 189ksi. Post-tensioning details are shown in Figure 4.4.5.2-3.

The construction stages were as follows:

Stage 1: Fabrication of precast girder segments.

Stage 2: Erection of precast girder segments on the pier and abutments.

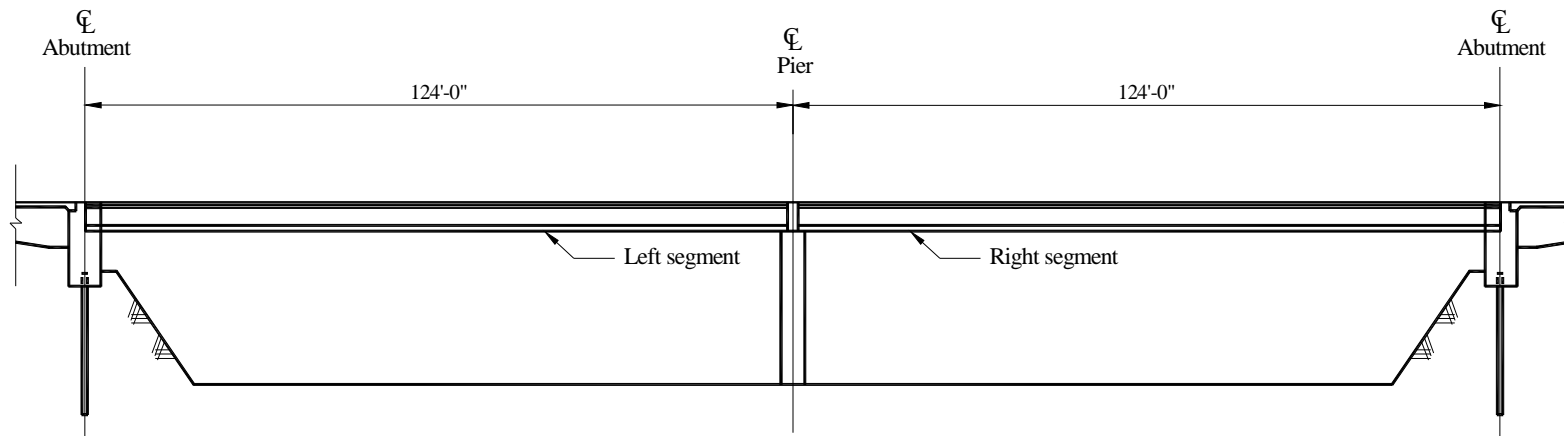
Stage 3: Construction of the diaphragm.

Stage 4: Post-tensioning.

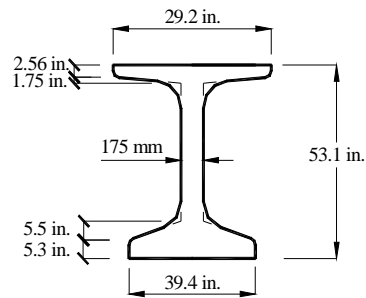
Stage 5: Placement of deck slab.

Stage 6: Construction of barriers

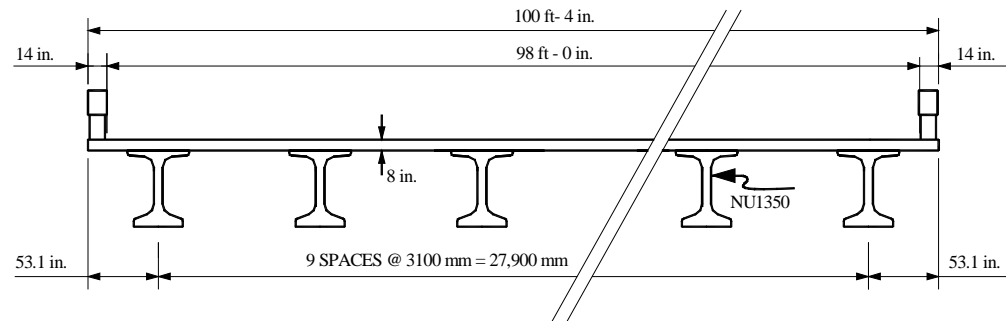
Additional Detailed Method input values are as follows. Relative humidity is 70%. Age at release is 1 day, age at post-tensioning is 30 days, age at deck placement is 60 days and age at final is 20,000 days. Post-tensioning secondary effect moment is 769k-in.



ELEVATION



SECTION - NU 1350
NOT TO SCALE



DECK CROSS SECTION
NOT TO SCALE

Figure 4.4.5.2-1 General Layout of the HW50 Bridge

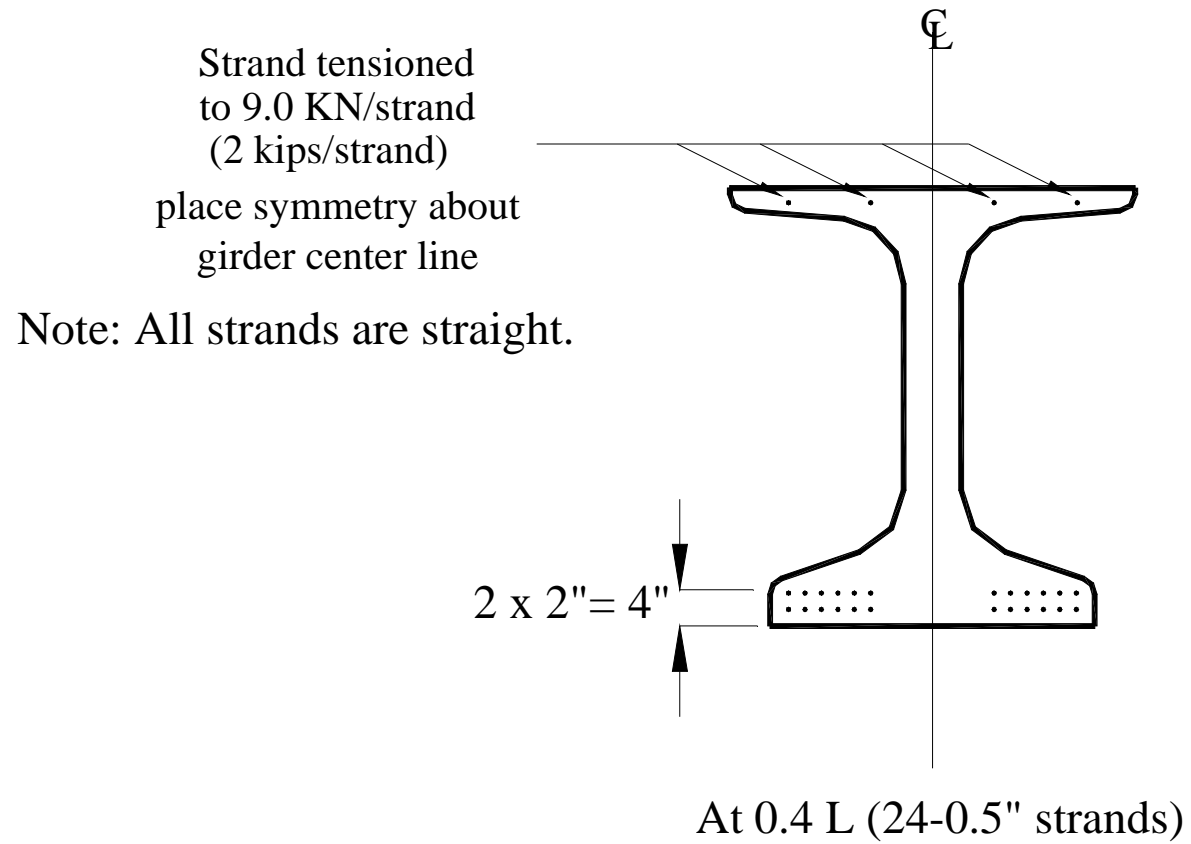
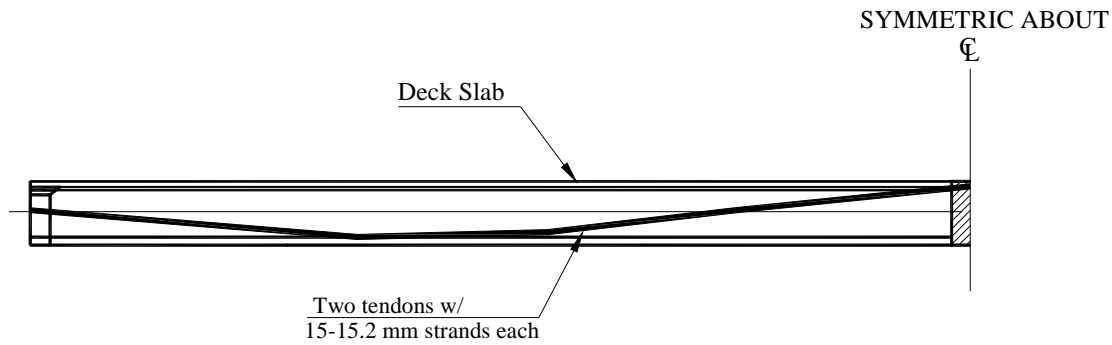
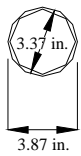


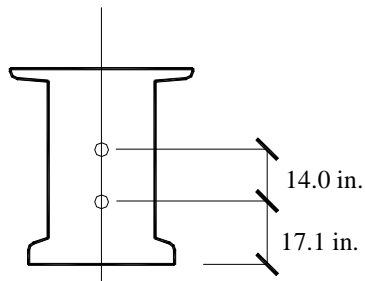
Figure 4.4.5.2-2 Pretensioning Scheme of the HW50 Bridge



POST-TENSIONING TENDON LAYOUT
NOT TO SCALE

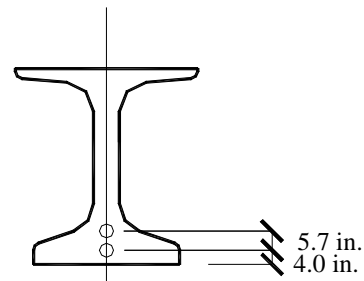


DUCT DETAIL
NOT TO SCALE



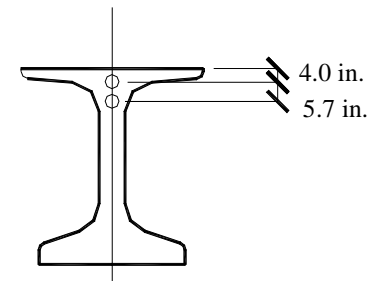
AT 0.4 L

NOT TO SCALE



AT 0.4 L

NOT TO SCALE



AT Pier

NOT TO SCALE

Figure 4.4.5.2-3 HW50 bridge post-tensioning details

The following is a time dependent loss comparison between the Detailed Method and Approximate Formulas.

	Detailed Method Loss (ksi)	Approximate Formula Loss (ksi)	Approximate Formula / Detailed Method Ratio
Formula #1 Pretensioning Loss At Time of Post-Tensioning	7.64	6.65	0.870
Formula #2 Pretensioning Loss At Final Time	29.23	32.69	1.118
Formula #3 Post-Tensioning Loss At Final Time	26.12	29.48	1.129

Table 4.4.5.2-1 Loss Prediction Comparison, Highway-50 Bridge

From the results above we see that all three approximate formulas conservatively predicted time dependent prestress loss in the pretensioning and post-tensioning steel in the Highway-50 Bridge. Formula #1 underestimated loss by 0.99ksi, or 13.0%. This value is within the 20% range found in the parametric study. Formula #2 overestimated loss by 11.8%. This is slightly outside of the 8% range found in the parametric study. Formula #3 was the most conservative, overestimating loss by 12.9%, slightly outside the 10% range in the parametric study.

There are a number of reasons for the overestimation of the approximate formulas for the pretensioning steel and post-tensioning steel at final time. One of the most conservative assumptions made during the parametric study was that cracking was not allowed in the precast section over the pier. This significantly increases the level of post-tensioning for a given span. The Highway 50 bridge used two tendons with 15 strands each, a total of 30 strands, and a jacking stress of 189ksi. This configuration would have resulted in a concrete tensile stress in the precast section over the pier with full live load greater than the 537 psi allowed ($0.19f'_c$). To keep the precast section from cracking over the pier with the given jacking stress of 189ksi, each girder line would have required three tendons with 12 strands each, 6 more strands than included in the bridge. This additional post-tensioning would have resulted in larger prestress loss predictions by the Detailed Method.

Another relevant assumption made in the parametric study is that the maximum stress in the tendon after friction and seating losses was $0.7f_{pu}$ or 189ksi. This usually allowed a jacking stress of 196ksi or so. The Highway 50 bridge used a jacking stress of 189ksi, lower than the 196ksi assumed in the study, which after friction and seating losses gave a stress at 0.4L of 179.1ksi. Had a jacking stress of 196ksi been used with the three tendon profile described above, the tendon stress at 0.4L would have been 185.2. The lower stress at 0.4L used in the Highway 50 bridge partially explains the reason for the lower loss predictions by the Detailed Method than the approximate formulas.

The list of assumption that were made in the development of the approximate formulas that would have caused them to estimate losses over-conservatively continues. The time at which deck placement was assumed to occur was 180 days. On the Highway-50 bridge Detailed Method analysis, the deck was placed at 60 days. Since deck placement reduces the compressive stress on the concrete at the location of the prestressing steels, an earlier deck placement would have reduced creep at final time.

A thicker deck was used on the Highway-50 bridge than was assumed. This would have resulted in a larger dead to live load ratio, reducing creep.

All of the above contributed to loss over-prediction by the approximate formulas.

4.5 CONCLUSIONS AND SUGGESTED RESEARCH

Approximate formulas have been developed to predict time dependent prestress loss in both pretensioning and post-tensioning steel in spliced girder bridges. The formulas are conservative and easy to use. The level of conservatism in loss predictions at final time is reasonable in two span bridges but less reasonable in single span structures. A wider range of bridge configurations needs to be investigated to confirm the accuracy of the formulas for two span applications and to modify the formulas, or possible develop new formulas, for single span structures. Formulas also need to be developed to predict these same losses in two-stage post-tensioned applications.

CHAPTER 5

POST-TENSIONING QUALITY CONTROL

5.1 INTRODUCTION

5.1.1 Problem Statement

The importance of protecting the corrosion sensitive post-tensioning steel has come into focus in recent years. After the collapse of two post-tensioned structures in England and the recent discovery of corroded tendons in several Florida bridges, many owners began to investigate their grouted post-tensioned structures more closely. Numerous investigations found that typical grout mixes, equipment, and procedures used in the past, as well as field inspection procedures, were not adequate to protect the post-tensioning steel. This research project seeks to determine what changes, if any, need to be made to the Nebraska Department of Roads Post-Tensioning Special Provisions to ensure that the full, corrosion free design life of post-tensioning tendons in Nebraska's bridges will be attained.

5.1.2 General Post-Tensioned Performance

Post-tensioned concrete (as opposed to pre-tensioned concrete) is a type of prestressed concrete in which the strands or bars are placed in longitudinal or transverse ducts and tensioned after the hardening of the concrete. The prestressing force is transferred through end anchorages such as the one shown in Figure 5.1.2 – 1.

Proper tendon grouting is critical to obtain the required structural bond and tendon corrosion protection. The primary causes of corrosion in post-tensioning tendons are standing bleed water,

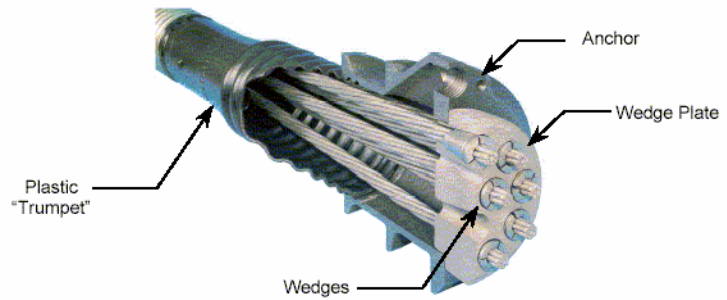


Figure 5.1.2 – 1 Post-Tensioning Anchorage

water infiltration, reactions caused by chemical admixtures, and exposure to de-icing chemicals. These often result from one or more of the following: the use of high bleed grout, poor design details, relaxed inspection oversight, relaxed construction and grouting operations and weak construction specifications. Each of these will be addressed in the following pages.

Post-tensioned concrete technology developed rapidly during the 1960s. In much of the work done since that time, the majority of grouts used in construction have been a simple mixture of Portland cement and water. Water cement ratios were typically specified between 0.47 to 0.53, with expansive and/or non-bleeding admixtures sometimes specified. In general these grouts appear to be performing satisfactorily. However, on some projects, especially in aggressive environments such as marine and northern climates where chlorides or sulphates were encountered, these grouts did not perform as expected (PTI Committee).

The focus of most of the attention surrounding post-tension tendon corrosion has been segmental bridge construction, and rightly so. By nature, segmental bridges are more susceptible to chloride ingress than their spliced concrete I-girder counterparts, even with

the, “no tensile stress allowed in the top of the deck after all losses, in the longitudinal and transverse directions”, requirement found in many post-tensioned box girder specifications . Joints between bridge segments have sometimes provided aggressive chloride ions unhindered access to the tendon duct. Wet joint spliced I-girder construction, although susceptible to its own set of problems, is a more corrosion resistant system.

With the wide spread use of new materials and technology in the last 10 years, the possibilities are far ranging with regard to additional controls that the Design Engineer can exert on the properties of the grout in both the fresh and the hardened states. These improvements are especially helpful in applications like bridge decks where de-icing salt is applied or in salt water environments, both of which may cause severe exposure of the post-tensioning elements.

It’s important to realize, before we begin the plunge into the recent national and international horror stories surrounding post-tension tendon corrosion, that historically, post-tensioned construction has had an excellent track record. Significant corrosion does not happen often. But when it does, the costs are high.

To illustrate the overall success of prestressed concrete bridge construction, the 1997 National Bridge Inventory taken by the Federal Highway Administration showed the following table:

Bridge Type	# of Bridges	Percent of Total	# Deficient	Percent of Deficient
Steel	196,741	42.2	63,930	61.2
Timber	43,446	9.3	20,896	20.0
Reinforced Concrete	141,558	30.4	19,421	18.6
Prestressed Concrete	84,400	18.1	3,170	3.0
Segmental Box	250	0.1	0	0.0
TOTALS	466,395		104,457	

**Table 5.1.2 – 1: Federal Highway
Administration National Bridge Inventory
Data, 1997**

Note that only 3% of prestressed bridges of all types (including post-tensioned) were found to be structurally deficient, and no segmental bridges were rated structurally deficient.

The second edition of ASBI’s “Durability Survey of Segmental Concrete Bridges”, published in September of 2002, found that, “segmental bridges are performing well with time”. The survey found no structurally deficient segmental bridges, and found that 99% had a superstructure rating of “satisfactory” (6) or higher on a scale of 0 to 9 with 0 being, “Failed condition, out of service, beyond corrective action”, and 9 being, “Excellent condition”. The survey also found prestressed concrete bridges to be the best performing system on the market. This survey is conducted every 5 years.

From these and other statistics we conclude that post-tensioned concrete bridge structures are good long term performers. We would do well to improve small problem areas rather than to seek an alternative system.

5.2 BACKGROUND AND LITERATURE REVIEW

5.2.1 Recent Problems

A look at the small number of post-tensioned bridges that have received so much attention nationally in recent years will also show the excellent performance of post-tensioned bridge technology. Internationally, England was the first location to have significant problems. In 1967 the Bickton Meadows footbridge collapsed suddenly due to tendon corrosion. It was built in 1952 and was of segmental construction with thin mortar joints. Both the precast units and mortar joints were of extremely poor quality. It was reported that the precast units were cracked and honeycombed when delivered to the site to the extent that grout appeared at the surface of the units during the grouting operation, i.e. grout squirted out of the bridge.

On December 4, 1984 at about 7:00am, the Ynys-y-Gwas bridge in the neighborhood of Port Talbot in Wales collapsed. It was a 60 foot long single span bridge of segmental construction. The investigation revealed that the segments were joined with thin, highly permeable mortar joints. Moisture, chlorides and oxygen had ready access to the tendons. Tendon corrosion took place at the transverse joints. There was no evidence of distress prior to failure (Woodward et. al).

These two collapses, along with a number of other less severe problems, led the United Kingdom's Ministry of Transportation to place a ban on the construction of new bonded post-tensioned bridges in 1992 – a very conservative response. This ban was partially lifted in 1996.

The United Kingdom's experience with precast segmental construction has been significantly different the United States'. Along with the two corrosion induced failures,

there have been a number of durability problems with bonded post-tensioned structures. Specifically these problems have been related to thin mortar joints, poor design and construction practices and mistakes made during the design and/or construction of the bridges (NCHRP 20-7). We conclude then that the problems in the U.K. are not due to intrinsic durability problems with precast segmental bonded post-tension construction. Lessons can still be learned, however, including the need for more stringent grouting requirements and inspection procedures to insure that post-tensioned tendons are completely encapsulated in a high quality grout.

Now turning our attention closer to home, in the spring of 1999 an examination of the 234 post-tensioned tendons on the Niles Channel Bridge in Florida revealed severe corrosion damage on two of these tendons. The Niles Channel Bridge is a 4,580ft low-level externally post-tensioned segmental bridge over seawater. It was concluded that initial corrosion was a result of the absence of grout due to bleed in the corroded areas. It was also concluded that corrosion continued due to the voids being recharged with water leaking through the concrete cover at the anchorages. One tendon was replaced. (FDOT, May 2000)

On August 28, 2000 during a routine inspection of the Mid-Bay Bridge in Florida (one of two inspections the bridge receives each year), “significant distress” was noted in a post-tensioning tendon. Mid-Bay is a 141 span, 19,270ft long precast segmental externally post-



Figure 5.2.1-1 First Distressed Tendon Discovered on The Mid-Bay Bridge

tensioned bridge. The polyethylene sheathing surrounding the distressed tendon was cracked, exposing the tendon's high strength prestressing strands and surrounding grout. Several strands were fractured as shown in Figure 5.2.1-1.



Figure 5.2.1-2 Mid-Bay's "Pulled Out" Tendon

This observation led to an immediate "walk-through" inspection to check for similar distress in other tendons. During this inspection it was discovered that a tendon in another span had failed by pulling out of the expansion joint diaphragm, along with its steel duct (Corven 2001) as shown in Figure 5.2.1-2, a traumatic sight for any bridge engineer. The anchor head of the failed tendon is shown in Figure 5.2.1-3.

A rigorous inspection regiment followed consisting of bore-scope inspections, vibration testing, Mag-Flux testing and a number of others. It became clear that the tendons of the Mid-Bay Bridge were not grouted as specified. Little or no grout was found in the anchorage immediately behind the anchor head of the failed tendon. As a result of this discovery, each of the remaining ten anchors in the span containing the failed tendon were bore scoped. Each of these anchorages showed significant voids in the anchors and corroded strands. Grout quality was found to be a primary cause for the presence of voids. Eleven of Mid-Bay's 840 tendons were replaced in 2000.



Figure 5.2.1-3 Anchor Head of Mid-Bay's Failed Tendon

Another noteworthy grouting problem was discovered in Florida's I-75/I-595 interchange. It consists of nine precast segmental box girder bridges, each of internal bonded post-tensioned construction with epoxy joints. It was constructed between 1986 and 1989. During a routing inspection water leakage was discovered at a few joints. In the process of repairing these joints, a number of ungrouted ducts were found. The corrosion dangers are obvious, as well as the unbonded construction that was assumed to be bonded in design.

And finally Florida's Sunshine Skyway Bridge, constructed in 1986, has perhaps received the most attention of any U.S. bridge reported to have experienced tendon corrosion problems. The bridge is located over lower Tampa Bay on the west coast of Florida and has a total length of 4.1 miles. It consists of a 4000



Figure 5.2.1-4 Florida's Sunshine Skyway Bridge

foot cable stayed main span as well as high and low-level approach spans. During a routine inspection of high-level approach pier interiors in August of 2000, severe tendon

corrosion was discovered in one of the piers. A comprehensive inspection followed. Three of the four post-tensioning tendons in the troubled pier were severely corroded. One of these tendons



Figure 5.2.1-5 Corroded Tendon at Anchorage in Sunshine Skyway's Troubled Pier

had experienced failure in 11 of its 17 strands. The grout material found in the cap region of this pier at the corrosion locations was chalky and weak. High chloride content permeated the corrosion protection system. Figure 5.2.1-5 shows the corroded tendon at the anchorage location. The pour backs in a number of piers were found to have cracks that could allow water to leak into voided areas inside trumpets and permeate the chalky grout to areas below the trumpet. Other problems were found as well. Significant tendon corrosion problems were found in the pier cap as well as on internal tendons. Grout in some columns had been contaminated with chloride. Also, a significant number of vertical external tendon polyethylene ducts had cracks and/or hollow sounding areas. Repair costs were approximately \$150,000.

Contrary to appearances at this point, all the United States' problems haven't been in Florida. The Boston Central artery felt the influence of tendon corrosion as well, but at a different stage in the process. Problems with the Sunshine Skyway prompted extensive inspection of the project during construction. During inspections bleed water voids were discovered as well as some large voids in ducts in both segmental and precast structures. Officials immediately alerted the grouting crews to the problem and changed the grout specification to a thixotropic grout. No corroded tendons were found.

So how do all these problems show the excellent performance of post-tensioned construction? It would seem quite the opposite – that these problems show poor performance. The fact that each one of these instances of corrosion is so earth shattering to the post-tensioning community and so widely publicized is testimony in itself to the scarcity of such problems. Tendons in post-tensioned bridges rarely experience significant corrosion. So when they do, everyone hears about it. Worldwide experience

with grouted tendons for over half a century has proven that cementitious grout provides excellent protection for prestressing steel. What we are observing is a potential Achilles Heel with the system, not a fundamental flaw. So protect the heel well.

5.2.2 The Engineering Community Responds

The flood gates of post-tensioning corrosion prevention literature have opened in the last ten years or so in an attempt to combat the rare but still frustratingly present case of post-tensioning steel corrosion. Articles, bulletins, and conference papers covering everything from tendon durability to grouting, plastic duct systems, factory applied corrosion protection, grouting admixtures, thixotropic grout, bleed testing, etc...

The Post-Tensioning Institute responded with their Specification For Grouting of Post-Tensioned Structures. Many of the revisions made to the Nebraska Department of Roads' Post-Tensioning Special Provisions are based on recommendations made in this document. It is intended to provide minimum requirements for the selection, design and installation of cementitious grouts and ducts for steel post-tensioned systems used in concrete construction. It was first published in February of 2001, has been updated once and has a second update on the way soon. The Nebraska Department of Roads' Special Provisions update was based partially on the most recent and as of yet unpublished version.

It was post-tension tendon corrosion that served as the catalyst for the American Segmental Bridge Institute's Grouting Certification Program. This training has taken place four times so far – in the fall of 2001, twice in 2002 and in the spring of 2003. A fall 2003 training is also scheduled. The author had the privilege of attending the spring

2003 training. The purpose of the ASBI training program is to provide supervisors and inspectors of grouting operations with the training necessary to understand and implement grouting specifications for post-tensioned structures. It's not designed primarily with the engineer in mind, but engineers can gain great insight into the world of grouting (yes, it is its own world) by attending the training.

5.3 GROUTING

5.3.1 Grout for Post-Tensioning Steel Corrosion Prevention

One of the two primary purposes of post-tension grout is the prevention of corrosion. The other purpose being structural bond, of course. Neither of these purposes is achieved when the tendon is not completely surrounded by grout as shown in the bore scope photo in Figure 5.3.1-1 (FDOT).



Figure 5.3.1-1 Bore Scope Photo Showing an Ungrouted Section of Tendon in the Mid-Bay Bridge

Post-tensioning grout is made up of Portland cement, potable water, various admixtures and pozzolans with no coarse aggregate and usually no fine aggregate. Basic properties used to describe a grout are bleed, segregation, permeability, fluidity, set time, strength and volume change. The most important of these for our purposes will be bleed. Properties like segregation and permeability are also important for corrosion prevention, but a grout that has good anti-bleed properties will necessarily have low permeability and not segregate.

A review of some of the basics of steel corrosion in concrete will help us to see the importance of post-tensioning grout. When water and oxygen are in the presence of steel,

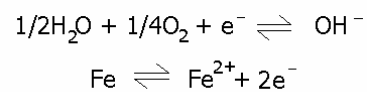
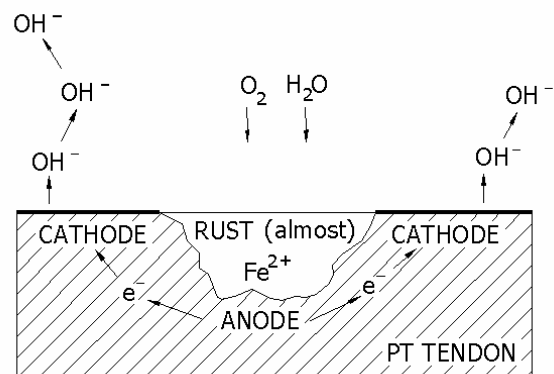


Figure 5.3.1-2 Initial Reaction Leading To Rust

redox potential exists. Redox potential is simply the presence of electromotive forces, i.e. electrons wanting to move. This potential leads to the oxidation (loss of electrons) of iron in the steel. Steel is defined as iron that contains carbon up to about 1.7% as an essential alloying constituent. Along with the iron oxidation, the reduction (addition of electrons) of water and oxygen in contact with the steel forms hydroxide ions (OH⁻). This redox reaction is illustrated in Figure 5.3.1-2. The rusting steel surface acts as the anode, gaining electrons and forming an iron cation. The adjacent steel surface acts as the cathode, losing electrons and forming hydroxide. The Fe cations (Fe⁺⁺) are subsequently changed to oxides of iron by a number of complex reactions that go beyond the scope of this explanation. The volume of the reaction products is several times the volume of the iron.

Both concrete and grout normally provide reinforcing steel with excellent corrosion protection. The high alkaline (basic, having a pH > 7) environment in concrete results in the formation of a tightly adhering oxide (OH⁻) film which passivates the steel and protects it from corrosion. “The exact composition of the thin and normally

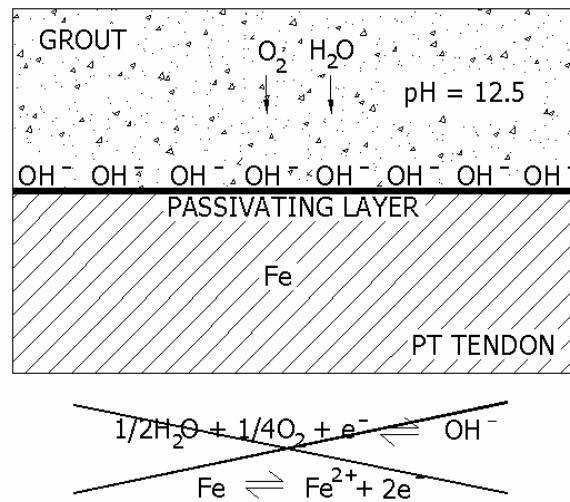


Figure 5.3.1-3 Passivating Film Formed By Good Quality Grout

invisible film has been difficult to determine. It seems clear, however, that it is made up of chemical combinations of oxygen and is simply called an oxide film.” (ACI

Committee 222). The integrity and protective quality of the film depend on the alkalinity of the environment. Since grout has a pH higher than 12.5, it is usually an excellent medium for protecting steel from corrosion. Figure 5.3.1-3 illustrates the passivating layer formed on post-tensioning steel by good quality grout. This is all in addition to the grout acting as a low permeability barrier that prevents corrosive agents from gaining access to the steel.

There are a number of different theories that attempt to explain exactly what happens when chlorides (Cl⁻) come in contact with this oxide film. One way or another, chlorides break down the film and accelerate the reaction beyond that which occurs when water and oxygen come into contact with unpassivated steel. “Only under

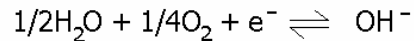
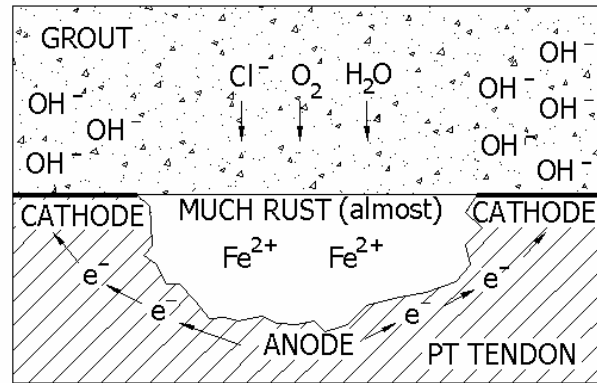


Figure 5.3.1-4 The effect of Chlorides On Steel Corrosion

conditions where salts are present or the concrete cover has carbonated does the steel become vulnerable to corrosion” (ACI Committee 222). Figure 5.3.1-4 illustrates this reaction.

In addition to these corrosion issues, high-strength steels, like those used in post-tensioning, suffer from additional corrosion woes. High strength prestressing steels show a far more sensitive reaction to corrosion attack than reinforcing steels. For example, if a mild reinforcing bar loses half of its cross sectional area, it loses about half of its

capacity. If a wire of a prestressing strand loses half of its cross sectional area, it may lose closer to $\frac{3}{4}$ of its capacity. Strands, having a very high strength and relatively large ratio of surface to cross-sectional area, has to be protected against corrosion



Figure 5.3.1-5 Typical Corrosive Pitting Found in the Sunshine Skyway's Corroded tendons

to a high degree. Figure 5.3.1-5 shows typical corrosive pitting found in the Sunshine Skyway's troubled pier (FDOT).

5.3.2 Bleed

Bleed is the process of sedimentation of a solution – in this case water and solid particles consisting of cement, admixtures, and pozzolans or fine sand, if used. Bleed water tends to migrate to higher points or in long tendons, may congregate at

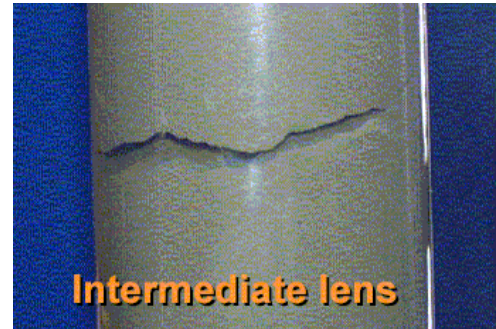


Figure 5.3.2-1 Grout Column with Intermediate Lens Formation

intermediate lenses. Separated water can become trapped in the tendon. Figure 5.3.2-1

shows an intermediate lens (VSL). Bleed is a small problem for concrete but can be devastating to a post-tensioning grout.

For strand type tendons there is also an additional mechanism of water transport. Seven-wire strands consist of six wires wrapped spirally and tightly around a slightly larger diameter center wire. The space between the six wires is large enough to permit passage of water, but not most of the cement particle sizes. Figure 5.3.2-2 shows the

interstitial areas in a 7-wire strand (FDOT).

The water can then travel through the interstitial areas between the core wire and the outer wires. Since the specific gravity of grout is about twice that of water, the water is forced through the spaces between the outer wires and up the strand causing exaggerated

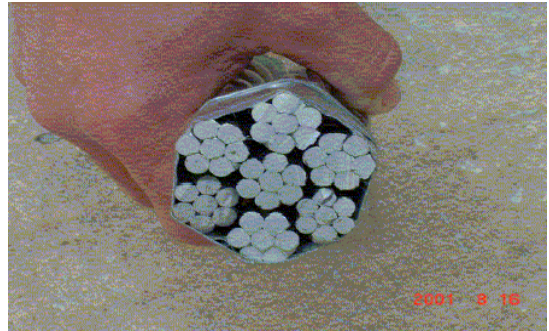


Figure 5.3.2-2 Interstitial Areas Of 7-Wire Strands

bleed. This is known as “wicking”. Wicking generally transports water along the length of the strand to the highest point. It actually reduces, but does not eliminate, the formation of intermediate lenses because it reduces the w/c ratio of the filtered grout.

Bleed can be a long-term concern in post-tensioned grout applications. Bleed water trapped in the duct cannot be readily evaporated. It is usually reabsorbed by the hardened grout and results in a void. Whether there is a void or entrapped bleed water, potential corrosion sites exist particularly if corrosion-causing contaminants are available. Corrosion often initiates before the bleed water has a chance to be reabsorbed. This can be due to the presence of corrosive agents in the bleed water taken from admixtures.

Bleed pockets typically form at high points in the duct due to bleed water traveling upwards. This high point may be at the top of a vertical duct, at an anchorage region, or at the crest of a draped tendon. Higher vertical rises result in

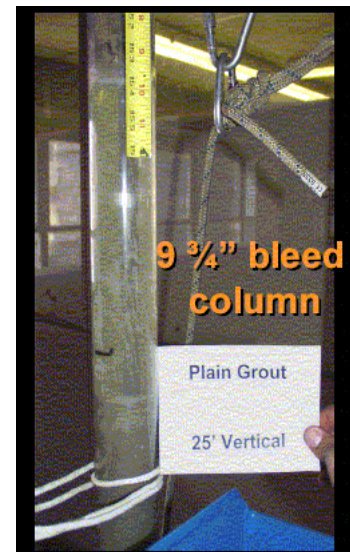


Figure 5.3.2-3 Bleed in Vertical Tendons

higher pressure heads and will require stronger anti-bleed properties. The amount of bleed may be considerable in a grout that does not contain bleed-reducing agents (Schokker 2003). Figure 5.3.2-3 shows bleed at the top of a twenty five foot tall duct containing a 7-wire strand and a standard water-cement grout (VSL). Almost ten inches of bleed accumulated. This speaks volumes to understanding Florida's pier grout bleed problems.

5.3.3 Thixotropic Grout

In order to achieve low or no bleed grout, in most cases a thixotropic grout consistency is required. Merriam-Webster's defines thixotropy as, "the property of various gels of becoming fluid when disturbed as by shaking" (Merriam-Webster) Ketchup is an example of a material that has a certain degree of thixotropy – when you hit the bottle you provide the agitation to start it flowing. Thixotropy is also a desirable quality to have in paint.

A thixotropic grout is simply one that exhibits gel-like properties at rest, but that becomes fluid when agitated (by mixing and pumping). The anti-bleed property of thixotropic grout causes it to retain water rather than allowing segregation. A gelling agent (also known as a thixotropic agent or stabilizer) must be added as an admixture to the grout to achieve strong anti-bleed and thixotropic properties. The degree of bleed resistance required is related to the elevation change of the duct. Ducts with larger elevation changes will typically experience more bleed due to the increased driving pressure at the bottom of the grout column. Prepackaged grouts with strong anti-bleed properties are likely to contain this type of admixture. The anti-bleed admixtures tend to

increase set time, but when used at the proper dosage set times remain under 12 hours (Schokker 2003). Fly ash and silica fume may, but will not necessarily, reduce bleed and contribute to thixotropy to a lesser extent. Admixtures such as viscosity modifiers, superplasticizers and expansive admixtures do not make a grout thixotropic and are not adequate alone to control bleed. Proper proportions of high range water reducer and a gelling agent will provide optimum anti-bleed characteristics (Schokker 2003).

Even though the bleed water can be controlled with a water retentive admixture, there is a plastic reaccommodation of the grout, prior to grout setting, which will reduce the vertical height of the grout (Schokker 2003). To ensure more complete filling of the duct, admixtures that cause grout expansion during the plastic stage may be used. Expansive admixtures, however, are not a solution to bleed and should not be used as such.

After years of using cement-water (non-thixotropic) grouts, most thixotropic grouts may look “too thick”, leading to the misconception that they will be difficult to pump. Actually, grout with a given w/c ratio will pump more easily if the water is not allowed to separate (Schupack 1984). Thixotropic grout is just a different type of material and we must re-

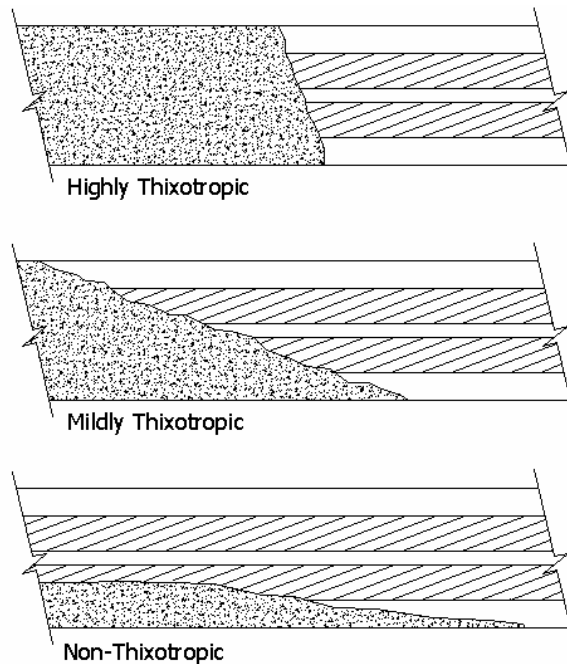


Figure 5.3.3-1 Change In Flow With Degree Of Thixotropy

educate ourselves to be comfortable with its properties.

Different grout mixes will exhibit very different flow patterns. Highly thixotropic grouts will tend to flow as a wall of grout, filling the entire duct cross-section as the grout front progresses, “including the interstices in the strand.” (Schokker 2003) This conclusion by Schokker seems to contradict our understanding of the wicking process, but is an interesting observation, none the less. Wicking occurs because water is able to penetrate between the wires in the strand but cementitious particles are not.

Non-thixotropic grouts will flow more like water. Figure 5.3.3-1 illustrates the difference in flow between grouts with varying degrees of thixotropy. Most prepackaged grouts will exhibit flow somewhere in the range between highly and mildly thixotropic (Schokker 2003). A highly thixotropic grout can actually push water through the duct without becoming mixed with it. This helps ensure that the grout mix in the mixer is the same grout mix that is in the duct. It also means that for relatively shallow drapes, high point vents may be less critical.

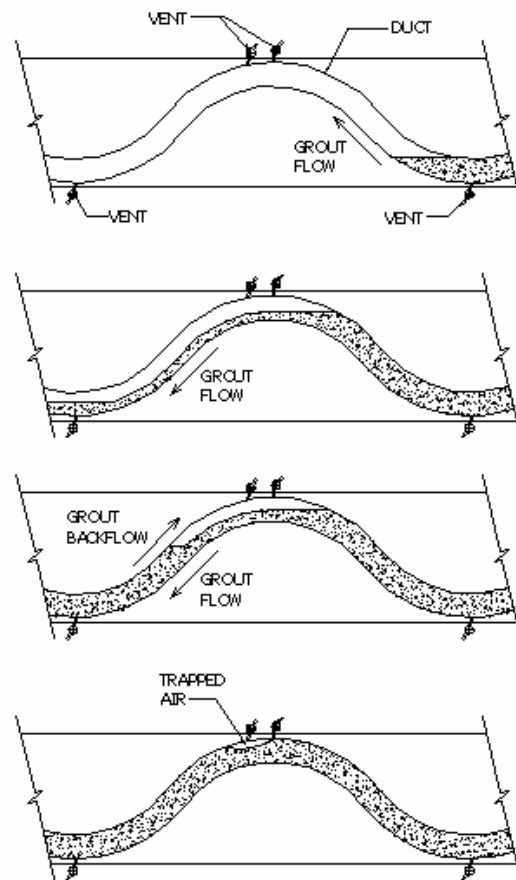


Figure 5.3.3-2 Non-Thixotropic Grout Flow, Backflow, and Proper Venting at Crest of Draped Tendon

In a draped duct, non-thixotropic grout will run down the slope in the duct, filling the bottom of the duct first, and then backflow. This backflow will entrap air and any water that remains in the duct, making proper venting critical. Backflow is illustrated in Figure 5.3.3-2. Notice the two vents at the tendon crest. Investigations have shown that there is a tendency for air and water voids to form just past duct high points (PTI 2001). A second vent located a minimum of three feet beyond the crest vent is recommended to remedy the problem.

5.3.4 THIXOTROPIC GROUT TESTING

Tests are available to test for a variety of grout properties from permeability to volume change to strength. Two of the most important tests with respect to corrosion prevention are bleed and fluidity.

5.3.4.1 BLEED TESTING

Conventional means for testing bleed of grout are described in ASTM C 940. This test method calls for the placement of a freshly mixed grout sample into a 1000mL graduated cylinder. The grout is allowed to sit undisturbed for 3 hours with periodic measurements of the total sample settlement and volume of bleed water. Following the allotted time, the bleed water is decanted and the volume is measured and reported as a percentage of the original volume.

This procedure does not subject the grout sample to column pressure (as in tendons with a vertical rise) nor the wicking effect of prestressing strand and, therefore, is not representative of field conditions. An alternative method investigated involves a

slight modification to the ASTM C 940 method as photographed in Figure 5.3.4.1-1 (VSL). A multiple strand bundle can be placed in the graduated cylinder to simulate the filtering effect. Care must be taken to make sure that the strand wires do not separate during cutting. If the strand weave is loosened during handling, it will have less wick action and will not be representative of field conditions.



Figure 5.3.4.1 – Modified ASTM C 490

Also, this method does not account for the higher pressure in tall tendons. However, a test method has been developed that combines the filter effect and higher pressure to test grouts for use in tall prestressing tendons. The apparatus consists of a commercially available filtration funnel, stand, pressure supply with gauge and valve, and bleed water collection container as shown in Figure 5.3.4.1-2. The procedure involves filling the funnel with grout, screwing the cap on the funnel, placing the funnel in the frame, connecting the air supply, allowing grout to rest in the funnel for ten minutes, pressurizing the funnel to the desired level to simulate a given vertical rise, maintain pressure for five minutes, recording bleed water volume



Figure 5.3.4.1-2 Schupack Filter Test Setup

and correlating the bleed volume with allowable bleed volumes for a given vertical rise. A complete description of the apparatus and procedure can be found in the PTI Guide Specification. It is also included in the revised Nebraska Department of Roads Post-Tensioning Special Provision.

5.3.4.2 Fluidity

The standard test for fluidity/pumpability has been the flow cone (ASTM 939). This test was appropriate for plane cement-water grouts of the past, but is not effective in measuring the pumpability of highly thixotropic grouts. A modified version of the standard flow cone, called the modified flow cone method in the PTI Guide Specification for Grouting of Post-Tensioned Structures, was developed in the 1970s. In order to maintain a driving head on the grout in the flow cone, the grout is filled to the top of the cone. The time to fill a liter container is the flow time.

Since we are most interested in the water content of the grout, it follows that we would want to check the density. The flow cone has traditionally been the method of choice for verifying water content but may not be a reliable indicator of such because flow cone efflux times vary depending on a number of factors other than water content. A common way to check



Figure 5.3.4.2-1 Mud Balance Test

density in the field is through the use of a mud balance. This test is quick and easy, as shown in Figure 5.3.4.2-1 (ECO Grouting Specialists, Ltd.). The cup is filled with grout

and capped, the outside is wiped off to remove excess grout, and the balance is used to find the density of the grout. Grout densities range from 1.7 to 2.3 relative to water. In the field, the mud balance reading should stay at or above the minimum reading used for prequalification testing to limit water content beyond that tested in the lab. Using the mud balance in conjunction with the flow cone ensures that the grout pumped into the ducts is as close to the grout tested in the lab as possible.

5.3.5 EARLY HISTORY OF THIXOTROPIC GROUT

Thixotropy, as a desirable property for fluids in a variety of engineering applications, is nothing new. Neither is the desire for a thixotropic post-tensioning grout. Only in recent years has its value been widely recognized. Since the late 1960s, however, research has been done on the development of thixotropic grouts for tall vertical tendons. Morris Schupack was the lead man in the early years of thixotropic grout development.

The earliest research in this area was in an attempt to allow power companies to move from unbonded to bonded tendons in their secondary nuclear containment structures. A thixotropic admixture for grouting 150 ft tall tendons was developed in the late 1960s to this end. At that time, the ability for grout to penetrate between single wire tendons bunched together on a tight radius was unknown. Research addressed grout sedimentation and penetration (Schupack 1970).

Schupack observed some interesting phenomenon. He says, *“It is also important to remember that in the first 8 to 10 hours after mixing, the free water at the top (of the test specimen) has to be observed because it has been found that re-absorption of the water occurs, and the bleeding phenomenon is obscured.”* The fact that bleed water is

reabsorbed by the hardened grout leaving a void in a duct is a well established phenomenon. He also observed that locking off the tendon under pressure did not help the problem of sedimentation and resulting voids.

Tests were performed to better understand wicking. Strand pulled through a die after stranding, leaving smaller interstitial areas, were tested against standard strands and loosely twisted strands. Strand pulled through a die exhibited wicking similar to strand not pulled through a die. Loosely twisted strand contained areas between the outer six wires too great to act as a filter.

Laboratory and field tests with the gelling agent consistently showed the elimination of sedimentation in bar type tendons. Surprisingly, however, the gelling agent tested performed poorly on strand type tendons – a difficulty to be overcome with future research. Methods were recommended to remove bleed water from the top of grout columns. Schupack also found that it was difficult to completely surround single wire

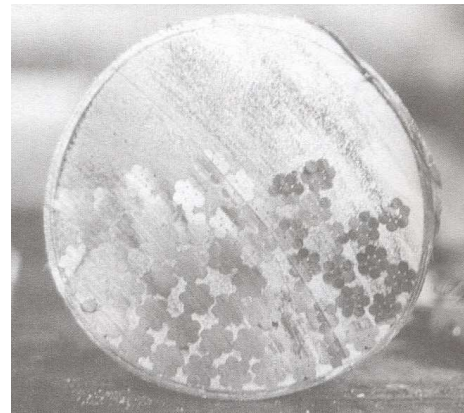


**Figure 5.3.5-1 Tendon Section,
Grout Penetration Between
Strands**

tendons on a curvature with grout, but that strand type tendons did not have this problem. Figure 5.3.5-1 shows a section of a tendon tested by Schupack in the 1960s. Thixotropic grout was found to penetrate between strands well, even in large tendons.

Schupack continued the development of his gelling admixture with a view toward grouting 200ft tall strand type tendons in another nuclear containment structure (Schupack 1974). The benefits of mixing with a shear mixer and pre-blending the

admixture with the cement were recognized, as well as the need to develop a testing method for bleed resistance that could simulate the pressure head and bleed exhibited by a tall column of grout. An appropriate pressure filter test was developed. (see Figure 5.3.4.1-2) Thixotropic grout pumpability, penetrability, setting time, strength, and porosity were also examined. An admixture was successfully developed to meet the 200ft demand, accompanied by the following conclusion: “...for tendons with any vertical rise, the proper use of the grouting admixture (thixotropic agent) will greatly minimize or eliminate the bleed phenomenon.” Just to emphasize the point, this was thirty years ago.

In more recent years, research has been conducted to directly correlate the results from the Schupack Filter Test to the bleed resistance in a strand type tendon with a given elevation change and pressure head to aid in determining the required bleed resistance (Schokker 2002). In other words, if you have a given elevation change, what results do you need from your grout using the Schupack filter test to ensure that you will not have bleed. The recommendations resulting from these tests were included in the Post-Tensioning Institute’s “Specification for Grouting of Post-Tensioned Structures”. The Federal Highway Administration and the Texas Department of Transportation, along with others have conducted pressure filter testing of many different grout formulations. The conclusion in many cases has been to specify commercially available pre-bagged grout instead of a grout developed in house. It might not sound like such a difficult undertaking, but developing a zero-bleed but still fluid post-tension grout with acceptable permeability, segregation, set time, strength, and volume change characteristics that does not contribute to steel corrosion is a daunting task. The post-tensioning industry is

leaning heavily toward the use of pre-bagged grouts. Many state agencies have updated their grouting specifications accordingly. Florida, the United States' very own 54,000 sq. mi. corrosion laboratory, has been a leader in this area. This is also reflected in the revised Nebraska Department of Roads Post-Tensioning Special Provision.

5.3.6 Thixotropic Grout Mixing

A special kind of mixer called a colloidal or high shear mixer comes strongly recommended by thixotropic grout manufacturers. Mixing action that typically occurs as concrete is mixed in a paddle mixer does not occur with post-tensioning grout. As the paddles churn the concrete, coarse and fine aggregate grind together and break up lumps of cementitious material. And even with this mixing action, concrete mixes containing silica fume, with its incredibly small particle sizes, sometimes still contain lumps.

Post-tensioning grout has no coarse aggregate and rarely contains fine aggregate. The mixing action in regular concrete that serves to break up lumps of cementitious material is absent. Thixotropic grouts often contain silica fume. Therefore, complete particle wetting in a post-tension grout is very difficult without a mixer suited to the task.

The problem is amplified with thixotropic grouts. The consistency of the gel that forms when the grout is at rest and consequently its bleed resistance depends highly on the degree of particle wetting. A highly thixotropic grout may be only mildly thixotropic if not mixed well.

Therefore thixotropic grout manufacturers often specify colloidal mixers. Figure 5.3.6-1 is a picture of a typical colloidal mixer. A colloid is simply a substance that consists of particles dispersed throughout another substance. A colloidal mixer is

designed to mix such substances. The “mixer” in a colloidal mixer is a high shear centrifugal pump. The inlet and outlet of the pump facilitate a circulation of the grout around the mixing tank.. This type of mixing provides far greater particle wetting than a standard paddle mixer. Mixing drums are typically between eight and thirteen cubic feet.

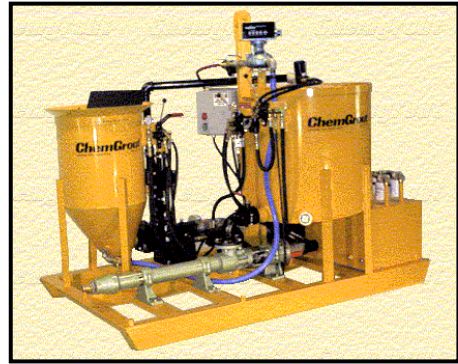


Figure 5.3.6-1 Colloidal Mixer

The grout plant containing the colloidal mixer must also contain an agitated storage tank. Thixotropic grout cannot be allowed to remain unagitated. Its thixotropic characteristics cause it to gel quickly. After mixing but before being pumped into the duct, the storage tank applies a degree of mechanical agitation to the grout much lower than the mixer. It may be a paddle mixer itself. The storage tank will be at least as large as the mixing tank.

5.4 INVESTIGATIVE METHODS

This section of the report deals with non-destructive evaluation techniques applied to post-tension tendons and ducts.

5.4.1 Borescope Inspection

A bore scope consists of a slender rod with a miniature camera mounted on the end. The camera's images are sent to a data acquisition system and then to a real-time monitor. The mini camera is inserted

into the post-tensioning duct via an approximately 3/4" diameter hole drilled in the concrete. Bore scope inspections have been used successfully to locate voids in grouted tendons worldwide.

Once the duct is located, this is by far the most reliable method of detecting

voids in grout. It is only mildly destructive, the damage being easily repaired. Figure 5.3.1-1 showed a bore scope photo of an ungrouted section of tendon in the Mid-Bay Bridge in Florida (Goni). Figure 5.4.1-1 shows typical patched bore scope inspection holes in a bridge deck in Ft. Lauderdale, Florida.

Although completely non-destructive evaluation of internal post-tensioned tendons is ideal, small scale destructive evaluation, like drilling holes for bore scope inspection, should be considered acceptable.



Figure 5.4.1-1 Ft. Lauderdale Airport Access Bridge in Florida

5.4.2 Impact Echo Testing

Impact-echo is a nondestructive testing technique typically used to locate discontinuities such as internal voids, cracks and delaminations in concrete. It has also been used to locate voids in grouted tendons. The impact-echo method uses a mechanical device to introduce a stress pulse to the surface of the concrete. These stress waves are reflected by internal interfaces (cracks, voids, rebar, etc.) and by boundaries of the structure. Reflected waves arrive at the surface where impact has occurred and produce displacements, which are measured by a receiving transducer. In principle, impact-echo is similar to a number of other non-destructive evaluation methods. Therefore, a considerable amount of time will be dedicated to it relative to other NDE methods in the following discussion. ASTM C-1383 gives a detailed description of impact-echo equipment and technology. Much of the following information relating to the impact-echo method was taken from Carino.

In practice, impact-echo testing relies on three basic components: 1) a mechanical impactor capable of producing short-duration impacts, the duration of which can be varied, 2) a high-fidelity receiver to measure the surface response, and 3) a data acquisition-signal analysis system to capture, process, and store the waveforms of surface motion. In order to accurately measure the surface motion, the transducer (high-fidelity receiver) has to be coupled effectively to the concrete surface. For most transducers, some type of grease-like material



**Figure 5.4.2-1
Commercial Impact-Echo
System**

is often used as a couplant. Modern impact-echo instruments are based on portable computers with data acquisition cards and accompanying software. Figure 5.4.2-1 shows the three components of a commercial impact-echo test system being used to test the web of a reinforced concrete beam (Carino).

When a disturbance is applied suddenly at a point on the surface of a solid, such as by impact, the disturbance propagates through the solid as three different types of waves: a P-wave, an S-wave and an R-wave.

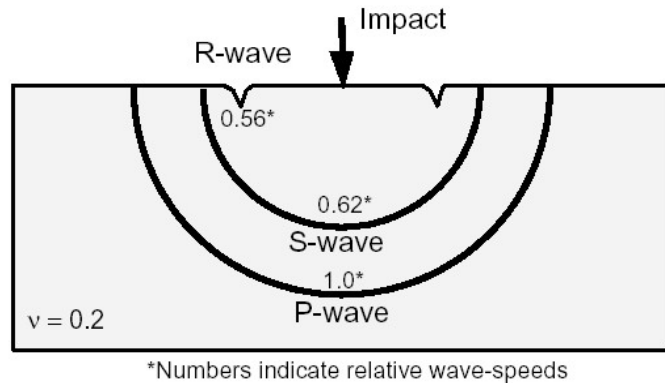


Figure 5.4.2-2 Stress Waves Caused by Impact at a Point

As shown in Figure 5.4.2-2, the P-

wave and S-wave propagate into the solid along spherical wave fronts. The P-wave is associated with the propagation of normal stress and the S-wave is associated with shear stress. There is also an R-wave that travels away from the impact along the surface.

The P-wave speed, S-wave speed and R-wave speed are each related to the Young's modulus of elasticity, E , Poisson's ratio, ν , and the density, ρ , of the material. For a Poisson's ratio of 0.2, which is typical of concrete, the S-wave speed is 61% of the P-wave speed and the R-wave speed is 92% of the S-wave speed.

When a stress wave traveling through material 1 is incident on the interface between a different material 2, a portion of the wave is reflected. The amplitude of the reflection is a function of the angle of incidence and is a maximum when the angle is 90° .

Figure 5.4.2-3 is a diagram of an impact-echo test on a plate with a large air void below the surface, similar to the slab shown in Figure 5.4.2-4. The P- and S-waves are reflected by internal defects or external boundaries.

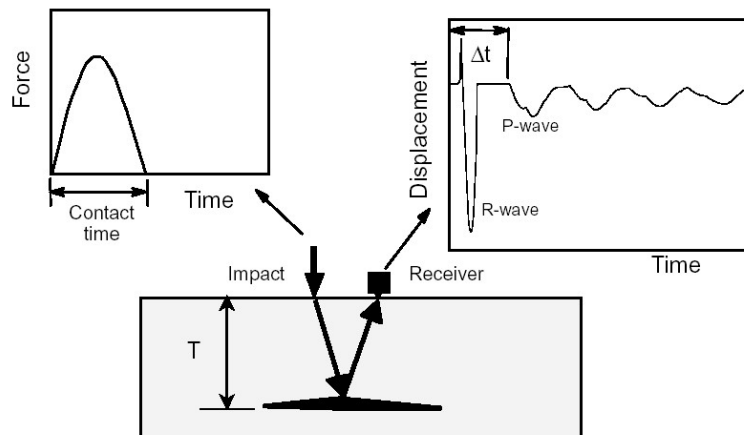


Figure 5.4.2-3 The Impact Echo Method

When the reflected waves, or echoes, return to the surface, they produce displacements that are measured by a receiving transducer. If the transducer is placed close enough to the impact point, the response is dominated by P-wave echoes (Carino). The right side of Figure 5.4.2-3 shows the pattern of surface displacements that would occur. The large downward displacement at the beginning of the waveform is caused by the R-wave, and the series of repeating downward displacements of lower amplitude are due to the arrival of the P-wave as it undergoes multiple reflections between the surface and the internal void.

A key development leading to the success of the impact-echo method was the use of frequency analysis of the recorded waveforms. In frequency analysis of impact-echo results, the objective is to determine the dominant frequencies in the recorded waveform. This is accomplished by using the fast Fourier transform technique to transform the recorded waveform into the frequency domain (Bracewell cited by Carino). The transformation results in an amplitude spectrum that shows the amplitudes of the various

frequencies contained in the waveform. For plate-like structures, the thickness frequency will usually be the dominant peak in the spectrum. The value of the peak frequency in the amplitude spectrum can be used to determine the depth of the reflecting interface.

Figure 5.4.2-4 illustrates the use of frequency analysis of impact-echo tests. The left graph shows the amplitude spectrum from a test over a solid portion of a 0.5 m thick concrete slab. There is a frequency peak at 3.42 kHz, which corresponds to multiple P-wave reflections between the bottom and top surfaces of the slab. The right graph shows the amplitude spectrum from a test over a portion of the slab containing a disk-shaped void.

The peak at 7.32 kHz results from multiple reflections between the top of the slab and the void (Carino).

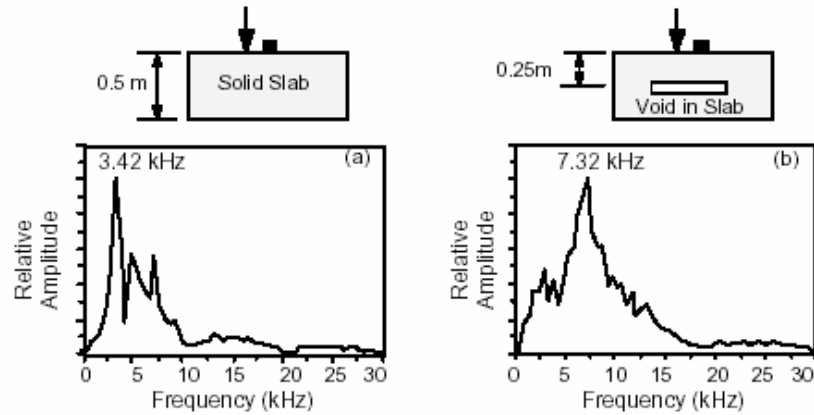


Figure 5.4.2-4 Examples of Amplitude Spectra From Impact-Echo Tests

Although the impact-echo method has many benefits over and against other NDE methods, as a means of locating voids within internally grouted post-tension tendons it has received mediocre reviews. Although relatively easy and inexpensive, the method is only accurate about 60% of the time (Goni). Often voids are “discovered”, but follow up bore scope investigations reveal otherwise. Investigators end up chasing false leads. Although a valuable method for detecting many other types of flaws in concrete as well as

determining slab depths, impact-echo testing is not recommended as an accurate method to detect the presence of voids in grouted post-tensioning tendon ducts.

5.4.3 Impulse Radar Testing

The purpose of impulse radar testing with respect to post-tensioning tendon inspection is to locate the tendon ducts, not to detect voids. Impulse radar testing is typically followed by bore scope investigation.

In practice, an impulse radar system consists of a transportable computer, a small monitor with a built-in keyboard, and one or more antennas. The antennas are connected to the computer through ports on a specialized data acquisition card. During measurement, the antenna is moved across the surface of the

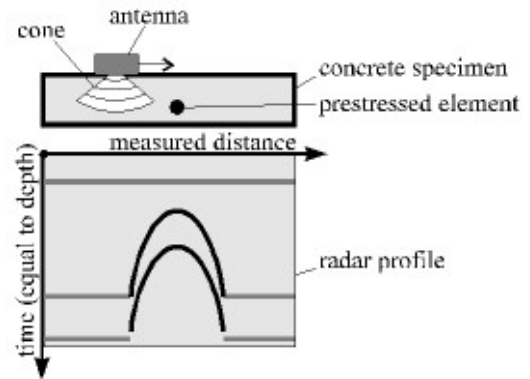


Figure 5.4.3-1 – Radar Profile of a Concrete and Rebar Specimen

concrete by hand. Figure 5.4.3-1 shows a specimen with a rebar in the middle and the corresponding simplified radar profile underneath. The antenna is moved in the direction of the arrow (Popel et. al.).

The antenna emits short impulses of electromagnetic waves. The waves spread in a shape that can roughly be approximated by the shape of a cone. If the electromagnetic waves hit an interface between two materials, a part of the wave is reflected as shown in Figure 5.4.3-2. The amount of

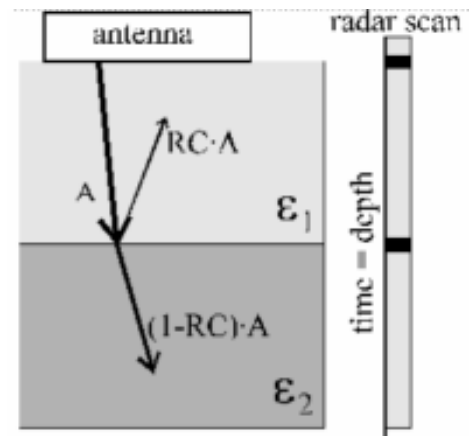


Figure 5.4.3-2 Reflection of a wave of intensity “A”, reflection coefficient “RC” and dielectric constants ϵ_1 and ϵ_2 .

reflection depends on the difference of the dielectric constants of the two materials. The reflected parts of the wave are received by the antenna. The intensity of the received reflections of one pulse are recorded in a single line along the vertical axis of the radar profile (Popel et. al. 1995).

Waves reflected from interfaces near the antenna are received earlier and display higher in the radar profile than waves reflected from interfaces far away. The intensity of the reflections is displayed in form of different colors. The recording of all the received reflections of one pulse is called a scan. When the antenna is moved, more scans are generated and displayed next to the previous scan. The sequential scans form the complete radar profile. The horizontal axis of the radar profile corresponds to the measured distance, while the vertical axis corresponds to the depth of the measured object. Because of the cone shaped radiation of the electromagnetic waves, interference patterns like the rebar in the middle of the specimen in figure 2 form a hyperbolic structure in the radar profile. The multiple hyperbolas are caused by multiple reflections of the wave between the rebar and the antenna. Figure 5.4.3-3 is a typical impulse radar record from a segmental bridge investigation in Ft. Lauderdale, FL (Goni).

Impulse radar testing has been found to accurately locate tendons in segmental bridge decks (Goni). A test can be performed in less than 5 minutes without cumbersome equipment or a large crew. This should be

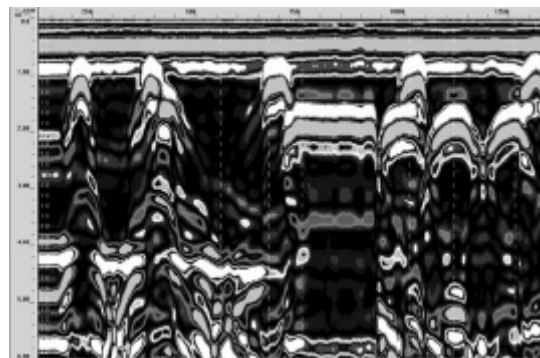


Figure 5.4.3-3 Typical Impulse Radar Record

given consideration as the method of choice for NDOR to locate the top tendon crest over the pier at the splice joint. It should be followed by bore scope inspection.

5.4.4 Magnetic Flux Leakage Testing

The purpose of magnetic flux testing is to identify post-tensioning strand corrosion and wire breaks. This immediately disqualifies it for our purposes of finding voids in ducts. A MFL test of a post-tensioning tendon consists of measuring changes in an induced magnetic field in the close vicinity of the post-tensioning tendon due to the presence of corrosion or fracture in the tendon. Figure 5.4.4-1 is a photo of the magnetic flux leakage testing device used for internal post-tensioning evaluation in the Ft. Lauderdale, Florida airport access bridge (Ghorbanpoor).

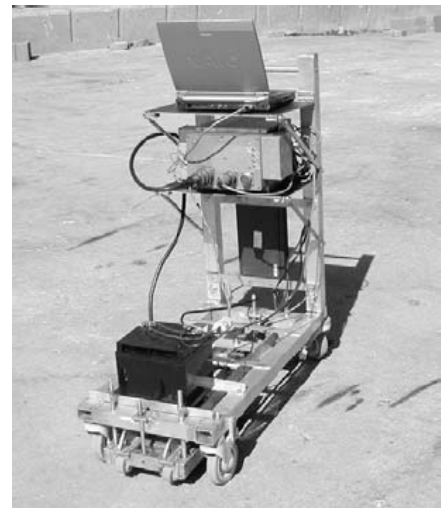


Figure 5.4.4-1 Magnetic Flux Leakage Testing Device For Internal Post-Tensioning

Although magnetic flux has had good results on external post-tensioning tendon inspections (Ghorbanpoor), reliable conclusions have been difficult to obtain with internally post-tensioned construction (Goni). Data collection is fast but interpretation requires time and expertise. MFL testing is also not able to evaluate tendons deep in concrete.

5.4.5 High Energy X-Ray (Linear Accelerator) Testing

The purpose of high energy X-Ray testing is to detect flaws inside concrete. This method holds great promise for a number of applications. It can accurately show defects in concrete 48" deep (Goni). In the future it may also allow the operator to view images in real time. However, it is very expensive and requires significant traffic control for public safety. A large perimeter safety zone is required to prevent X-Ray exposure. It also requires heavy equipment and is time consuming and cumbersome. X-Ray testing was used successfully to inspect grouted structures in the Boston Central Artery after the problems in Florida were publicized. Figure 5.4.5-1 is a photo of the X-ray testing device used for internal post-tensioning evaluation in the Ft. Lauderdale, Florida airport access bridge (Goni).



Figure 5.4.5-1 High Energy X-Ray Testing Device

If Nebraska had serious tendon corrosion problems and had a large number of bridges to inspect for voids, this method would be worth pursuing. However, with the limited number of PT bridges in this state and the small voids expected, a local investment in high-energy radiography equipment and training can not be justified at this time.

5.4.6 Conclusions

One of the problems often encountered when attempting to locate a post-tensioning duct using a NDE technique, such as impulse radar, is distinguishing between various material interfaces. For example, to locate the top post-tensioning duct over the pier section in an NU girder, the NDE method has to be able to “look past” two layers of rebar and 9 to 10 inches of concrete. This assumes the test is conducted in the splice region where shear reinforcement will not be present. The bottom layer of rebar consists of at least #4 and #6 bars at 6” O.C. longitudinal and #4 bars at 12” O.C. transverse. The top layer of rebar consists of at least #5 bars at 12” each way. There may be much more longitudinal deck steel present if ultimate negative moment capacity was a controlling factor. The interpretation of the recorded signal (radar profile) may require some expertise. However, it is the author’s opinion that a combination of impulse radar and bore scope inspection is still preferred for location and non-destructive evaluation of galvanized post-tension ducts.

5.5 OTHER PROTECTIVE MEASURES

In addition to making significant changes to the specifications related to grouting, a number of other protective measures were considered. This section briefly discusses these alternatives and makes a cost comparison.

5.5.1 Plastic Duct Systems

5.5.1.1 Background

The most fundamental change made recently to a number of state agencies' post-tensioning special provisions is the additional requirement that the duct system form an airtight and watertight protective barrier and to be formed from polyethylene. There are a number of benefits to such a system. First, this allows the complete encapsulation of the tendon. Because of the more effective details that are common on plastic duct systems, systems usually seal the tendon more effectively against the ingress of contaminants. This also allows for pressure testing the system after assembly to ensure a complete seal. The intention is that, if the duct is inadvertently not completely filled with grout (the possibility of which great pains are taken to avoid), the risk that this poses to the tendons is significantly reduced in that the sealed duct system will maintain a



**Figure 5.5.1.1-1 Dual Duct System
Incorporating Polyethylene Ducts in
Florida's Sunshine Skyway**

corrosion-free environment. Figure 5.5.1.1-1 shows a double duct system used on Florida's Sunshine Skyway. The interior duct is made of polyethylene.

Second, plastic duct systems allow for the complete electrical isolation of the tendon. This is impossible with a galvanized duct system. In highly corrosive environments electrical monitoring is sometimes desired. This is not Nebraska's situation.

Plastic ducts have been used for many years in prestressing technology for such applications as monostrands, ground anchors, stay cables and external tendons, mostly in the form of smooth pipes, not allowing transfer of bond stresses from the tendon to the structure. However, between 1968 and 1974 almost 1,000,000 feet of corrugated black polyethylene ducts were installed in bridges in Switzerland for bonded post-tensioning. After up to 30 years in use no deterioration of the polyethylene ducts has been observed in bridges eventually demolished or modified (FIB Bulletin 7).

Ducts for bonded post-tensioning have traditionally been made from steel strips with special corrugation. A long experience with these ducts is available for many different applications.

In recent years, however, the corrosive behavior of galvanized metal in harsh environments has been recognized. This speaks to the advantages of plastic duct systems over and against their galvanized counterparts. In the most recent publication of the "PTI Guide Specification for Grouting of Post-Tensioned Structures", section C2.7.1 addressing types of ducts reads, "Plastic ducts may add to the system durability by providing a non-corrosive impermeable layer between the concrete and the grout.

Galvanized steel ducts are not impermeable and may corrode in aggressive environments.”

In a paper published in the September-October 2002 issue of PCI Journal, Dr. John E. Breen and his colleagues report on the results of a 4 ½ year study conducted to investigate corrosion protection for internal tendons in segmental bridges. Although segmental bridge construction was the immediate concern, many of the conclusions and recommendations presented are applicable to all forms of internal, grouted post-tensioning tendons. Their findings are revealing. Regarding the 15 specimens containing steel ducts they write, “Galvanized steel ducts were corroded in all cases... (Galvanized steel) ducts were corroded *through* in nearly two-thirds of the specimens, eliminating the duct as corrosion protection for the prestressing tendon.” (Breen et. al.)

They conclude, “Galvanized steel post-tensioning ducts provide only limited corrosion protection for internal tendons, and may corrode through in severe exposure conditions or when low concrete cover has been provided. Plastic ducts provide a significant improvement in corrosion protection, limiting prestressing tendon corrosion to negligible levels and eliminating concrete cracking due to duct corrosion. Plastic post-tensioning ducts should be used for all internal tendons in applications where corrosion is a concern, including... environments where chloride-bearing deicing chemicals are used.”

Even after years of wide spread use, corrugated plastic duct systems for bonded post-tensioning are still relatively undeveloped compared to their galvanized counterparts. Currently products still differ widely in material properties, details, installation procedures and use on site. Therefore, they have not yet been standardized as

has been done for corrugated steel ducts or smooth PE pipes. They are also produced in relatively small quantities and therefore are typically much more expensive than corresponding steel ducts.

A number of states have specified plastic ducts for post-tensioning steel in bridge decks and galvanized ducts elsewhere. It's worth mentioning that the only type of bridge in which the Florida Department of Transportation allows corrugated metal ducts is the spliced I-girder.

Due to the current lack of standardization in plastic duct systems, State Department of Transportation Post-Tensioning Special Provisions often give significant attention to plastic duct specifications and testing.

Testing requirements may resemble the following (Minnesota DOT PT Special Provisions):

Corrugated plastic duct shall be designed so that a force equal to 40% of the ultimate tensile strength of the tendon will be transferred through the duct into the surrounding concrete in a length of 762 mm. Twelve static pull out tests shall be conducted to determine compliance of a duct with the force transfer requirement. If ten of these tests exceed the specified force transfer, the duct is acceptable. The Contractor shall provide to the Engineer certified test reports verifying that the duct meets the requirements of these special provisions in regard to force transfer.

To satisfy the intent of these tests, the results for static pull-out tests from previous projects utilizing identical duct and prestressing steel with similar concrete and grout material may be submitted to the Engineer in lieu of executing new pull-out tests. However, if the previous results are unacceptable or if there is a significant difference in the materials used, the Contractor shall provide results from new tests for this Project.

Specifications for polyethylene duct material may resemble the following

(Minnesota DOT PT Special Provisions):

Polyethylene duct for internal use shall be corrugated high-density material conforming to the requirements of ASTM D 3350 “Standard Specification for Polyethylene Plastics Pipe and Fittings” Type III, Class C, Category 5, Grade P33. The material thickness shall be 2.0 mm ± 0.26 mm.

Additional requirements for polyethylene duct are as follows:

<i>Property</i>	<i>Value</i>	<i>ASTM</i>	
<i>Charpy impact strength of notched specimens at 23degrees C</i>		<i>Greater than 35 kJ/m2</i>	<i>D256</i>
<i>Tensile impact strength of notched specimens at 23 degrees C</i>		<i>Greater than 130 kJ/m2</i>	<i>D1882</i>
<i>Carbon content</i>		<i>Greater than 2%</i>	

In addition to a lack of standardization, plastic ducts have been known to crack. Figure 5.5.1.1-2 is a photo taken in one of the Sunshine Skyway’s approach piers (FDOT). Though cracking has been observed primarily on externally post-tensioned systems, it could still be a strike against use in an internally post-tensioned system that may cause the duct to come into tension due to the flexure of the concrete member, i.e. Nebraska’s situation.



**Figure 5.5.1.1-2
Polyethylene Duct**

5.5.1.2 Nebraska's Situation

Plastic duct systems clearly offer more comprehensive corrosion protection for post-tensioning tendons than do galvanized duct systems. In highly aggressive environments, they provide a valuable barrier and allow the tendon to be monitored for electrical activity, i.e. corrosion, if desired. However, for Nebraska's circumstances, plastic duct systems are unfavorable for a number of reasons. Galvanized metal ducts are a standard product with established quality controls and multiple-source availability. The

most vulnerable location in a draped tendon in a spliced girder bridge is at crest locations over piers. And even at this Achilles Heel location, chlorides have to penetrate through at least 7"

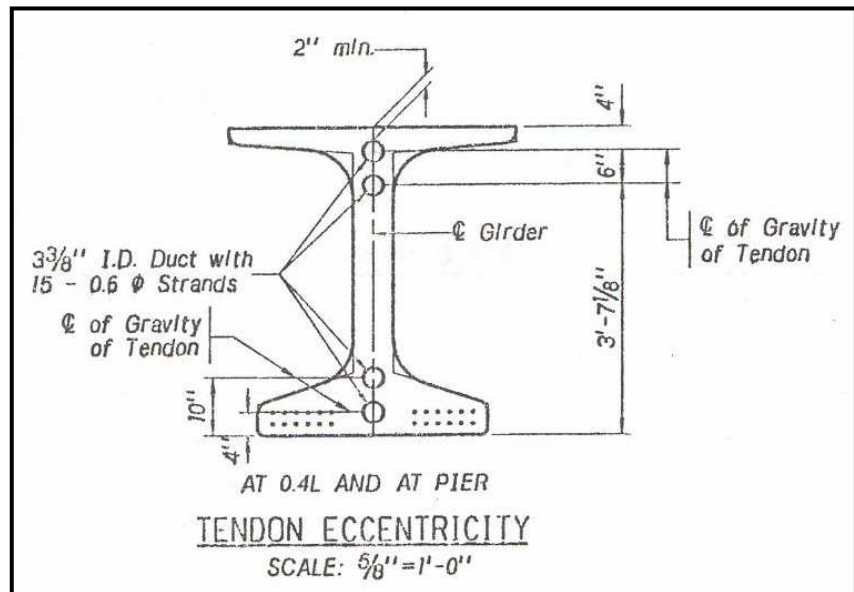


Figure 5.5.1.2-1 Detail, 2" Concrete Cover Over Duct

of deck concrete, 2"

of girder concrete, a sealed duct and a layer of thixotropic grout before reaching the tendon, which happens to be at the bottom of the duct at this location. Figure 5.5.1.2-1 shows a cross section of this location. This is a detail used by the Nebraska Department of Roads.

It could be argued that, in reality, the only true protective barrier in that whole system is the duct. The deck concrete will crack due to shrinkage even before live load is applied. So water can easily find its way to the top surface of the girder. Nebraska allows cracking in the girder concrete under live loads. So after a 50 year or so service life with these cracks opening and closing, it is reasonable to think that salt laden water could find its way to the duct. And if the duct is galvanized steel it is only a matter of time before it is corroded through.

So that leaves the grout as the final layer of protection. The problem here is that the grout will be even more cracked than the I-section. Post-tensioning is applied to the bridge before the duct is grouted, obviously. So the grout itself does not see any of the compressive stress that is locked into the I-section. It is essentially in a state of zero stress, even with post-tensioning in place. The only compressive stress the grout at the crest location will ever see in a single stage post-tensioned bridge is stress transferred to the grout due to the creep and shrinkage of the girder. This stress will be minimal.

Then the deck load is applied along with the superimposed dead load. This brings the grout at the crest location from zero stress to a level of tension beyond its modulus of rupture. The grout in the duct becomes permanently cracked due to the deck weight and superimposed dead load.

Finally, the live load is applied. This live load further opens the cracks already present in the grout. So to recap the situation: cracked deck, cracked girder, cracked grout. It seems like the only sure line of defense for the tendon is the duct. This most certainly argues for the use of non-corrosive plastic ducts instead of galvanized steel.

At the same time, however, the cracked I-section under live load disallows the use of plastic entirely. Cracks opening and closing in the girder concrete over the pier will cause fatigue cracking in the plastic. Plastic ducts are still unproven in this area. Galvanized ducts are as well, for that matter. To the author's knowledge, fatigue testing on galvanized ducts is not documented in the literature. But engineering judgment points us in the direction of steel being better able to resist the fatigue caused by the opening and closing of cracks in the I-section than polyethylene.

Plastic duct systems also allow the anchorage location to be completely sealed from chloride attack. In segmental bridge applications this can be a desirable specification. However, as shown in Figure 5.5.1.2-2, the post-tensioning tendon anchorage locations are encased in a large block of concrete. Chloride penetration at these locations does not seem likely.

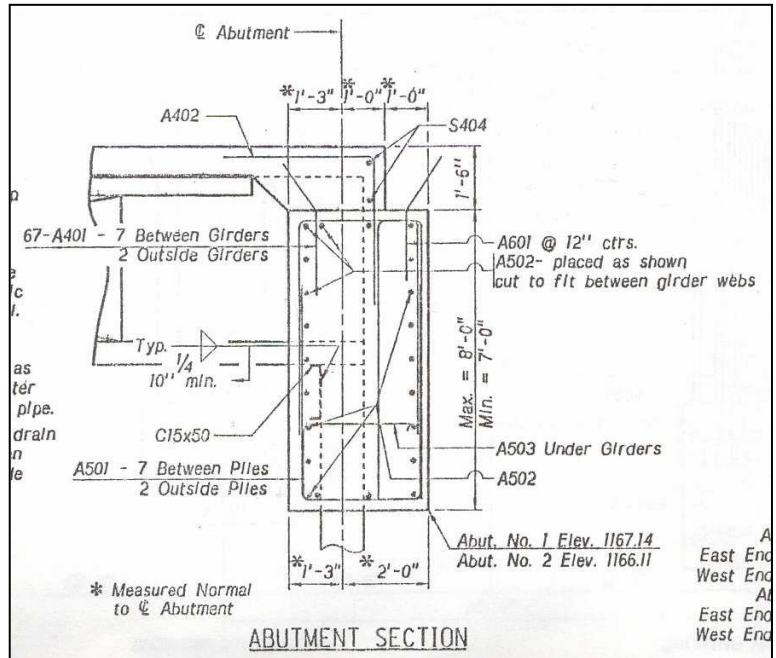
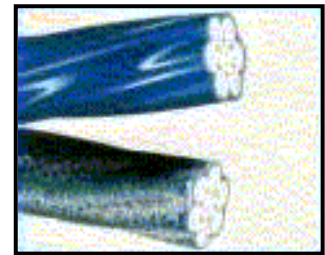


Figure 5.5.1.2-2 Detail Showing Concrete Encasement of Anchorage Region

5.5.2 Galvanized / Epoxy Coated Strand

Epoxy coating was considered as an alternative because of its great potential anticorrosive value. Figure 5.5.2-1 shows externally coated 7-wire epoxy strand. Experience has shown that an epoxy coated strand needs to have the interstices between wires completely filled with epoxy to avoid migration of water / humidity along the strand (Ganz). Coating Nebraska's strand would have brought with it a large group of additional concerns including the following:



**Figure 5.5.2-1
Externally Coated
Epoxy Strand**

Epoxy coated strand is expensive. Grit impregnated or not, it is available through only one supplier in the continental United States, Florida Wire and Cable, at a prohibitively high cost. Much more readily available uncoated strand costs much less. A cost comparison is presented in the next section of this report.

Anchorage seating losses for epoxy-coated strand are typically more than that for uncoated strand; the difference is often large enough to be significant (Breeze et. al.).

Additional care must be taken to avoid damaging the epoxy coating during shipping and installation. Damaged areas take time to repair. Also, small imperfections in the epoxy coating can lead to accelerated pitting corrosion at these locations (Ganz et. al.).

Final stressing of epoxy coated strand should be a single stroke operation because after one jacking cycle the jaws of the wedges can become contaminated with particles of epoxy; a second jacking cycle without cleaning the grips may result in a loss of gripping action (Breeze et. al.).

The use of epoxy-coated strand is not recommended with galvanized metal ducts; severe abrasion of the epoxy will occur during the stressing operation as the strand comes in contact with the spiral duct seams.

Although epoxy coated strand can provide a valuable additional layer of corrosion protection, the costs, especially financial, outweigh the benefits for Nebraska's situation.

Galvanized strand is another option briefly considered. It has long been used for wire in suspension cables and more recently in stay cables. Zinc coated prestressing steel however, is rarely used for post-tensioning. Few manufactures supply galvanized strand. Presently, no U.S. specification exists, which specifies the properties of galvanized strands suitable for post-tensioning applications and which specifies the zinc coating thickness requirements. Two ASTM specifications provide galvanizing guidelines.

Galvanized strand produced from 270ksi strand material, normally has a reduced 240ksi tensile strength and does not meet ASTM A 416 requirements. The approximately 800^oF temperature of the hot dipped galvanizing process changes the properties of the cold drawn steel wires.

Galvanized strand meeting the 270 grade requirement of ASTM A 416 is either produced from higher than 270 grade ungalvanized material, or the wires, after galvanizing, are further reduced in size by drawing them through a die or several dies (PTI Committee for Post-Tensioning System Certification). It is not necessary in Nebraska's situation.

5.5.3 Cost Comparison

In the interest of comparing the cost effectiveness of implementing commercially available pre-bagged thixotropic grout as compared with other corrosion prevention alternatives, a cost analysis was performed. The bridge used in the comparison was the N-50 interchange bridge in Sarpy County, Nebraska. It is a 250' long, 100'-6" wide two span bridge using spliced post-tensioned NU1350 girders. The splice occurs over the pier. There are 10 girder lines with a total of 20 post-tensioning tendons, 2 tendons per girder. Each tendon contains 15 strands. Assume a tendon length 10% longer than the bridge length to account for drape.

We begin by comparing the cost of steel vs. plastic ducts. Galvanized steel duct typically costs about \$0.96 per linear foot. Polyethylene duct costs about \$2.83 per linear foot. Given the bridge configuration above, we have a total duct length of 5,500'. The total cost of galvanized duct on this project would be about \$5,300 or \$0.21 per square foot of bridge deck. The total cost of polyethylene duct would be \$15,600 or \$0.62 per square foot of bridge deck, for a total cost increase of \$10,300 or an increase per square foot of \$0.41. Duct prices were obtained from a DSI sales representative.

Moving on to coated vs. uncoated strand. Given the bridge configuration above we have a total strand length of 82,500'. Uncoated 0.6" diameter 7-wire strand costs about \$0.24 per linear foot. Similar coated strand costs about \$0.73 per foot. The total cost of uncoated strand is \$19,800 or \$0.94 per square foot of deck. The total cost of



Figure 5.5.3-1 Post-Tensioning Grout Discharge

coated strand is about \$60,200 or \$2.85 per square foot of deck for a total cost increase of \$40,400 or \$1.90 per square foot. Strand cost was obtained from a Florida Wire and Cable representative.

Now to thixotropic vs. plain cement grout. Figure 5.5.3-1 shows post-tensioning grout discharge. A 3 3/8" I.D. duct has an area of 8.95in². A 15 strand tendon has an area of 3.26in² for a void area of 5.69in². This yields a void volume of 305cf assuming a factor of 1.4 to account for grout waste. A standard 94# sac of cement (S.G. = 3.15) mixed at a 0.45 w/c ratio yields 1.16cf of grout for a total sacs required = 263. A sac of cement costs about \$7.00 for a total grout cost of \$1,840 or \$0.07 per square foot of deck. Pre-bagged grout generally comes in smaller bags, 50# or so, and costs about \$16.50 per cubic foot of mixed grout for a total cost of \$5030 or \$0.20 per square foot of deck. This a cost increase of about \$3200 or \$0.13 per square foot of deck. Pre-bagged grout cost was obtained from a Sika representative.

To summarize, moving to plastic ducts instead of steel will increase cost about \$0.41/sf. Epoxy coated instead of uncoated strand will increase cost about \$1.90/sf. Thixotropic instead of plain cement grout will increase \$0.13/sf. This seals the case for a pre-bagged thixotropic grout. The minimal cost increase is clearly offset by the increase in durability.

It is also prudent to consider that a colloidal mixer will cost about \$7,500 more than an equivalent paddle mixer, meaning a paddle mixer with an additional agitation tank, comparable pump capacity capable of grouting a tendon within the maximum time allowed, etc... This initial investment will quickly pay for itself.

5.5.4 The Most Critical Protective Measure – Personnel

The most critical protective measure, one which cannot be easily fit into a cost comparison, is the knowledge and experience of the personnel involved in the grouting process. The grouting technicians, grouting supervisors, grouting inspectors, and design engineers all need to stay knowledgeable and involved. Post-tension grouting has progressed well beyond its infant stages when a five gallon bucket of water and a sac of cement mixed in a paddle mixer constituted a good grout. The engineering community knows better now.

Historically, grouting of post-tension tendons has been treated as an afterthought. It is, “what you do when the real construction work is done.” This kind of thinking leads the occasional ungrouted duct and various tendon corrosion horror stories that have been so well publicized in the last five years or so. Significant re-education is called for in the post-tension grouting community. This need for education is heavily reflected in the revised Nebraska Department of Roads Post-Tensioning Special Provisions.

5.6 CONCLUSIONS AND RECOMMENDATIONS

The conclusions reached in light of the previous discussion are reflected in the changes proposed to the Nebraska Department of Roads Post-Tensioning Special Provisions found in the appendices of this report. The following is a discussion of some of the major conclusions reached and changes recommended.

The largest body of changes proposed to the specification is to the grout itself. The protection of post-tensioning steel depends of the tendon being completely surrounded by quality grout. This calls for no less than a flowable and yet zero-bleed

product. Thixotropic grouts can meet both of these requirements. Commercially available pre-bagged grout manufacturers are typically not shy about advertising their ability to meet all the grout property requirements laid out in Table 5.1 of the Special Provisions. The need for specialized mixing equipment is also incorporated.

Recommendations were made for new production testing requirements. These ensure that a quality grout is being pumped into the tendon and a similar, undiluted grout is exiting the tendon.

Personnel requirements were removed from the plan notes and expanded in the Special Provisions. These focus on the State Inspector and on the Grouting Supervisor. Not included in the recommended changes were requirements for the Design Engineer. Obviously the Engineer needs to have at least and preferably a much greater knowledge base in post-tension grouting issues than the inspector and supervisor. It is recommended that Nebraska Department of Roads Engineers involved in writing the final Post-Tension Special Provisions attend the ASBI Grouting Training and become ASBI Grouting Training Certificate holders.

A grouting plan and optional pre-grouting conference are recommended. The submission of a grouting plan by the Contractor gives the Engineer insight into the level of understanding of the Contractor and gives the Engineer the opportunity to change procedures as necessary. The pre-grouting conference can be a valuable tool during these times of grouting re-education. It serves to help keep everyone knowledgeable and involved.

Provisions were also made to facilitate inspection of the tendon after the grouting operation. The idea behind these provisions is that when everything goes wrong, as it

occasionally will, the inspectors need to be able to physically look into the duct to see whether or not grout made it to the most critical locations. These may seem the most extreme of all the proposed changes but are not uncommon among other state agencies.

We believe that these, along with the additional changes made to the Nebraska Department of Roads' Post-Tensioning Special Provision, are a large step toward ensuring the full, corrosion free design life of post-tensioning tendons in Nebraska's bridges.

REFERENCES

- AASHTO, LRFD Bridge Design Specifications, Second Edition 1998 and Interims 1999 and 2000, American Association for State Highway and Transportation Officials, Washington, D.C.
- AASHTO, Standard Specifications for Highway Bridges, 16th Edition, American Association for State Highway and Transportation Officials, Washington, D.C., 1996
- Abdel-Karim, A.M., “Analysis and Design of Precast/Prestressed Spliced-Girder Bridges”, Dissertation presented to the University of Nebraska-Lincoln, NE, in partial fulfillment of the requirements for the degree of Doctor of Philosophy, 1991
- Abdel-Karim, A.M., and Tadros, M.K., “Design and Construction of Spliced I-Girder Bridges”, PCI JOURNAL, V. 37, No. 4, July-August 1992, pp. 114-122
- Abdel-Karim, A.M., and Tadros, M.K., “State-of-the-Art of Precast/Prestressed Concrete Spliced Girder Bridges,” Special Publication, PCI, 1992.
- ACI Committee 222R-96, “Corrosion of Metals in Concrete,” American Concrete Institute, Farmington Hills, MI, 1997, pp. 30
- ACI Committee 363, State-of-the-Art Report on High-Strength Concrete (ACI 363R-92),” Manual of Concrete Practice, American Concrete Institute, 55 pp.
- Al-Omaishi, N., “Prestress Losses in Pretensioned High-Strength Concrete Bridge Girders”, Ph.D. Dissertation, Department of Civil Engineering, University of Nebraska, Lincoln, NE, 2001
- ASTM C 940-87, “Standard Test Method for Expansion and Bleeding of Freshly Mixed Grouts for Preplaced-Aggregate Concrete in the Laboratory”, American Society for Testing and Materials, West Conshohocken PA, 1987
- Badie, S. S. and Tadros, M. K., “Flexural strength According to AASHTO LRFD Specifications,” PCI Journal, Vol. 44, No. 4, July-August 1999, pp. 122-127
- Bexten, K. A., Hennessey, S. and LeBlanc, B., “The Bow River Bridge-A Precast Record,” HPC Bridge Views, Issue No. 22, July/August 2002, Federal Highway Administration /National Concrete Bridge Council, <http://www.portcement.org/br/newsletters.asp>.
- Bracewell, R., “The Fourier Transform and its Applications”, 2nd Ed., McGraw-Hill Nook Co., 1978, 444 p.

Breen, J.E, Burdet, O., Roberts, C., Sanders, D., and Wollman, G., "Anchorage Zone Reinforcement for Post-tensioned Concrete Girders," NCHRP Report 356, TRB, National Research Council, Washington, DC, 1994

Breen et. al., "Evaluation of Corrosion Protection for Internal Prestressing Tendons in Precast Segmental Bridges, " PCI Journal, Prestressed Concrete Institute, Chicago, IL, September-October 2002, v.47, issue #5,

Breeze, Paul C. et. al., "Guidelines for the Use of Epoxy-Coated Strand," PCI Committee Report, PCI Journal, July-August 1993, p.26

Bridge Office Policies and Procedures (BOPP) Manual, Nebraska Department of Roads (NDOR), Lincoln, NE, 2001

Caroland, W. B., Deep, D., Janssen, H. H., and Spaans, L., "Spliced Segmental Prestressed Concrete I-Beams for Shelby Creek Bridge", PCI JOURNAL, V. 37, No. 5, September-October 1992, pp. 22-33

Concrete Society, The, "Grouting Specifications," Concrete, July/August 1993, p.23

Corven Engineering, Inc., "Mid-Bay Bridge Post-Tensioning Evaluation – Draft Report", Florida Department of Transportation, Feb, 2001, 55 pp.

Ficenec, J. A., Kneip, S.D., Tadros, M.K., and Fischer, L., "Prestressed Spliced I-Girders: Tenth Street Viaduct Project, Lincoln, Nebraska," PCI JOURNAL, V. 38, No. 5, September-October 1993, pp. 38-48

Fitzgerald. J. B., and Stelmack, T. W. "Spliced Bulb-Tee Girders Bring Strength and Grace to Pueblo's Main Street Viaduct", PCI JOURNAL, V. 41, No. 6, November-December 1996, pp. 40-54

Girgis, A., Sun, C., and Tadros, M.K., "Flexural Strength of Continuous Bridge Girders-Avoiding the Penalty in the AASHTO-LRFD Specifications," PCI JOURNAL, Vol. 47, No. 4, July/August 2002, pp. 138-141

Guide Specification for design and construction of Segmental Concrete Bridges, Second Edition, American Association of State Highway and Transportation Officials, Washington, DC, 1999

Kamel, M., "Innovative Precast Concrete Composite Bridge Systems," Ph.D. Dissertation, University of Nebraska-Lincoln, 1996

Loov's ., "Unified Design Recommendations for Reinforced, Prestressed and Partially Prestressed Concrete Bending and Compression Members," ACI Structural Journal V. 89, No. 2, March-April 1992, pp. 200-210

Loov, E.R., and Patnaik, A., k, "Horizontal Shear Strength of Composite Concrete Beams With a Rough Interface," PCI JOURNAL, Vol. 39, No. 1, January-February 1994, pp. 48-66

Ma, Z., Huo, X., Tadros, M. K., and Baishya, M., "Restraint Moments in Precast/Prestressed Concrete Continuous Bridges," PCI JOURNAL, Vol. 43, No. 6, November-December 1998, pp. 40-57

Ma, Z., Huo, X., Tadros, M.K. and Baishya, M. "Restraint Moments in Precast/ Prestressed Concrete Continuous Bridges," PCI JOURNAL, Vol. 43, No. 6, November-December 1998

Ma, Z., Saleh, M. A and Tadros, M.K., "Optimized Post-Tensioning Anchorage in Prestressed Concrete I-Beams," PCI JOURNAL, Vol. 44, No. 2, March-April 1999

Marshall, S. L., and Pelkey, R. E., "Production, Transportation, and Installation of Spliced Prestressed Concrete 'I' Girders for the Annacis Channel East Bridge", ACI SP93-33, American Concrete Institute, Detroit, MI, 1986

Mast, R. F., "Unified Design Provision for Reinforced and Prestressed Concrete Flexural and Compression Members," ACI Structural Journal, V. 89, No. 2, March-April 1992, pp. 185-199

Mills, D., Kenneth, C. T., and Marshall, S. L., "Design-Construction of Esker Overhead", PCI JOURNAL, V. 36, No. 5, September-October 1991, pp. 44-51

Mirmiran, A., Kulkarni, S., Castrodale, R., Miller, R., and Hastak, M., "Nonlinear Continuity Analysis of Precast, Prestressed Concrete Girders with Cast-in-Place Decks and Diaphragms," PCI JOURNAL, Vol. 46, No. 5, September-October 2001, pp. 60-80.

Nicholls, J. J., and Prussack, C., "Innovative Design and Erection Methods Solve Construction of Rock Cut Bridge", PCI JOURNAL, V. 42, No. 4, July-August 1997, pp. 42-55

PCI Bridge Design Manual, Precast/Prestressed Concrete Institute, Chicago, IL, 1997.

PCI Design Handbook Precast and Prestressed Concrete ,Fourth Edition, Precast/Prestressed Concrete Institute, Chicago, IL, 1992

Pierce, L. F. "Annacis Channel East Bridge", PCI JOURNAL, January-February 1988, V.33, No.1, pp. 148-157

Ronald, H. D., "Design and Construction Considerations for Continuous Post-Tensioned Bulb-Tee Girder Bridges," PCI JOURNAL, Vol. 46, No. 3, May-June 2001, pp. 44-66

Saleh, M.A., Einea, A., Tadros, M.K., "Creating Continuity in Precast Girder Bridges," Concrete International, Vol. 17, No. 8, 1995, pp. 431-595

Saleh, M., Tadros, M., "Effects of Post-Tensioning on Concrete Members," PCI JOURNAL, Vol. 46, No. 5, September-October 2001, pp. 104-109

Stephen J. Seguirant, "Effective Compression Depth of T-Sections at Nominal Flexural Strength," PCI JOURNAL, Vol. 47, No. 1, January-February 2002, pp. 100-105

Seguirant, Stephen J., "New Deep WSDOT Standard Sections Extend Spans of Prestressed Concrete Girders." PCI Journal, Vol. 43, No. 4, July-August 1998, pp. 92-119

Tadros, M.K., Al-Omaishi, N. Seguirant, S. J. and Gallt, J. G., "Prestress Losses in Pretensioned High-Strength Concrete Bridge Girders," National Cooperative Highway Research Program, NCHRP Report 18-07, Transportation Research Board, National Research Council, Washington DC, August 2002, 120 pp.

Tadros, M.K., Ghali, A., and Dilger, W. H., "Time-dependent Analysis of Composite Frames," ASCE Journal of Structural Engineering, V. 103, No. 4, April 1977, pp. 871-884

Van Lund, J. A., Kinderman, P. D., and Seguirant, S. J., "New Deep WSDOT Girders used for the Twisp River Bridge," PCI JOURNAL, V. 47, No. 2, March-April 2002, pp. 21-31